OUKA
The University of Osaka
Institutional Knowledge Archive

Title	STUDY OF HELIX-COIL TRANSITION IN POLYPEPTIDES
Author(s)	Norisue, Takashi
Citation	大阪大学, 1973, 博士論文
Version Type	VoR
URL	https://hdl.handle.net/11094/2159
rights	
Note	

The University of Osaka Institutional Knowledge Archive : OUKA

https://ir.library.osaka-u.ac.jp/

The University of Osaka

STUDY OF HELIX-COIL TRANSITION IN POLYPEPTIDES

TAKASHI NORISUYE

STUDY OF HELIX-COIL TRANSITION IN POLYPEPTIDES

A Doctral Thesis Submitted by

Takashi Norisuye

to the Faculty of Science, Osaka University

1973

Acknowledgments

This work was performed at the Fujita Laboratory, Department of Polymer Science, Osaka University. I am greatly indebted to Professor Hiroshi Fujita and Assistant Professor Akio Teramoto for drawing my attention to the present problem. It is a pleasure to thank them for their guidance, advice, and constant encouragement. I am very grateful to the late Dr. Kazuo Nagai for his valuable discussion and to Assistant Professor Shinsuke Yamashita, now at the School of Pharmacy of Tokushima University, for providing a PBLG sample. Mr. Mikio Matsuoka, Mr. Norio Sayama, and Mr. Kenji Kida helped me with polarimetric and vapor pressure measurements. Thanks are also due to all the members of the Fujita Laboratory for their contribution to this work and their friendship.

Finally, it is a pleasure to acknowledge the assistance of my wife Yasuko Norisuye who typed the manuscript. I also wish to express my gratitude to my father Kazuo Norisuye and my mother Kotoe Norisuye for their encouragement during the course of this work.

Contents

Chapter 1

Introduction

1-1. Introduction

During the last twenty years, biological macromolecules and their synthetic analogs have acquired rapidly growing interest in the field of polymer solution study. Synthetic polypeptides have received special attention because these polymers were shown to take up various conformations in solution, such as α-helix, β-form, and random coil, depending on the kind of polypeptide, solvent, temperature, and so forth.

It has been demonstrated for some polypeptides that their conformation undergoes a change from random coil to helix or vice versa, when the environmental conditions are varied. This helix-coil transition process has been investigated either theoretically or experimentally by a number of authors. Yet there remains much to be desired in the elucidation of this process and the changes in molecular properties accompanying it. The present thesis has been undertaken in the hope of obtaining more information which may ultimately aid in reaching the deeper understanding of polypeptide molecules in the helix-coil transition region.

1-2. Historical Survey

Doty, Blout, and coworkers[1-4] opened the door to the subsequent studies of synthetic polypeptides in solution when they showed from light-scattering and viscosity measurements that poly(γ-benzyl L-glutamate) (PBLG) assumed either the α-helical conformation of Pauling, Corey, and Branson[5] or randomly coiled conformation, depending upon the solvent in which it was dissolved. Doty and Yang[6] found from optical rotation measurements that a sharp thermal transition of PBLG from coil to helix took place in a dichloroacetic acid (DCA) — ethylene dichloride (EDC) mixture (75 vol% DCA). The transition behavior depended largely on the molecular weight of the sample, and, in contrast to analogous cases of protein denaturation, the helical conformation was stabilized at higher temperatures. Such "inverse" thermal transitions also have been observed for other synthetic polypeptides[7] when the solvent mixtures contained an "active" solvent such as DCA or trifluoroacetic acid, which is capable of forming hydrogen bonds with peptide residues. Doty and Yang predicted that in this type of transition the active solvent solvates the coiled residues of the polypeptide chain at low temperatures, but is liberated upon raising temperature to induce intramolecular hydrogen bonds between peptide residues. Calvin, Hermans, and Scheraga[8] demonstrated this prediction experimentally.

Although Klotz, Hanlon, and coworkers[9-12] suggested that the protonation of peptide residues by strong acids might be responsible for the transition, recent NMR studies[13-16] have lent support to the original solvation mechanism of Doty and Yang.

Another important contribution of Doty and Yang[6] was that average conformations of polypeptides can be determined from optical rotation and related spectroscopic measurements. There are excellent review articles[17,18] as for the developments in such a direction as well as the transitions of polypeptides.

Schellman[19] had attempted formulating the denaturation of protein or the helix-coil transition of polypeptide in terms of statistical mechanics before the work of Doty and Yang[6] appeared. His theory dealt with the "all or none" type of transition and ignored the possibility of alternation between the helical and coiled conformations within a polypeptide chain. The viscosity data of Doty[20] suggested, however, that the transition did not take place according to the all or none principle. Many investigators[21-28] subsequent to Schellman all took into account the alternation of helical and randomly coiled sections. Although the expressions of these authors are different in appearance, they all have a feature in common that the conformation of an uncharged homopolypeptide in the helix-coil transition region can be characterized by three parameters, N, u, and

σ. Here N is the number of peptide residues in the molecule, u is the equilibrium constant for the formation of helix from random coil, and σ is the helix-initiation or cooperativity parameter. Table 1.1 shows the correlation of the transition parameters used by various authors.

The first quantitative test of such a theory with experiment was made by Zimm, Doty, and Iso.[29] They tried to find a set of values for the transition enthalpy ΔH, transition entropy ΔS, and σ which allow the theory of Zimm and

Table 1.1. Comparison of the notation for the transition parameters used in various theories

Helix-initiation parameter	Equilibrium constant	Reference
σ	u	present notation
σ	s	Zimm and Bragg[22]
Z^{-2}	X^{-1}	Gibbs and DiMarzio[24]
y_{hc}^{2}	j_c/j_h	Peller[23]
α^2	σ	Nagai[27]
B^2	BC	Miyake[26]
v^2	w	Lifson and Roig[28]

Bragg[22] to fit the experimental curves of Doty and Yang.[6] Here ΔH and ΔS are related to ln u by

$$\ln u = -\frac{1}{RT}(\Delta H - T\Delta S) = -\frac{1}{RT}(1 - \frac{T}{T_c}) \qquad (1\text{-}1)$$

where T is the absolute temperature, R is the molar gas constant, and $T_c = \Delta H/\Delta S$ is the temperature at the midpoint of the transition where ln u vanishes. They found that ΔH = 890 cal/mol and $\sigma = 2 \times 10^{-4}$. Zimm and Bragg[22] suggested from a theoretical point of view that σ would be relatively insensitive to the kind of polypeptide and solvent species.

Applequist[30] derived from the theory of Zimm and Bragg

$$\lim_{N\to\infty} [\partial f_N/\partial(1/T)]_{T=T_c} = -\frac{\Delta H}{4\sqrt{\sigma}\,R} \qquad (1\text{-}2)$$

where f_N is the helical content of the polypeptide molecule having N degrees of polymerization. According to this equation, the magnitude of the ratio $\Delta H/\sqrt{\sigma}$ may be available from the slope of an f_N vs. T curve at $f_N = 1/2$ for infinitely large N. Thus if either ΔH or σ is known, the other can be estimated. Applequist used this equation to estimate ΔH values for several systems, assuming $\sigma = 2 \times 10^{-4}$. Calorimetric measurements of ΔH have been undertaken by several groups of authors.[31-44] Such measurements were combined with Applequist's equation to estimate σ. However, the numerical values of ΔH and σ obtained by different

authors for the same polypeptide-solvent system were at variance with each other. In all these treatments, it was assumed that the parameters ΔH, ΔS, and σ are independent of temperature. Such an assumption may not be justified theoretically.

As a result of these efforts of the previous investigators, we now have a considerable amount of data for ΔH, and know that the value of σ depends appreciably on the kind of polypeptide, in contrast to the earlier suggestion of Zimm and Bragg.[22] Hayashi, et al.,[45] showed for poly(β-benzyl L-aspartate) (PBLA) that σ depended largely on solvent, too. Moreover, their data for the inverse transition of PBLA appeared to indicate that ΔH depends upon temperature.

Recently, Okita, Teramoto, and Fujita[46] proposed for the estimate of σ and ΔH a simple procedure which is free from the restrictions inherent in the previous ones. It utilized data for f_N as a function of N at fixed solvent conditions, and was applied successfully to the transition curves of poly-N^5-(3-hydroxypropyl)-L-glutamine (PHPG) in water-methanol mixtures.

Following the first attempt by Schellman,[47] Peller,[48] Gibbs and DiMarzio,[24] and Bixon and Lifson[49] have theoretically investigated effects of an active solvent on helix-coil transition by taking explicitly its interactions with peptide residues into account. However, little has been done yet to test their theories with experiment.

The mean-square radius of gyration, $\langle S^2 \rangle$, defines average dimensions of a polymer molecule in solution and can be determined directly from light-scattering measurements. Nagai[27] was the first to investigate theoretically $\langle S^2 \rangle$ and related quantities of polypeptide molecules in the helix-coil transition region. Later, Miller and Flory[50] and several authors[51-54] made similar studies. It has been shown that under certain conditions of σ and N the theoretically calculated curves for $\langle S^2 \rangle$ vs. ln u (that for $\langle S^2 \rangle$ vs. f_N as well) have a shallow minimum in the vicinity of ln u = 0 and that the shape of the curves is very much influenced by σ. Teramoto, Fujita, and coworkers[45,46,55] demonstrated, though qualitatively, the correctness of these theoretical predictions in terms of intrinsic viscosity data. Ptitsyn and coworkers[51,56,57] published similar studies.

For quantitative test of these theories direct experimental data for $\langle S^2 \rangle$ are needed, although the measurements are much more difficult than those of intrinsic viscosity. In addition, as pointed out by Nagai,[27] light-scattering measurements may not yield correct $\langle S^2 \rangle$, since a polypeptide molecule in the transition region must be reckoned as a copolymer consisting of alternate helical and randomly coiled sections which may have different specific refractive index increments.

Recently, Okita, Teramoto, and Fujita[58] obtained from extensive light-scattering measurements on PHPG in mixtures

of water and methanol data for $\langle S^2 \rangle$ over the entire range of the helix-coil transition. These data, when analyzed in terms of the procedure developed in the present work, indicated that a PHPG molecule in the transition region can be approximated by an alternate sequence of α-helical rods and random coils. Strazielle, Dufour, and Marchal[59] found from light-scattering measurements on PBLG in various mixtures containing DCA that the preferential adsorption of DCA to the polymer solute was remarkable for most of the solvent mixtures they examined. They also presented data for $\langle S^2 \rangle$ in the transition region, but gave no quantitative analysis of them. These are the only data available at present for $\langle S^2 \rangle$ of polypeptide in the transition region. Need for more experimental data are apparent.

The conclusion of Doty, et al.,[2,4] from light-scattering and viscosity measurements that PBLG in helix-forming solvents takes the form of straight rod consisting of the α-helix has been substantiated by studies of other solution properties such as dielectric dispersion,[60] flow birefringence,[61-63] and non-Newtonian viscosity.[64] However, a number of papers[65-73] also have appeared which threw doubt on the rigidity of the molecule in helicogenic solvents. Some groups of authors[65-69] considered that the shape of a polypeptide in helix-forming solvent was better represented by a wormlike chain of Kratky and Porod,[74] since the pitch of the helix per monomeric residue, h, derived from various

methods were shown to be a decreasing function of molecular weight. Miller and Flory[50] inferred that such flexibility of helical polypeptide would be caused either by random deviation of bond rotation angles from the α-helical values or by occasional interruptions of the helix by sequences of randomly coiled residues. No conclusion is yet established as to which of these interpretations is more reasonable.

1-3. Purposes and Contents of This Work

The main theme of the present thesis is the relationship between dilute solution properties of a polypeptide molecule and its conformation. For an investigation of this relationship we have to consider factors responsible for determining the chain conformation on one hand, and to examine conformation-dependent properties in the transition region on the other hand. The literature survey given in the preceding section shows that existing data pertinent for this purpose are scarce and insufficient. We therefore attempted accumulating relevant data, mostly with PBLG, and deriving theoretical expressions necessary to analyze them.

Chapter 2 concerns the theory of helix-coil transition in polypeptide and its application to transition curves of PBLG in mixtures of DCA and EDC and of DCA and cyclohexanol. In the next chapter, theoretical equations for u, ΔH, and σ are derived by taking the effects of solvation into account and tested with experimental data for PBLG and PBLA.

In Chapter 4, a simple expression for $\langle S^2 \rangle$ is derived from the exact expression of Nagai[27] by using the approximation introduced by Okita, et al.,[46] and a method for analyzing $\langle S^2 \rangle$ data is proposed. Furthermore, the particle scattering function is calculated on the basis of Nagai's model,[27] with the copolymer nature of interrupted helices being taken into account.

Chapter 5 deals with light-scattering measurements on PBLG and analyzes the data in terms of the method developed in Chapter 4. The last chapter presents intrinsic viscosity data for PBLG in various solvents. They are discussed in connection with the light-scattering data presented in Chapter 5.

Chapter 2

Helix-Coil Transition of Poly(γ-Benzyl L-glutamate)

2-1. Introduction

As mentioned in Chapter 1, the conformation of a helix-forming polypeptide molecule in the helix-coil transition region can be characterized by three parameters, N, σ, and u. Experimental determination of these parameters is basic for a quantitative discussion of various physical properties of the polypeptide molecule in dilute solution. Okita, Teramoto, and Fujita[46] have recently proposed an elegant method appropriate for this purpose. We shall first describe the theory of helix-coil transition due to Nagai,[27] from which the method of Okita, et al.,[46] has been derived. This method is then used to determine the transition parameters σ and u, and also the transition enthalpy ΔH for PBLG in mixtures of dichloroacetic acid (DCA) and ethylene dichloride (EDC) and in a mixture of DCA and cyclohexanol (CHL). Finally, we shall compare the resulting values of σ and ΔH with those obtained for the same systems by previous authors.[29,32,33,35,38,40]

2-2. Theoretical

2-2-1. Statistical Model and Formulation of Nagai's Theory

First, we quote the statistical mechanical model and

the partition function for Nagai's theory.[27] Let us consider a polypeptide chain consisting of N monomeric residues which are numbered 1, 2, 3, ..., N from the carboxyl terminal and each of which consists of an identical peptide residue, (-CO-CHR'-NH-). Here R' denotes the side chain attached to the α-carbon. The NH group of the i-th residue is assumed to form a hydrogen bond with the CO group of the (i + 4)-th residue if, and only if, the (i + 1)-, (i + 2)-, and (i + 3)-th residues are in the α-helical conformation. The polypeptide chain at intermediate stages of the transition consists of alternate sequences of helical and randomly coiled sections. Its conformational state is described by a sequence of digits one and zero

000011111100111011110O•••

where the digit one corresponds to the state in which the residue is "distorted" so as to form a helical section, and the digit zero corresponds to the state in which the residue is "undistorted" or involved in a randomly coiled section. In the developments to follow, two sequences, 010 and 0110, are excluded for the reason that only one or two consecutive distorted residues may not produce an intramolecular hydrogen bond.

To be consistent with the α-helical structure mentioned above, it is necessary to consider not only the nearest neighbor interaction but also the interaction among essentially

three (at most four) consecutive residues. Thus our problem is typical of the one-dimensional Ising problems, and may be treated by the matrix method. This method utilizes the transition probability matrix whose $k\ell$-element represents the probability that one (ℓ-th) of all the states possible for the (i - 1)-, i-, and (i + 1)-th residues will follow one (k-th) of all the states possible for the (i - 2)-, (i - 1)-, and i-th residues. Each element is determined from the statistical weights or the Boltzmann factors for seven possible sequences of three consecutive residues defined by

111	u
101	1
011	$\sqrt{\sigma}$
001	1
110	$\sqrt{\sigma}$
100	1
000	1

where

$$\sqrt{\sigma} = \exp[-(F_d - F_c)/RT] \qquad (2\text{-}1)$$

$$\epsilon = \exp(-F_h/RT) \qquad (2\text{-}2)$$

and

$$u = \sqrt{\sigma}\,\epsilon \qquad (2\text{-}3)$$

Here R is the gas constant, T is the absolute temperature, and F_c, F_d, and F_h are free energies per mole of "undistorted"

residues, "distorted" residues, and of hydrogen bonds, respectively. It is implicitly assumed that these quantities contain the contributions from interactions of solvent molecules with polypeptide residues. Hence, they are regarded as potentials of mean force. The statistical weight of unity was assigned for the sequences 101, 001, 100, and 000, because the free energy of a random coil residue was chosen as the standard, regardless of the states of the nearest-neighbor residues.

In terms of the statistical weights given above, the transition probability matrix $\underset{\sim}{P}$ for Nagai's model is written

$$\underset{\sim}{P} = \begin{bmatrix} u & 0 & 0 & 0 & \sqrt{\sigma} & 0 & 0 \\ 0 & 0 & \sqrt{\sigma} & 0 & 0 & 0 & 0 \\ u & 0 & 0 & 0 & 0 & 0 & 0 \\ 0 & 0 & \sqrt{\sigma} & 0 & 0 & 0 & 0 \\ 0 & 1 & 0 & 0 & 0 & 1 & 0 \\ 0 & 0 & 0 & 1 & 0 & 0 & 1 \\ 0 & 0 & 0 & 1 & 0 & 0 & 1 \end{bmatrix} \qquad (2\text{-}4)$$

Since the first and the N-th residues cannot be involved in a helical section, the matrices associated with the first and the N-th residues are given by

$\underset{\sim}{P}_c$ = the matrix whose (7,4) and (7,7) elements are equal to unity and all others equal to zero

(2-5)

and

$\underset{\sim}{P}_a$ = the matrix whose (5,6), (6,7), and (7,7) elements are equal to unity and all others equal to zero, (2-6)

respectivily.

The partition function Z_N of the polypeptide chain is then given by

$$Z_N = \text{SAE}\,[\underset{\sim}{P}_c \underset{\sim}{P}^{N-2} \underset{\sim}{P}_a] \tag{2-7}$$

where the symbol "SAE" indicates the sum of all elements of the matrix in the succeeding brackets. We define the right-hand and left-hand eigenvectors, $\underset{\sim}{v}(\lambda_i)$ and $\underset{\sim}{w}(\lambda_i)$, as

$$\begin{aligned} \underset{\sim}{P}\underset{\sim}{v}(\lambda_i) &= \lambda_i \underset{\sim}{v}(\lambda_i) \\ \underset{\sim}{w}(\lambda_i)\underset{\sim}{P} &= \lambda_i \underset{\sim}{w}(\lambda_i) \\ \underset{\sim}{w}(\lambda_i)\underset{\sim}{v}(\lambda_j) &= \delta_{ij} \end{aligned} \tag{2-8}$$

where δ_{ij} is Kronecker's delta, and λ_i is one of the four roots of the characteristic equation

$$\lambda_i^{\,2}(\lambda_i - u)(\lambda_i - 1) = \sigma u \tag{2-9}$$

$$(\lambda_1 > \lambda_2 > \lambda_3 > \lambda_4)$$

Solution of equation (2-8) gives

$$\underset{\sim}{v}(\lambda_i) = \left(1 \;\; \frac{\sqrt{\sigma}\,u}{\lambda_i^{\,2}} \;\; \frac{u}{\lambda_i} \;\; \frac{\sqrt{\sigma}\,u}{\lambda_i^{\,2}} \;\; \frac{\lambda_i - u}{\sqrt{\sigma}} \;\; \frac{\lambda_i - u}{\sqrt{\sigma}} \;\; \frac{\lambda_i - u}{\sqrt{\sigma}}\right)^{tr} \tag{2-10}$$

$$\underset{\sim}{w}(\lambda_i) = C(\lambda_i)\left(1 \; \frac{\sqrt{\sigma}}{\lambda_i^2} \; \frac{\lambda_i - u}{u} \; \frac{\lambda_i - u}{\sqrt{\sigma}\, u} \; \frac{\sqrt{\sigma}}{\lambda_i} \; \frac{\sqrt{\sigma}}{\lambda_i^2} \; \frac{\lambda_i - u}{\sqrt{\sigma}\, u}\right) \tag{2-11}$$

and

$$C(\lambda_i) = \lambda_i(\lambda_i - 1)[4\lambda_i^2 - 3(1 + u)\lambda_i + 2u]^{-1} \tag{2-12}$$

where the symbol tr indicates the transposed or column vector. Since the matrices $\underset{\sim}{P}$ and $\underset{\sim}{P}^{N-2}$ may be expanded as

$$\underset{\sim}{P} = \sum_i \lambda_i \underset{\sim}{v}(\lambda_i)\underset{\sim}{w}(\lambda_i) \tag{2-13}$$

$$\underset{\sim}{P}^{N-2} = \sum_i \lambda_i^{N-2} \underset{\sim}{v}(\lambda_i)\underset{\sim}{w}(\lambda_i) \tag{2-14}$$

by using the relation

$$\mathrm{SAE}\,[\underset{\sim}{P}_c \underset{\sim}{v}(\lambda_i)\underset{\sim}{w}(\lambda_i)\underset{\sim}{P}_a] = (u\sigma)^{-1} C(\lambda_i)\lambda_i^3(\lambda_i - u)^2 \tag{2-15}$$

we obtain

$$Z_N = \sum_i \lambda_i^N(\lambda_i - u)[4\lambda_i^2 - 3(1 + u)\lambda_i + 2u]^{-1} \tag{2-16}$$

According to Nagai, the helical content f_N of a polypeptide chain having N degrees of polymerization is expressed by

$$f_N = N^{-1} \sum_i \langle \mu_i \rangle = N^{-1} \partial(\ln Z_N)/\partial \ln\sqrt{\sigma} \tag{2-17}$$

where $\langle \mu_i \rangle$, the average probability that the i-th residue is "distorted" or involved in a helical section, is given by

$$\langle \mu_i \rangle = Z_N^{-1} \, \mathrm{SAE}[\underset{\sim}{P}_c \underset{\sim}{P}^{i-2} \sqrt{\sigma} (\partial \underset{\sim}{P} / \partial \sqrt{\sigma})^{N-i-1} \underset{\sim}{P}_a] \qquad (2\text{-}18)$$

It may be noted that $\langle \mu_i \rangle$ is not the fraction of intact hydrogen-bonded residues but the fraction of residues in the helical state. Use of the relations

$$\mathrm{SAE}[\underset{\sim}{P}_c \underset{\sim}{v}(\lambda_m) \underset{\sim}{w}(\lambda_n) \underset{\sim}{P}_a] = (u\sigma)^{-1} \lambda_m (\lambda_m - u) \lambda_n^{\,2} (\lambda_n - u) C(\lambda_n) \qquad (2\text{-}19)$$

and

$$\underset{\sim}{w}(\lambda_m) \sqrt{\sigma} (\partial \underset{\sim}{P} / \partial \sqrt{\sigma}) \underset{\sim}{v}(\lambda_n) = \lambda_n^{-1} C(\lambda_m) [\lambda_m \lambda_n + \lambda_m (\lambda_m - u) + \lambda_n (\lambda_n - u)] \qquad (2\text{-}20)$$

allows equation (2-18) to be written

$$\langle \mu_i \rangle = Z_N^{-1} (\sigma u)^{-1} \sum_{m,n} C(\lambda_m) C(\lambda_n) (\lambda_m - u)(\lambda_n - u) \lambda_m^{\,i-1} \lambda_n^{\,N-i}$$

$$\times [\lambda_m \lambda_n + \lambda_m (\lambda_m - u) + \lambda_n (\lambda_n - u)] \qquad (2\text{-}21)$$

Here the summation must be taken over both m and n (=1, 2, 3, and 4).

Now we define f by the term associated with the largest eigenvalue λ_1 in equation (2-21). It follows that

$$f = (\lambda_1 - 1)(3\lambda_1 - 2u)[4\lambda_1^{\,2} - 3(1+u)\lambda_1 + 2u]^{-1} \qquad (2\text{-}22)$$

This quantity denotes the probability that a particular residue in the chain having infinitely large N is "distorted," and hence it is the helical content for an infinitely long chain.

2-2-2. Approximate Expressions

By substitution of equation (2-21) into (2-17), Nagai[27] obtained a rigorous expression of f_N for finite N. Recently, Okita, et al.,[46] have derived a simple approximate expression for f_N from Nagai's exact one and have offered a procedure for evaluating σ and u from experimental data for f_N. In what follows, we derive simple expressions for Z_N, f_N, and related quantities, using the approximations introduced by Okita, et al., who utilized the fact that the σ value is of the order of 10^{-4} for most polypeptide-solvent systems.

If $\sqrt{\sigma}$ is assumed to be much smaller than unity, the four eigenvalues of equation (2-9) may be expanded in powers of $\sqrt{\sigma}$ to give[46]

$$\lambda_1 = 1 + \sqrt{\sigma}\,(z + \sqrt{1 + z^2}) + O(\sigma) \tag{2-23}$$

$$\lambda_2 = 1 - \sqrt{\sigma}\,(z - \sqrt{1 + z^2}) + O(\sigma) \tag{2-24}$$

$$\lambda_3 = \sqrt{\sigma} + O(\sigma) \tag{2-25}$$

$$\lambda_4 = -\sqrt{\sigma} + O(\sigma) \tag{2-26}$$

where z is defined by

$$z = (\ln u)/2\sqrt{\sigma} \tag{2-27}$$

It follows from equation (2-27) that

$$u = 1 + 2\sqrt{\sigma}\,z + O(\sigma) \tag{2-28}$$

Substituting equations (2-23) and (2-28) into (2-22), we obtain

$$f = (1/2)(1 + z/\sqrt{1 + z^2}) + O(\sqrt{\sigma}) \qquad (2\text{-}29)$$

Solution of equation (2-29) for z gives

$$z = (2f - 1)/2[f(1 - f)]^{1/2} \qquad (2\text{-}30)$$

Inserting this equation into equations (2-23) and (2-24), we obtain

$$\lambda_1 = 1 + \sqrt{\sigma}\sqrt{f/(1-f)} + O(\sigma) \qquad (2\text{-}31)$$

$$\lambda_2 = 1 - \sqrt{\sigma}\sqrt{(1-f)/f} + O(\sigma) \qquad (2\text{-}32)$$

Thus the four eigenvalues can be expressed in terms of σ and f, instead of σ and u.

The partition function, Z_N, consists of the four terms associated with the four eigenvalues. The relative magnitudes of these terms may be determined by $(\lambda_2/\lambda_1)^N$, $(\lambda_3/\lambda_1)^N$, and $(\lambda_4/\lambda_1)^N$ in comparison with unity. From equations (2-31) and (2-32), the factor $(\lambda_2/\lambda_1)^N$ may be written

$$(\lambda_2/\lambda_1)^N = \exp\,[-N\sqrt{\sigma}/\sqrt{f(1-f)}] \qquad (2\text{-}33)$$

Since the right-hand side of this equation attains a maximum at f = 1/2, we obtain

$$(\lambda_2/\lambda_1)^N \leq \exp\,(-2N\sqrt{\sigma}) \qquad (2\text{-}34)$$

This equation was first derived by Lifson and Roig[28] from their theory, and it was shown that $(\lambda_2/\lambda_1)^N$ is negligible in comparison with unity within 1 % if $N\sqrt{\sigma} > 2.3$. A similar conclusion has been derived by Okita, et al.,[46] and by Poland and Scheraga.[75]

It is seen from equations (2-25), (2-26), and (2-31) that $(\lambda_3/\lambda_1)^N$ and $(\lambda_4/\lambda_1)^N$ are of the order of $(\sigma)^{N/2}$, and hence the terms in Z_N involving λ_3 and λ_4 are negligibly small even if N is quite small.

Therefore, combining equations (2-22) and (2-23) with (2-16), subject to $\sqrt{\sigma} \ll 1$, we find that

$$Z_N = (1 - f)\lambda_1^N + f\lambda_2^N \qquad (2\text{-}35)$$

When $N\sqrt{\sigma} > 2$, this equation reduces to

$$Z_N = (1 - f)\lambda_1^N \qquad (2\text{-}36)$$

Since the cyclic condition[76,77] leads Z_N to λ_1^N, the factor (1 - f) is considered to represent the end effect. Equation (2-35) or (2-36) can be derived also from the expression of Zimm and Bragg[22] for Z_N.

With $\langle\mu_i\rangle$ calculated by equations (2-12) - (2-35) we obtain

$$f_N = (f/N) \sum_i [1 - (\lambda_2/\lambda_1)^i - (\lambda_2/\lambda_1)^{N-i} + (\lambda_2/\lambda_1)^N] \times \{1 + [f/(1-f)](\lambda_2/\lambda_1)^N\}^{-1} \qquad (2\text{-}37)$$

Substitution of equation (2-33) into (2-37), followed by replacement of the summation over i by an integral from zero to N, gives the eqation of Okita, et al:

$$f_N = f\left\{1 - 2\sqrt{f(1-f)}/N\sqrt{\sigma} + [1 + 2\sqrt{f(1-f)}]\exp[-N\sqrt{\sigma}/\sqrt{f(1-f)}]\right\}$$
$$x\left\{1 + [f/(1-f)]\exp[-N\sqrt{\sigma}/\sqrt{f(1-f)}]\right\}^{-1} \qquad (2\text{-}38)$$

Alternatively, this equation can be derived by substituting equation (2-35) into (2-17).

If the product $N\sqrt{\sigma}$ is larger than 2, the terms associated with $\exp[-N\sqrt{\sigma}/\sqrt{f(1-f)}]$ may be dropped. This simplification corresponds to the neglect of the second term on the right-hand side of equation (2-35). Thus it follows that

$$f_N = f - 2f^{3/2}(1-f)^{1/2}/N\sqrt{\sigma} \qquad (2\text{-}39)$$

provided that $N \gg 1$, $\sqrt{\sigma} \ll 1$, and $N\sqrt{\sigma} > 2$. A similar dependence of f_N on N has already been derived by Lifson and Roig[28] from their theory, although the coefficient of N^{-1} was expressed in terms of the larger two eigenvalues.

Table 2.1 compares the approximate values of f_N computed by equation (2-39) with the exact ones[27] for $N = \infty$, 1200, and 600, and $\sigma = 2 \times 10^{-4}$. It is seen that equation (2-39) is a good approximation to the exact equation over essentially the entire range of helix-coil transition.

The method of Okita, et al., for evaluating u and σ makes use of equation (2-39). It predicts that a plot of

Table 2.1. Comparison of the exact and approximate expressions for the helical content f_N; σ is taken to be 2.0×10^{-4}

z	N = ∞		N = 1200		N = 600	
	exact	approx.	exact	approx.	exact	approx.
-2.163	0.051	0.046	0.050	0.045	0.049	0.044
-1.570	0.085	0.078	0.082	0.076	0.079	0.073
-0.736	0.211	0.204	0.201	0.194	0.191	0.184
-0.447	0.303	0.296	0.287	0.280	0.271	0.264
-0.069	0.472	0.465	0.444	0.438	0.416	0.411
0.000	0.507	0.500	0.477	0.471	0.448	0.441
0.196	0.603	0.596	0.569	0.562	0.534	0.527
0.362	0.677	0.670	0.640	0.633	0.603	0.596
0.823	0.825	0.818	0.788	0.781	0.751	0.744
1.224	0.894	0.887	0.861	0.854	0.828	0.821
1.955	0.951	0.945	0.926	0.920	0.901	0.894
2.645	0.972	0.968	0.953	0.947	0.933	0.927
3.311	0.982	0.979	0.966	0.962	0.950	0.945

f_N vs. N^{-1} at fixed solvent conditions gives a straight line, whose ordinate intercept I (= f) and slope S are related to $\sqrt{\sigma}$ by

$$\sqrt{\sigma} = -2(I/S)[I(1 - I)]^{1/2} \qquad (2\text{-}40)$$

Combination of this equation with equations (2-27) and (2-30) gives

$$\ln u = -2I(2I - 1)/S \qquad (2\text{-}41)$$

Thus experimental determinations of I and S lead to the evaluation of σ and u. If the values of u are obtained as a function of temperature, the enthalpy change ΔH for the helix-coil transition may be evaluated by the thermodynamic relation:

$$\Delta H = -R\partial(\ln u)/\partial(1/T) \qquad (2\text{-}42)$$

In this way, the basic parameters σ and u together with the transition enthalpy ΔH can be determined from measurements of f_N as a function of N at fixed solvent conditions. Since this method involves no restriction other than $N \gg 1$, $\sqrt{\sigma} \ll 1$, and $N\sqrt{\sigma} > 2$, the values of σ, u, and ΔH so obtained correspond to the specific temperature and solvent chosen for the measurements of f_N. This allows the experimental investigation of σ and ΔH as functions of temperature, solvent species, and solvent composition.

The fraction of hydrogen bonded residues, θ_N, has received more attention than f_N by many workers.[22-24,28] An approximate expression for θ_N was derived by a process similar to that leading to equation (2-38). The result

showed that $f_N = \theta_N$ under the condition that $N \gg 1$ and $\sqrt{\sigma} \ll 1$.

In calculating average conformations, we have exclusively used Nagai's theory, though this theory is essentially the same as that of Zimm and Bragg.[22] In both theories, two sequences, 010 and 0110, are excluded for the reason mentioned before. On the other hand, in the model of Lifson and Roig,[28] these two sequences are included and given statistical weights of $\sqrt{\sigma}$ and σ, respectively. In this connection, Poland and Scheraga[75] remarked that the conformation of the entire chain might be influenced by excluding conformations in which either 010 or 0110 exists. However, the results thus far presented may be little affected by inclusion of the 010 and 0110 states provided $\sqrt{\sigma} \ll 1$. In fact, it can be shown that if $\sqrt{\sigma} \ll 1$ both Nagai's theory and Lifson-Roig's give the same expression for f_N.

2-3. Experimental

2-3-1. Polypeptide Samples

γ-Benzyl L-glutamate (BLG) purchased from the Peptide Center of Osaka University was converted to γ-bynzyl L-glutamate-N-carboxy-anhydride (NCA) by the method of Blout and Karlson.[3] BLG crushed to powder and dried in vacuum was suspended in tetrahydrofuran, which amounted to about five times of BLG in weight, and then phosgen was bubbled through at 50°C. After 1.5 hours, a clear solution was obtained.

This solution was concentrated under reduced nitrogen atmosphere, and then n-hexane was added until crystallization of NCA began. The NCA was purified by repeated crystallization under nitrogen atmosphere first from a chloroform solution and then from an ethyl acetate solution with n-hexane as a precipitant.

Polymerization of NCA was carried out at room temperature with dioxane as a solvent and triethylamine as an initiator. The concentration of NCA was adjusted to about 5 % (wt/vol) and the mole ratio of NCA to initiator to 70. The resulting viscous solution was poured with vigorous stirring into a large volume of ethanol to isolate the polypeptide formed. The polymer obtained was divided into two parts by fractional precipitation from an 0.2 % (wt/vol) methylene chloride solution with methanol as a precipitant. The volume ratio of methanol to methylene chloride was estimated from the data of Cosani, et al.[78] The higher-molecular-weight portion, which amounted to 90 % of the whole material, was chosen for the present study. This fraction is designated sample E-1 in the subsequent presentation. In addition to this sample, the following four samples was also used.

Samples E-3, E-4, and A-IV were appropriate middle fractions obtained by similar fractional precipitation of two original samples. One for samples E-3 and E-4 had been obtained by polymerization with triethylamine as an initiator, and one for A-IV with sodium methoxide as an initiator.

Sample A-6 was an unfractionated polymer which had been prepared by Nakagawa, et al.,[79] by polymerization in dimethylformamide (DMF) with n-butylamine as an initiator. Kinetic evidence[79,80] had suggested that this last sample would be nearly monodisperse in molecular weight. So no further fractionation was effected on it. Each of these samples was precipitated from a methylene chloride solution into methanol, freeze-dried from a dioxane solution, and dried overnight in a vacuum oven at 40°C.

2-3-2. Preparations of Polypeptide solutions

Polypeptide solutions were made up gravimetrically by mixing weighed amounts of polypeptide sample and solvent under nitrogen atmosphere. The solutions thus obtained with DCA-EDC mixtures as solvent were sufficiently stable over 20 hours when kept below 40°C. On the other hand, mixtures of DCA-CHL were quite unstable at temperatures above 30°C. It was perhaps so because oxidation of CHL or ester formation between the solvent species occurred. Therefore, polypeptide samples were dissolved first in DCA and then a proper amount of CHL was added, and measurements, particularly at higher temperatures, were made as quickly as possible. The reason why we dared to select this solvent mixture for the present work was its appropriateness for light-scattering measurements (see Chapter 5).

2-3-3. Solvents

Fractionally distilled triethylamine (bp 89.4°C), tetrahydrofuran (bp 67.3°C), dioxane (bp 102.2°C), chloroform (bp 61.4°C), ethyl acetate (bp 77.3°C), EDC (84.5°C), DMF (bp 41.0 - 42.0°C/ 11 mm Hg), and CHL (bp 67.5 - 68.0°C/ 16 mm Hg) were used. DCA was distilled twice with concentrated sulfuric acid under reduced nitrogen atmosphere, and the fraction bioling at 61 - 64°C at 3 mm Hg was collected and immediately used.

With the aid of a Bauch-Lomb precision Sugger Refractometer the refractive indices of various DCA-EDC mixtures and DCA-CHL mixtures at 20, 25, and 30°C and of DMF at 25°C were measured for light of wavelengths 436, 546, and 589 nm. Densities of these liquids were determined pycnometrically at various temperatures. Necessary values of density and refractive index for other solvent compositions and temperatures were obtained by either interpolation or extrapolation.

2-3-4. Molecular Weight Determination

Number-average molecular weights $\bar{M}_n$ of the chosen samples of PBLG were determined from osmotic pressure measurements made at 25°C with DMF as a solvent. Use was made of a Mechlolab Model 502 high-speed membrane osmometer fitted with gel cellophane membranes for samples E-1 and E-3 and with Sartrious Ultrafine Filters of the type Super Dense

for samples E-4, A-IV, and A-6.

Weight-average molecular weights $\bar{M}_w$ of samples E-1 and E-3 were determined by light scattering and those of samples E-4, A-IV, and A-6 by sedimentation equilibrium, with DMF at 25°C as a solvent. Details of the light-scattering measurements are deferred to Chapter 5. Sedimentation equilibrium data were taken in a Beckman-Spinco Model E ultracentrifuge equipped with the Rayleigh interference optical system and a Kel-F coated 12 mm double-sector cell. The partial specific volume of PBLG in DMF at 25°C was taken to be 0.786 ml/g.[79]

2-3-5. Optical Rotation Measurements

Data for optical rotation as a function of temperature were obtained at the wavelemgth of 436 nm for DCA-EDC systems and at 546 nm for a DCA-CHL system (91.7 wt% DCA) by the use of a JASCO Model DIP-SL automatic polarimeter with a jacketed 10-cm cell. Optical rotatory dispersion (ORD) measurements were performed on a Yanagimoto Model ORD 185 recording spectropolarimeter for DCA-EDC systems and on the JASCO automatic polarimeter for DCA-CHL systems. The resulting curves were analyzed in terms of the Moffitt plot[81] (with λ_o taken to be 212 nm as usual) to determine the Moffitt parameter b_o. Mean residue rotations $[m']_{436}$ at 436 nm calculated from the ORD diagrams for PBLG-DCA-EDC systems were compared with the polarimeter values at the corresponding wavelength and external conditions in order to check the

accuracy of the ORD apparatus used.

For refractive indices needed to convert optical rotation to $[m']_\lambda$ directly measured values or those estimated from them and the literature values by Sellmeier's equation were used.

It was found that $[m']_{436}$ for PBLG in DCA-EDC mixtures scarcely depended on polypeptide concentration up to 1.5 g/dl. Since subsequent data were taken at concentrations below 1 g/dl, $[m']_\lambda$, $[\alpha]_\lambda$, and hence any quantities deduced from them may be taken as referring to infinite dilution.

2-4. Results and Discussion

2-4-1. Molecular Weights

Figure 2.1 shows the results from the osmotic pressure measurements. Values of $(\pi/RTc)^{1/2}$ are plotted against c with the expectation that this type of plot may facilitate more reliable estimate of $\overline{M}_n$ and second virial coefficient A_2.[82]

Table 2.2 summarizes the values obtained for $\overline{M}_n$, $\overline{M}_w$, and A_2. The polypeptide samples chosen are fairly homogeneous with respect to molecular weight when judged from their ratios of $\overline{M}_w$ to $\overline{M}_n$. Although equation (2-39) is concerned with a monodisperse polypeptide sample, it is still valid for polydisperse samples if N in the equation is replaced by its number-average $\overline{N}_n$, as has been pointed

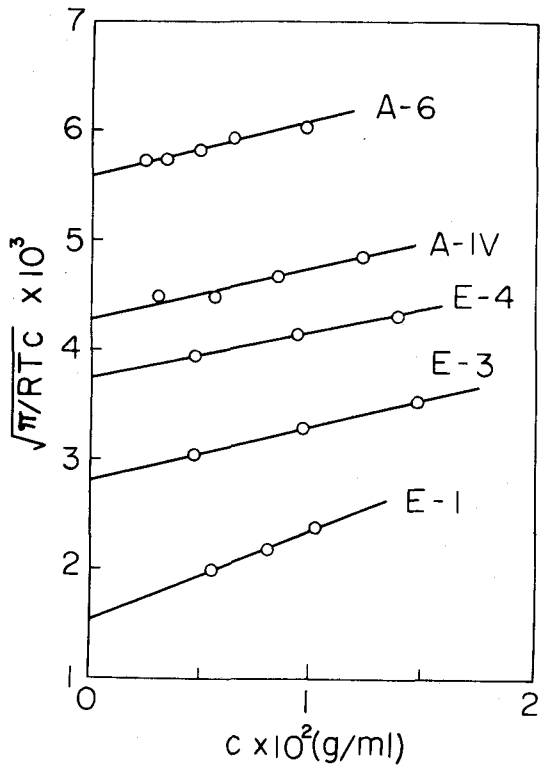

Figure 2.1. Plots of $(\pi/RTc)^{1/2}$ vs. concentration c for the indicated samples in DMF at 25°C.

out by Okita, et al.[46] Therefore, $\bar{M}_n$, rather than the weight-average $\bar{M}_w$, will be used in the subsequent analysis of data for the helix-coil transition.

2-4-2. Estimate of Helical Content from ORD Data

It is generally assumed that the helical content f_N for a polypeptide molecule is related to the Moffitt parameter b_o by

Table 2.2. Numerical data of molecular weight and second virial coefficient for PBLG in DMF at 25°C

Sample code	Osmotic pressure		Light scattering or Sedimentation equilibrium		$\bar{M}_w/\bar{M}_n$
	$\bar{M}_n \times 10^{-4}$	$A_2 \times 10^4$ (ml mol/g^2)	$\bar{M}_w \times 10^{-4}$	$A_2 \times 10^4$ (ml mol/g^2)	
E-1	$42._2$	2.4_4	$56._7$	2.2_4	1.3_4
E-3	$12._8$	2.8_0	$15._8$	2.7_8	1.2_3
E-4	7.1_4	3.2_5	8.0_8	$7._1$	1.1_3
A-IV	5.4_9	4.0	6.3_5	$5._8$	1.1_6
A-6	3.2_0	$5._5$	3.7_0	$8._4$	1.1_6

$$f_N = (b_o - b_o^C)/(b_o^H - b_o^C) \qquad (2\text{-}43)$$

where b_o^C and b_o^H denote the b_o values for random coil and helix, respectively. For this equation to be used in practice the values of b_o^C and b_o^H must be determined from appropriate experiments.

For PBLG-DCA-EDC systems, a value of 45.3 to b_o^C was assigned. This is the b_o value obtained in pure DCA at 25°C with a PBLG sample of relatively low molecular weight ($\bar{M}_v = 2.2 \times 10^4$; $\bar{M}_v$ stands for viscosity-average molecular

weight). On the other hand, a value of - 700 was assigned to b_o^H, which is the b_o value obtained in pure EDC at 25°C with another sample of very high molecular weight ($\overline{M}_v$ = 50 x 10^4). The latter assignment is based on the fact that EDC is one of the strongest helix-supporting solvents for PBLG.

Although equation (2-43) offers one of the most reliable means for the evaluation of helical content of a polypeptide in solution, its practical use suffers inconvenience because the experimental determination of b_o is not simple. This inconvenience can be circumvented, however, if, as has been demonstrated by Teramoto, Nakagawa, and Fujita,[55] there is a unique relation between mean residue rotation $[m']_\lambda$ at some specified wavelength λ and b_o for the system considered. This is because the former can be determined more directly and accurately than the latter. Such a relation for PBLG-DCA-EDC systems is shown in Figure 2.2. Here data for different samples at various solvent conditions are incorporated in order to cover the entire range of b_o. All the plotted points fall on a single curve which may be represented approximately by two straight lines intersecting at $-b_o$ = 630, indicating that in the region of $-b_o$ smaller than 630 there exists a linear relation between $[m']_{436}$ and b_o regardless of solvent composition and temperature. The branch above $-b_o$ = 630 will not be used for the present analysis, because the data in this region are too few to

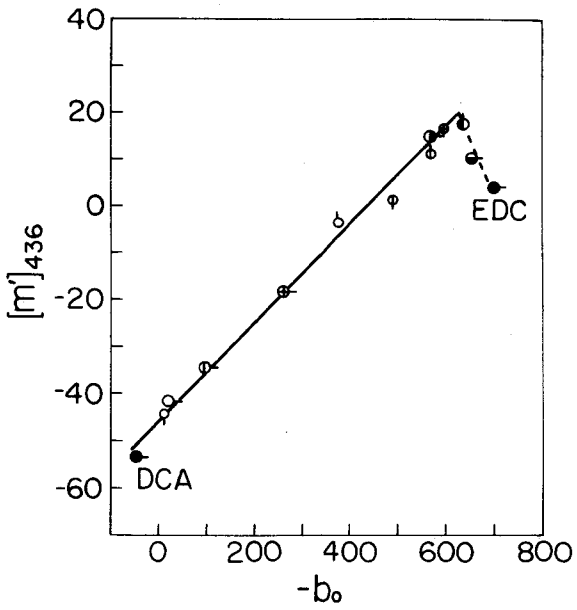

Figure 2.2. Relationship between $[m']_{436}$ and Moffitt parameter b_o for PBLG in DCA-EDC mixtures. (○) $\bar{M}_v$ = 1.4 x 10^4, (◐) $\bar{M}_v$ = 2.2 x 10^4, and (⊕) A-6 in 70 vol% DCA. (◑) A-6 and (◐) E-1 in 50 % DCA, (◒) $\bar{M}_v$ = 50 x 10^4 in 3 % DCA and (●) in pure DCA and EDC (see text). Small circles indicate the data of Teramoto, et al.,[55] in DCA-EDC: (○) 76 %, (◐) 70 %, and (⊕) 64 %. The temperatures at which the data were taken are indicated by pips: (◔) 30°C, (◔) 25°C, and (◔) 20°C.

conclude the existence of a unique relation between $[m']_{436}$ and b_o.

Now we substitute $[m']_{436}$ for b_o in equation (2-43) with the aid of the solid line shown in Figure 2.2. The result is

$$f_N = ([m']_{436} + 50.7)/78.4 \quad \text{for } -b_o < 630 \qquad (2\text{-}44)$$

which allows conversion of the measured values of $[m']_{436}$ for PBLG in DCA-EDC mixtures to helical contents. It should be noted that equation (2-44) differs appreciably from the relation employed by Zimm, Doty, and Iso[29] in an analysis of the experimental data of Doty and Yang[6] for PBLG in DCA-EDC mixtures. When equation (2-44) is used, the specific rotation they assigned to perfect helix gives an f_N as small as 0.9.

ORD data for PBLG in DCA-CHL mixtures were taken at wavelengths 578, 546, 436, and 405 nm by the use of a JASCO automatic polarimeter. Measurements were also made on an EDC solution at 25°C, and a value of -655 ± 15 was obtained for b_o. This b_o value is different from -700 obtained by the use of the ORD spectropolarimeter, but compares favorably with the reported values.[17,83] A b_o value of 105 was obtained with DCA on the JASCO polarimeter. The differences between our two b_o values in EDC as well as those in DCA are not due to experimental errors but chiefly to the difference in the span of wavelength. To be consistent with this finding, we assume that for PBLG in DCA-CHL mixtures $b_o^H = -655$ and $b_o^C = 105$ in the analysis of optical rotation data taken on the JASCO polarimeter.

Figure 2.3 shows the relationship between specific rotation at 546 nm, $[\alpha]_{546}$, and b_o for PBLG in DCA-CHL

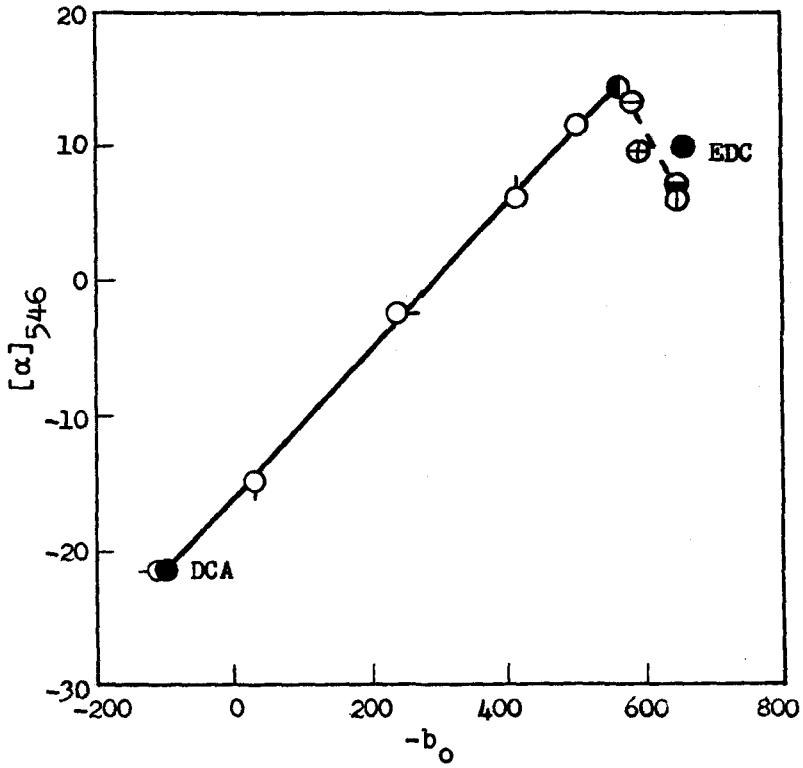

Figure 2.3. Relationship between specific rotation at 546 nm, $[\alpha]_{546}$ and $-b_o$ for PBLG in DCA-CHL mixtures. (◑) $\bar{M}_v$ = 46 x 10^4 in 50 % (wt% of DCA), (◒) E-4 in 50 %, (⊕) A-X (see Chapter 5) in 67 %, (⊖) $\bar{M}_v$ = 46 x 10^4 in 80 %, (◐) $\bar{M}_v$ = 46 x 10^4 in 90 %, and (○) $\bar{M}_v$ = 46 x 10^4 in 91.6 %. The temperatures at which the data were taken are indicated by pips: (◔) 21°C, (○-) 19°C, (◔) 17°C, (-○) 10°C, and no pip 25°C.

mixtures. The plot is represented by two straight lines (solid and broken lines) intersecting at b_o = -560, and the solid line gives the following relation for f_N:

$$f_N = ([\alpha]_{546} + 21.5)/41.2 \quad \text{for } -b_o < 560 \qquad (2\text{-}45)$$

2-4-3. Features of Helix-Coil Transition

Figure 2.4 shows typical results from polarimeter measurements on sample E-3 in DCA-EDC mixtures of different compositions. The composition of each mixture is indicated by vol% of DCA at 25°C. This convention is used in all subsequent presentations, except for data in DCA-CHL mixtures. As shown above, $[m']_{436}$ is linearly related to the helical content, so that Figure 2.4 can be taken to indicate how the helical content of sample E-3 in DCA-EDC mixtures changes

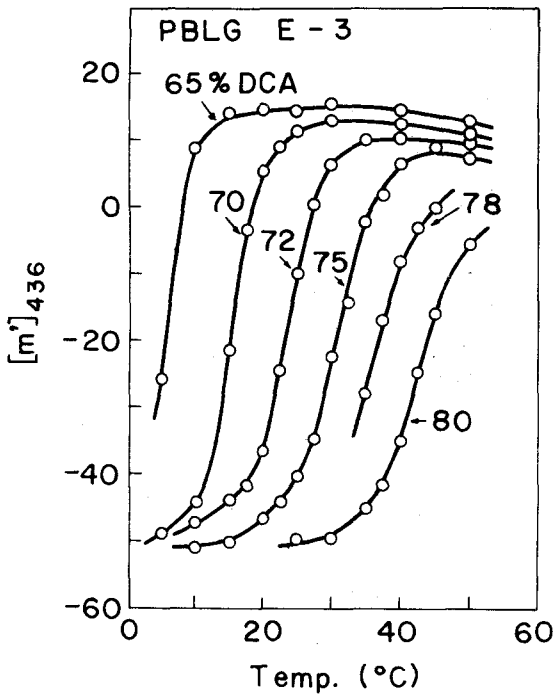

Figure 2.4. Temperature dependence of $[m']_{436}$ for sample E-3 in DCA-EDC mixtures. Composition of each DCA-EDC mixtures is indicated by vol% of DCA at 25°C.

with temperature. It is seen that as the composition of EDC decreases, the transition from coil to helix shifts toward higher temperature and becomes slightly gradual. These features are in accord with the observations of previous investigators.[55,84] Furthermore, each transition curve has a broad maximum and decreases gradually at higher temperatures. Since this region of $[m']_{436}$ lies within the branch of $-b_o$ below 630, the decrease in $[m']_{436}$ implies that in $-b_o$. A similar decreases of $-b_o$ at higher temperatures can be seen in the data of Nakajima and Hayashi[84] for PBLG and poly(γ-methyl L-glutamate) in DCA-EDC mixtures. These findings imply that the helical content decreases on the helix side as the temperature is raised. One can attribute it to the solvent effects upon the helix-coil transition such as discussed theoretically by Peller[48] and by Gibbs and DiMarzio.[24] We shall consider this problem in greater detail in the next chapter.

Figure 2.5 illustrates plots for $[m']_{436}$ vs. temperature in a DCA-EDC mixture (70 vol% DCA) as a function of the molecular weight of PBLG. The decrease in molecular weight broadens and shifts the transition curve toward higher temperature. These results bear close resemblance to those observed for this system by previous workers,[6,29,55,85] and are consistent with the theoretical predictions.[22,24,27,28] Figure 2.6, in which data in a DCA-CHL mixture (91.7 wt% DCA) are plotted, also confirms this conclusion.

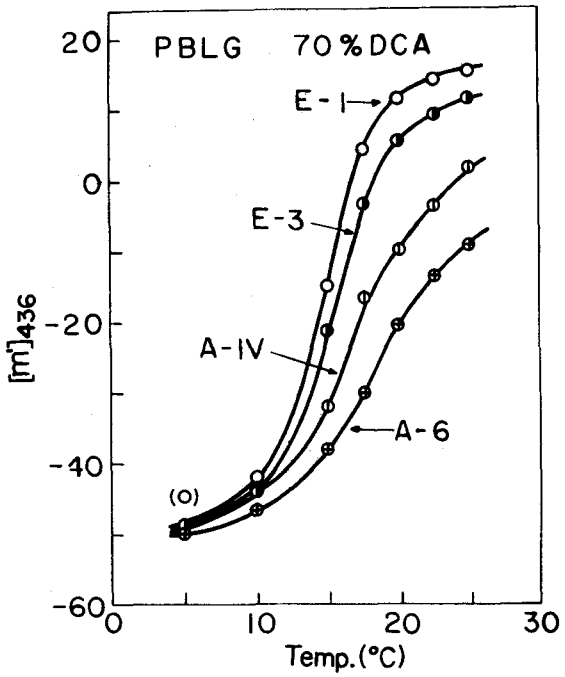

Figure 2.5. Temperature dependence of $[m']_{436}$ for PBLG in a DCA-EDC (70 vol% DCA) mixture as a function of molecular weight.

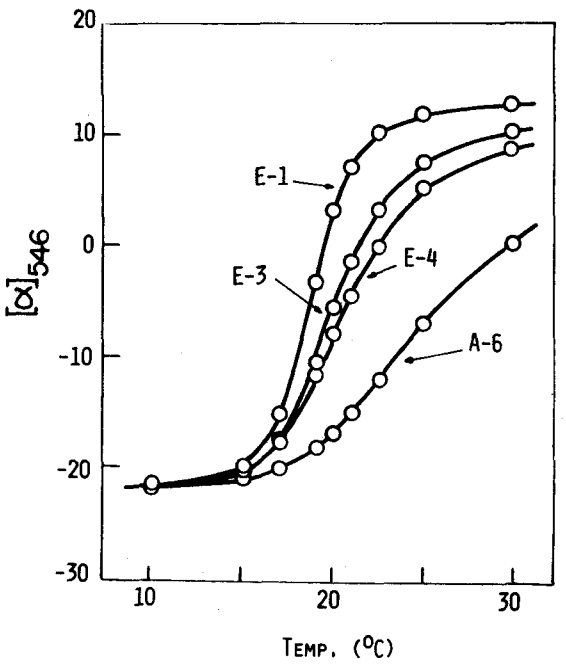

Figure 2.6. Temperature dependence of $[\alpha]_{546}$ for PBLG in a DCA-CHL (91.7 wt% DCA) mixture as a function of molecular weight.

2-4-4. Evaluation of Transition Parameters

We have calculated necessary values of f_N for the application of equation (2-39) from measured values of $[m']_{436}$ and $[\alpha]_{546}$ by making use of equations (2-44) and (2-45), respectively. Figures 2.7 and 2.8 illustrate for DCA-EDC (65 and 70 % DCA) mixtures the resulting plots of f_N vs. $\bar{N}_n^{-1}$ as functions of temperature. As required by theory, the data points at each temperature follow a straight line over the

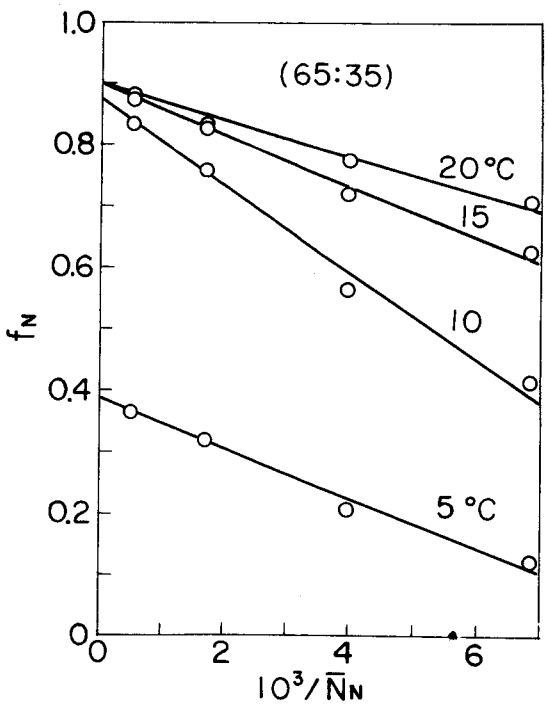

Figure 2.7. Plots of f_N vs. $\bar{N}_n^{-1}$ for PBLG in a DCA-EDC (65:35) mixture.

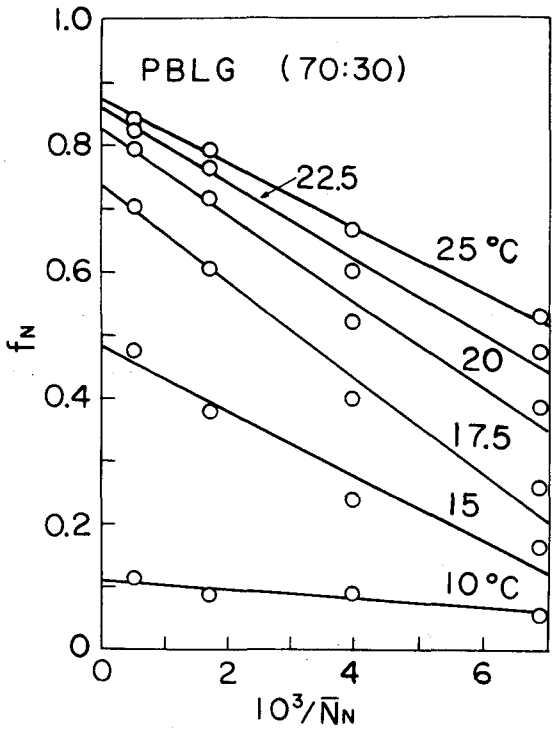

Figure 2.8. Plots of f_N vs. $\bar{N}_n^{-1}$ for PBLG in a DCA-EDC (70:30) mixture.

range of abscissa indicated. Figure 2.9 shows similar results for a DCA-CHL (91.7 wt% DCA) mixture. The plotted points scatter considerably in the vicinity of the mid-point of the transition, so that no accuracy may be claimed of the straight line (hence their intercepts and slopes) drawn through such points. The scatter of the plotted points is attributed to the difficulty of handling this mixed solvent. It was found that a small variation in DCA content affected appreciably the observed values of $[\alpha]_{546}$ and hence the

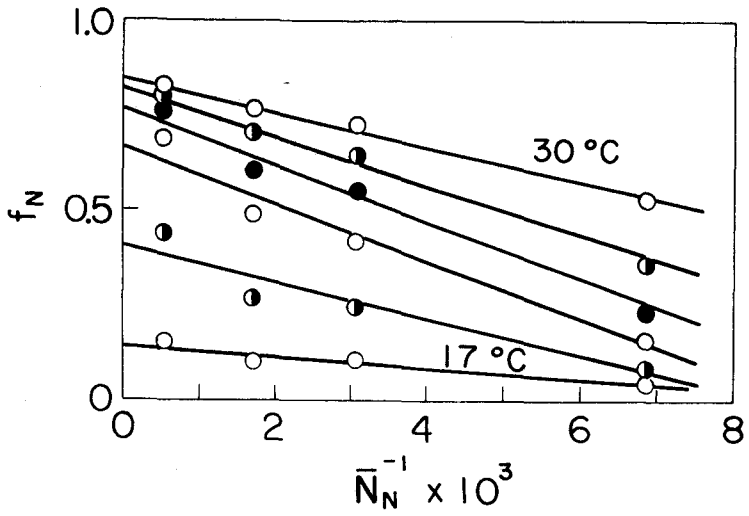

Figure 2.9. Plots of f_N vs. $\bar{N}_n^{-1}$ for PBLG in the DCA-CHL mixture (91.7 wt% DCA) at 30, 25, 22.5, 21, 19, and 17°C from top to bottom.

transition curves.

In all cases treated, the slope S first increased with f, passed through a maximum, and finally decreased as f approached unity. This trend is essentially the same as that observed for poly-N^5-(3-hydroxypropyl)-L-glutamine in mixtures of water and methanol by Okita, et al.[46]

Numerical data for $\sqrt{\sigma}$ and ln u obtained by equations (2-40) and (2-41) are summarized in Tables 2.3 and 2.4. It is seen that the values of $\sqrt{\sigma}$ at fixed solvent compositions stay nearly constant in the temperature region where the substantial portion of the helix-coil transition occurs.

Table 2.3. Numerical values of the transition parameters σ, ln u, and ΔH for PBLG in DCA-EDC mixtures

Solvent composition (vol% of DCA at 25°C)	Temp. (°C)	f	$\sqrt{\sigma} \times 10^2$	$(\ln u) \times 10^2$	ΔH_c (cal/mol)	T_c (°C)
65	5	0.38_7	0.93	-0.43		
	10	0.87_4	0.82	1.84		
	15	0.89_8	1.3_1	3.4_4		
	20	0.89_9	1.8_3	4.8_5		
	25	0.88_0	(2.2)	6.8_9	800 ± 50	5.1
70	5	0.03_0	---	$-5._2$		
	10	0.10_8	1.0_0	-2.5_3		
	15	0.48_2	0.93	-0.07		
	17.5	0.73_6	0.85	0.91		
	20	0.82_6	0.92	1.57		
	22.5	0.86_0	0.99	2.06		
	25	0.87_3	1.1_3	2.54	780 ± 50	15.2
72	17.5	0.16_2	0.8_7	-2.2_8		
	20	0.22_0	0.88	-1.19		
	22.5	0.45_1	0.88	-0.17		
	25	0.67_3	0.86	0.63		
	27.5	0.79_4	0.82	1.20		
	30	0.83_6	0.90	1.64		
	35	0.84_0	1.2_9	2.0_1	720 ± 40	23.5

Table 2.3. (continued)

Solvent composition	Temp. (°C)	f	$\sqrt{\sigma} \times 10^2$	(ln u)$\times 10^2$	ΔH_c (cal/mol)	T_c (°C)
75	22.5	0.10_4	1.1_4	-2.9_6		
	25	0.15_6	0.9_0	-1.7_1		
	27.5	0.26_1	0.9_1	-0.99		
	30	0.48_3	0.87	-0.06		
	32.5	0.60_1	0.97	0.40		
	35	0.75_2	0.86	1.00		
	37.5	0.78_6	1.00	1.39		
	40	0.81_9	1.0_3	1.71	600 ± 50	$30._7$
78	34.9	0.38_2	0.9_0	-0.4_4		
	37.1	0.57_3	0.8_5	0.2_5		
	39.2	0.69_1	0.8_6	0.7_2		
	41.7	0.74_6	0.8_8	1.0_0		
	44.1	0.77_8	0.9_4	1.2_6	580 ± 60	$36._3$
80	35	0.08_5	0.7_2	-2.1_3		
	37.5	0.14_7	0.7_6	-1.5_2		
	40	0.26_7	0.81	-0.85		
	42.5	0.44_3	0.81	-0.19		
	45	0.58_0	0.81	0.26		
	50	0.65_7	0.9_2	0.64	500 ± 50	$43._3$

Thus, in the range of solvent composition studied, we have an average $\sqrt{\sigma}$ of 0.95×10^2 for PBLG in DCA-EDC mixtures and of 0.92×10^{-2} in the DCA-CHL mixture. At high temperatures where the helical content approaches a limiting value on the helix side, $\sqrt{\sigma}$ appears to increase markedly with temperature.

Table 2.4. Numerical values of the transition parameters $\sqrt{\sigma}$, ln u, and ΔH for PBLG in a mixture of DCA and CHL (91.7 wt% DCA)

Temp. (°C)	f	$\sqrt{\sigma} \times 10^2$	(ln u)$\times 10^2$	ΔH_c (cal/mol)	T_c (°C)
10	0				
15	0.04_5	0.8_3	-3.6_4		
17	0.14_0	0.7_3	-1.7_3		
19	0.4_1	0.8_5	-0.3_2		
20	0.5_5	0.8_8	0.1_8		
21	0.6_6	0.8_7	0.5_7		
22.5	0.76_1	0.8_7	1.0_6		
25	0.82_2	0.9_8	1.6_5		
30	0.845	1.4_0	2.6_7	860 ± 80	$19._5$

Although we are not confident of whether this phenomenon is real or not because of experimental uncertainty, it is possible to give an explanation for it in terms of a specific interaction between a pair of DCA molecules and a randomly coiled residue. This point will be discussed in the next chapter.

Figure 2.10 shows plots of ln u vs. 1/T for the six DCA-EDC mixtures studied. The data points for each solvent composition follow a curve having downward curvature. This result implies that the enthalpy changes ΔH for the helix-coil

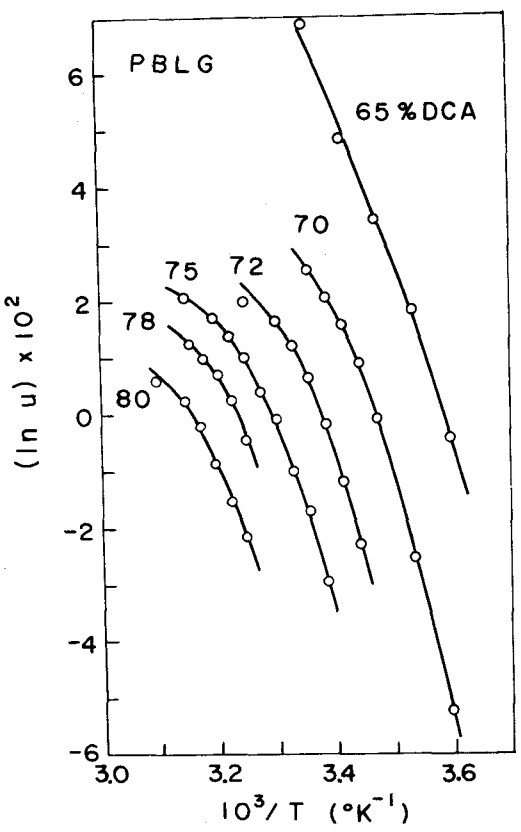

Figure 2.10. Plots of ln u vs. 1/T for PBLG in DCA-EDC mixtures of the indicated DCA contents.

transition of PBLG in the solvent considered decrease with increasing temperature and that the degree is more conspicuous for higher DCA content. Figure 2.11 illustrates the temperature dependence of ΔH for DCA-EDC mixtures. The uncertainty in the graphical determination of ΔH is represented by the vertical segments attached to the plotted points. In Figure 2.12, a plot similar to Figure 2.10 is shown for the DCA-CHL mixture. It can be seen that ΔH for this system also depends

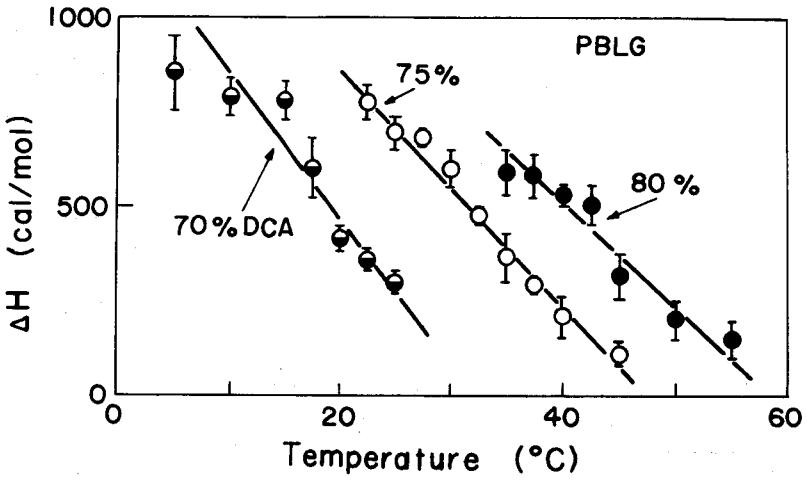

Figure 2.11. Temperature dependence of the transition enthalpy ΔH for PBLG in DCA-EDC mixtures.

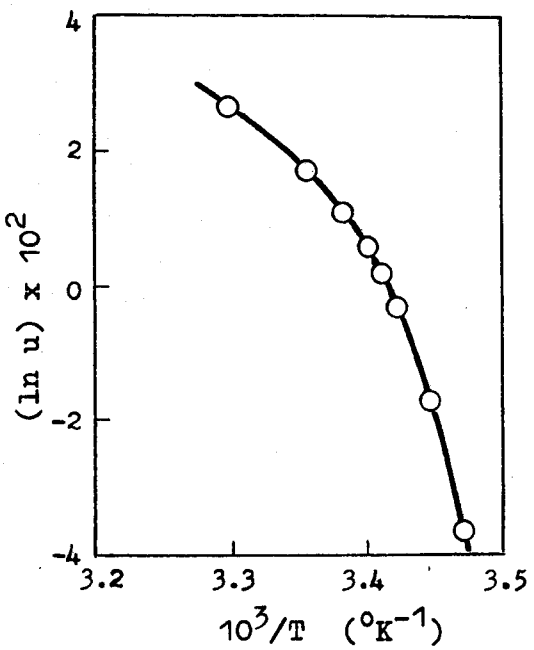

Figure 2.12. Plots of ln u vs. 1/T for PBLG in the DCA-CHL mixture.

considerably upon temperature. In Tables 2.3 and 2.4, therefore, we present only the values of ΔH_c, i.e., the value of ΔH at $T = T_c$.

Essentially, the method used in this work to evaluate σ and ΔH is a kind of curve-fitting method, but it seems superior to the method of Zimm, et al.,[29] since it involves no trial-and-error process and can be applied to the case where these parameters vary with temperature. For a system with temperature-dependent σ and ΔH, the values of these parameters will depend on what portion of an experimentally given curve of f_N vs. temperature is considered important in fitting a theory to experiment. The difference between our values and those of Zimm, et al., ($\sqrt{\sigma} = 1.4 \times 10^{-2}$ and $\Delta H =$ 890 cal/mol) may be accounted for by this idea; we emphasized the portion of transition curve where f_N changed from about 0.1 to 0.9, whereas Zimm, et al., had attempted curve-fitting over a nearly complete range of transition with a single set of temperature-independent σ and ΔH.

2-4-5. Comparison with Calorimetric Data

Three types of calorimetric measurements have been made for PBLG in DCA-EDC mixtures by several groups of authors; heat capacity,[32,33,35] heat-of-dilution,[38] and heat-of-solution[40] measurements. The transition enthalpy ΔH is defined as the change in enthalpy accompanying the conversion of one mole of peptide residues from randomly coiled state to helical state at a given temperature T and a fixed

solvent composition x. Since the calorimetric measurements are associated with processes in which the temperature or the solvent composition is changed, they provide certain averages of ΔH: temperature average (in the case of heat capacity) and solvent-composition average (in the case of either heat-of-dilution or heat-of-solution).[86] Therefore, data from calorimetric measurements may not be amenable to direct comparison with ΔH unless ΔH is independent of T and x. Moreover, comparison among calorimetric data themselves may not be adequate if they are associated with different averaging processes.

Let us consider the enthalpy change derived from heat-capacity measurements. Here we confine ourselves to a high-molecular-weight polypeptide dissolved in solvent mixtures consisting of a helix-breaking solvent and a helix-forming solvent, such as DCA-EDC mixtures. The additional heat per mole of peptide residues absorbed upon a small change in temperature dT equals the enthalpy change ΔH at T multiplied by the accompanying change in helical content $(df)_x$ at a fixed x. Mathematically,[31]

$$\Delta C_P \, dT = \Delta H(df)_x \quad \text{or} \quad \Delta H(\partial f/\partial T)_x \, dT \qquad (2\text{-}46)$$

where ΔC_P denotes the excess heat capacity per mole of peptide residues. Integration of both sides of this equation leads to

$$\langle \Delta H \rangle_x = \int_{T_o}^{T_m} \Delta C_P \, dT = \int_0^{f_m} \Delta H(df)_x \qquad (2\text{-}47)$$

Here T_o is a temperature arbitrarily chosen in the region where the polypeptide molecule is in randomly coiled state, and f_m indicates the value of f for the temperature T_m, above which no more conversion to helical conformation appears to take place. Experimentally, T_m and T_o are defined as the temperatures at which a C_p vs. T curve touches the base line corresponding to the helix and coil sides, respectively. The quantity on the right-hand side of equation (2-47) can be evaluated if ΔH and f are obtained as functions of temperature.

Figure 2.13 illustrates plots of ΔH vs. f constructed

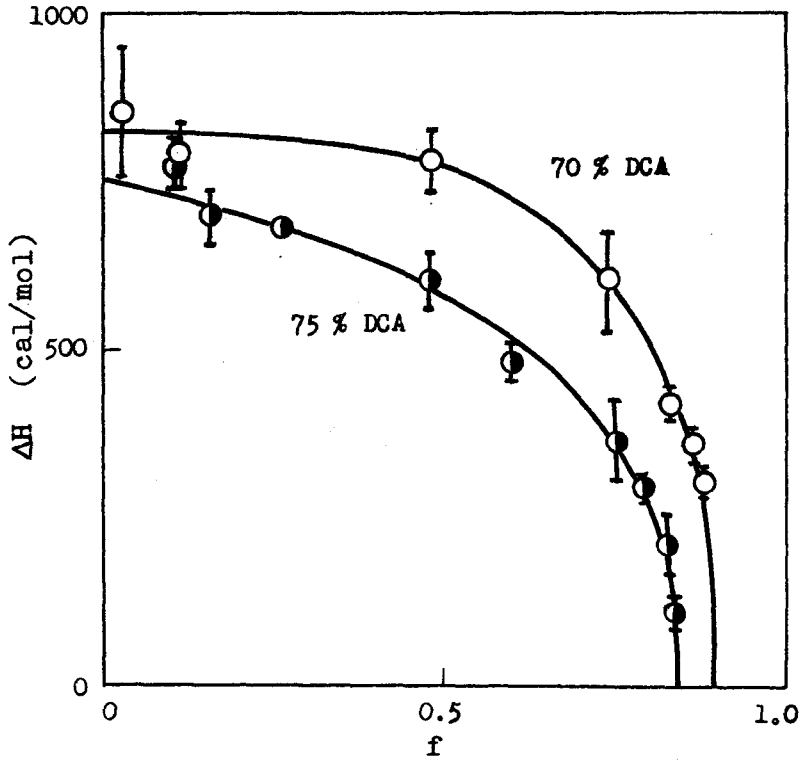

Figure 2.13. Dependence of ΔH on helical content f for PBLG in DCA-EDC mixtures (70 and 75 vol% DCA).

from the author's data for PBLG in DCA-EDC mixtures (70 and 75 % DCA). It is seen that ΔH falls to zero at an f value appreciably smaller than unity. This implies that even if the polypeptide chain is so long that its end effect may be ignored, it cannot be thermally converted to a perfect helix in the solvent mixture considered. The value of f corresponding to $\Delta H = 0$ may be taken to be f_m. Thus, $\langle \Delta H \rangle_x$ for PBLG in these DCA-EDC mixtures are obtained as the area of the domain under each solid curve in Figure 2.13. The values of $\langle \Delta H \rangle_x$ obtained in this way for PBLG in DCA-EDC mixtures are summarized in Table 2.5, together with ΔH_c (given in Table 2.3) and the reported values from direct calorimetric measurements.[32,33,35,38,40]

Our values for $\langle \Delta H \rangle_x$, plotted against T_c in Figure 2.14, in which the heat capacity data of Karasz, O'Reilly, and Bair[33,35] are included, are in excellent agreement with those of Karasz, et al. This agreement may be taken as support, though indirect, to the reliability of our determination of ΔH and f.

From heat-capacity measurements, Ackermann and Neumann[32] found that the values of $\langle \Delta H \rangle_x$ for PBLG in DCA-EDC mixtures decreased linearly with polypeptide concentration and that, at any fixed solute concentration, they increased systematically with decreasing DCA content. However, when the data were extrapolated to zero concentration, the effect of solvent composition virtually disappeared. The infinite-dilution

Table 2.5. Comparison with calorimetric data for the enthalpy change accompanying the helix-coil transition of PBLG in DCA-EDC mixtures

Solvent composition (vol% of DCA)	ΔH_c or $\langle \Delta H \rangle_T$ (cal/mol)	$\langle \Delta H \rangle_x$ (cal/mol)	f_m	T_c (°C)	Reference
65	800 ± 50	730 ± 100	0.90	5.1	This work
70	780 ± 50	630 ± 50	0.87	15.2	
72	720 ± 40	560 ± 50	0.84	23.5	
75	600 ± 50	490 ± 50	0.83	30.7	
78	580 ± 60	440 ± 60	0.81	36.3	
80	500 ± 50	360 ± 50	0.80	43.3	
75		525 ± 80		26.0	33
66[a]		670 ± 50		8.5	35
82[a]		380 ± 50		40.0	35
		950 ± 20			32
	750 ± 100			25[b]	38
	650 ± 30			30[b]	40

a) Data for deuterated PBLG in deuterated DCA-EDC mixtures.
b) Temperature at which the measurements were made.

value of $\langle \Delta H \rangle_x$ so obtained is significantly larger than all the data listed in Table 2.5. From the marked concentration dependence displayed in the data of Ackermann and Neumann,[32]

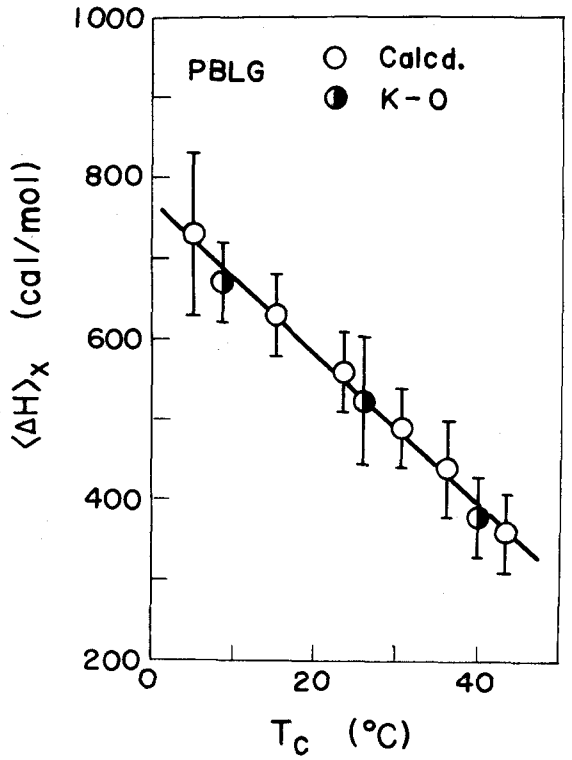

Figure 2.14. Plots of $\langle\Delta H\rangle_x$ against the transition temperature T_c for PBLG in DCA-EDC mixtures. (○) calculated values from the present data by using equation (2-65) and (◑) data of Karasz, O'Reilly, and Bair[33,35] from heat-capacity measurements.

one might conclude, as Ackermann and Neumann claimed, that this discrepancy would be associated with finite polymer concentrations at which the other authors performed measurements. However, it seems a little hazardous to accept this conclusion because, as mentioned before, our data for ΔH and hence $\langle\Delta H\rangle_x$ calculated therefrom can be taken as those at

infinite dilution. A similar argument may be applied to the data of Giacometti, et al.,[40] who conducted heat-of-solution measurements at as low a concentration as 0.2 g/dl. On the other hand, the measurements of Ackermann and Neumann were confined to fairly high concentrations. Therefore, it is not certain whether the linear relation they found applies down to lower concentrations. Nothing more than speculative can be said about this discrepancy until heat-capacity data at such low concentrations become available.

Finally we consider the enthalpy changes derived from heat-of-dilution and heat-of-solution measurements for PBLG in DCA-EDC. Since in these measurements data were taken by changing the solvent composition from a perfect coil solvent DCA to a perfect helix solvent EDC at constant temperature, the estimated enthalpy change $\langle \Delta H \rangle_T$ may correspond to

$$\langle \Delta H \rangle_T = \int_0^1 \Delta H (\partial f / \partial x)_T \, dx = \int_0^1 \Delta H \, (dx)_T \qquad (2\text{-}48)$$

It has been theoretically predicted[86] that $\langle \Delta H \rangle_T$ may be replaced approximately by ΔH_c. Figure 2.15 checks this prediction with data for PBLG in DCA-EDC mixtures.

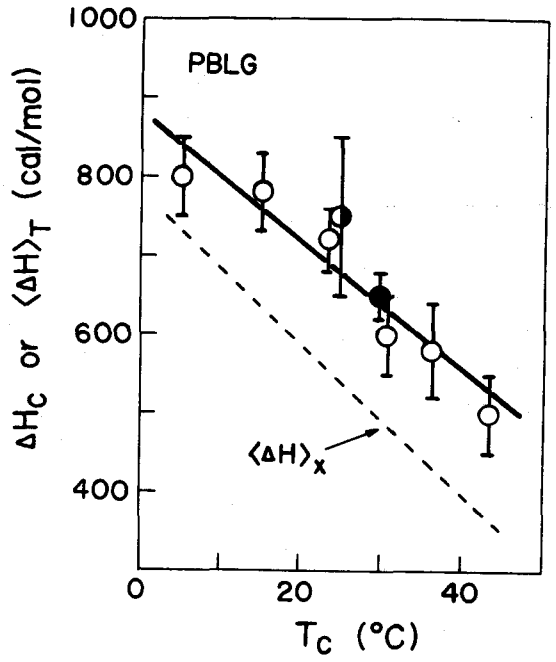

Figure 2.15. Comparison of our ΔH_c values with $\langle \Delta H \rangle_T$ from heat-of-solution and heat-of-dilution measurements for PBLG in DCA-EDC mixtures. (○) present data of ΔH_c, (◑) heat-of-dilution data of Kagemoto and Fujishiro,[38] and (●) heat-of-solution data of Giacometti, et al.[40] The dashed line indicates the dependence of $\langle \Delta H \rangle_x$ on T_c shown in Figure 2.14.

Chapter 3

Solvent Effects on Helix-Coil Transition in Polypeptides

3-1. Introduction

The theory of helix-coil transition developed in Chapter 2 has not explicitly taken into account solvent effects. Schellman[47] first considered this problem, and his study was followed by several authors,[24,48,49] who used statistical models, hereafter referred to as independent interaction models. In these models, each active solvent was assumed to interact independently with free NH and CO groups. Although the interaction between the active solvent and peptide residues may not be cooperative, this assumption seems to be inadequate when the active solvent is a carboxylic acid. Because carboxylic acids in solvent of low dielectric constant exists as cyclic dimers stabilized by two hydrogen bonds,[87] they may not interact independently with each active site of peptide residues.

In this chapter, a theory of helix-coil transition which may apply in such circumstances is developed, and the results are used to interpret experimental data for PBLG and poly(β-benzyl L-aspartate) (PBLA) in DCA-EDC mixtures.

3-2. Theoretical

3-2-1. Molecular Mechanism of Solvation

We consider a polypeptide molecule dissolved in a binary mixture which consists of an active solvent (e.g., carboxylic acid) and an inert solvent. Here by "inert solvent" we mean an organic liquid which has no specific interaction with peptide residues. It may have interactions with the polypeptide if they are not affected by the conformational state of the macromolecule. The α-helical structure of the polypeptide molecule is stabilized by intramolecular hydrogen bonds between NH and CO groups of peptide residues. It transforms to a random coil with the breaks of such hydrogen bonds to produce free NH and CO groups, which in turn may be stabilized by hydrogen bonding with the active solvent molecules.

It is well known that carboxylic acids in solvent of low dielectric constant exist as dimer. For example, DCA is considered to dimerize as[87]

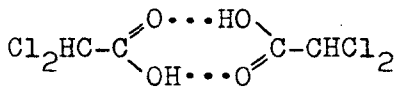

Here each of the three dots represent a hydrogen bond. If each dimerized DCA were to hydrogen bond independently with either free NH or CO group in peptide residues with the loss of the two hydrogen bonds indicated by the three dots, the number of hydrogen bonds would remain unchanged before and after the reaction, and hence the system would not be stabilized enthalpically. It is more likely that the free NH and

CO groups belonging to a given peptide residue may react in pair with a DCA dimer. We propose the following reaction for this process:

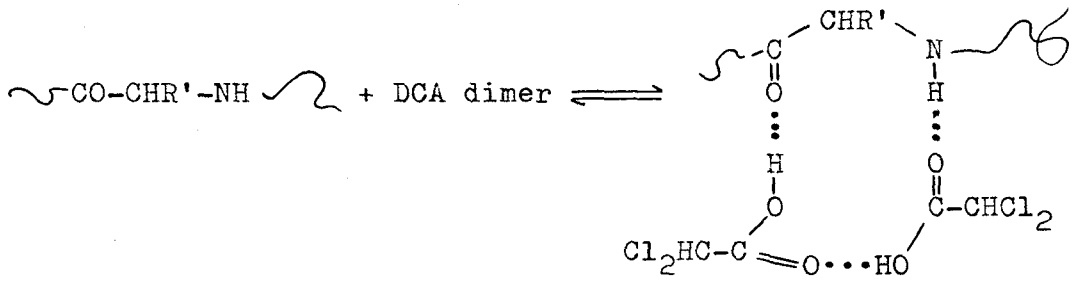

where R' denotes the side chain attached to the α-carbon. This reaction is acceptable from a stereochemical point of view, and moreover, the system is stabilized enthalpically because of the production of an extra hydrogen bond.

3-2-2. Effects of Solvation on the Transition

We enumerate the necessary statistical weights, choosing the central monomeric residue in the OOO conformation in the inert solvent as the standard of free energy. We denote by σ_o and u_o the value of σ and u in the inert solvent. The free energy of each peptide residue, when dissolved in a transition mixture, may be lowered by solvation with active solvent molecules, and hence its statistical weight should alter. To account for this effect, Peller[48] and Bixon and Lifson[49] proposed to multiply the statistical weight of a peptide residue by a factor of (1 + Ka) if the residue considered contains a site which is accessible to hydrogen

bonding with the active solvent. The statistical weight ζ for the 000 sequence may then be written

$$\zeta = 1 + K\underline{a} \qquad (3\text{-}1)$$

where K stands for the equilibrium constant for the proposed reaction and $\underline{a}$ is in this case the activity of the dimerized active solvent. This expression is equivalent to that of Birshtein and Ptitsyn,[88] although they did not consider the pairwise interaction.

All the sequences except for 000 may not allow the binding of the dimer. For the seven sequences, therefore, the statistical weights are given by

Conformations	Statistical weights
111	u_o
101	1
011	$\sqrt{\sigma}_o$
001	1
110	$\sqrt{\sigma}_o$
100	1
000	$\zeta = 1 + K\underline{a}$

We can construct the partition function Z_N^o of the polypeptide molecule from the statistical weights given above. In this case, as shown by Bixon and Lifson,[49] it is convenient to factorize Z_N^o as

$$Z_N^o = \zeta^N Z_N \qquad (3\text{-}2)$$

It immediately follows from the definition that Z_N represent the partition function when the central residue in the 000 conformation is chosen as the standard and given a statistical weight of unity. Constructing the matrices $\underset{\sim}{P}$, $\underset{\sim}{P}_c$, and $\underset{\sim}{P}_a$ associated with the statistical weights so normalized and following the procedure of Nagai[27] (see Chapter 2), we obtain

$$Z_N = \sum_i \sigma u \lambda_i^N (\lambda_i - 1)^{-1} [5\lambda_i^4 - 4(1+u)\lambda_i^3 + 3u\lambda_i^2 - \zeta\sigma u]^{-1} \tag{3-3}$$

and

$$\lambda_i^2(\lambda_i - 1)(\lambda_i - u) = \sigma u[1 + K\underline{a}\lambda_i^{-1}(\lambda_i - 1)] \tag{3-4}$$

where

$$u = u_o/(1 + K\underline{a}) \tag{3-5}$$

$$\sqrt{\sigma} = \sqrt{\sigma}_o/(1 + K\underline{a})^2 \tag{3-6}$$

Although he did not consider the effect of solvent binding explicitly, Nagai[27] derived expressions for the partition function and characteristic equation of more general applicability, special examples of which are equations (3-3) and (3-4).

We have already shown in Chapter 2 that the two larger eigenvalues, λ_1 and λ_2, are sufficient to calculate the partition function and the helical content in actual systems. If value of $K\underline{a}$ is not too large in comparison with unity,

we can expand these eigenvalues in powers of $\sqrt{\sigma}$. Recently, Puett and Ciferri[89] have reported K values ranging from 0.2 to 2.8 for PBLG in various mixtures containing DCA. Thus we assume Ka to be of the order of unity or less.

Introducing the variable z defined by $(\ln u)/2\sqrt{\sigma}$, we obtain equations (2-23) and (2-24) for the larger two eigenvalues. Carrying out further calculations, we arrive at the same expression of Z_N as equation (2-35) and obtain for Z_N°

$$Z_N^{\circ} = \zeta^N[(1 - f)\lambda_1^N + f\lambda_2^N] \qquad (3\text{-}7)$$

Since the helical content f_N is expressed by[27]

$$f_N = N^{-1}\partial(\ln Z_N^{\circ})/\partial \ln\sqrt{\sigma}_o$$

$$= N^{-1}\partial(\ln Z_N)/\partial \ln\sqrt{\sigma} \qquad (3\text{-}8)$$

we obtain equation (2-38) or (2-39) for f_N. Consequently, the values of $\sqrt{\sigma}$ and u evaluated by making use of equations (2-40) and (2-41) should be related to $\sqrt{\sigma}_o$ and u_o through equations (3-6) and (3-5), respectively. The statistical weight for the end residue of a helical section, $\sqrt{\sigma}_o$, is not equal to $\sqrt{\sigma}$. However, since it always appears in pair with the factor $(1 + Ka)^{-2}$ to form $\sqrt{\sigma}$, σ can be identified with the cooperativity parameter and may be used for the discussion of conformation-dependent properties without going into details of the solvent effect. A similar argument may apply to equation (A-5) for the independent interaction model given

in Appendix. Thus it follows that the cooperativity parameter may be affected by the solvent binding, contrary to the suggestion by Zimm and Bragg[22] and by Gō, Gō, and Scheraga.[90]

Substitution of equation (3-5) into (2-42) gives

$$\Delta H = \Delta H_o - \frac{K\underline{a}}{1 + K\underline{a}} \Delta H_1 \qquad (3\text{-}9)$$

with

$$\Delta H_1 = \Delta H_a - \Delta H_m \qquad (3\text{-}10)$$

where

$$\Delta H_o = -R\,\partial(\ln u_o)/\partial(1/T) \qquad (3\text{-}11)$$

$$\Delta H_a = -R\,\partial(\ln K)/\partial(1/T) \qquad (3\text{-}12)$$

$$\Delta H_m = R\,\partial(\ln \underline{a})/\partial(1/T) \qquad (3\text{-}13)$$

Here ΔH_o is the molar enthalpy change accompanying the formation of intramolecular hydrogen bonds between peptide residues in the inert solvent, ΔH_a is the molar enthalpy change for the complex formation between a dimer of the active solvent and a pair of free CO and NH groups, and ΔH_m is the partial molar enthalpy of the dimerized active solvent in the mixture considered.

Since $-RT \ln u_o$ is defined as the free energy difference between coil and helix in the inert solvent, we may write

$$\ln u_o = - \frac{\Delta H_o}{R} \left(\frac{1}{T} - \frac{1}{T_c^o}\right) \qquad (3\text{-}14)$$

Here T_c^o is the temperature at which $\ln u_o$ vanishes, and it may be regarded as the transition temperature for the helix-coil transition in the inert solvent. From equations (3-5) and (3-14) and the condition that $u = 1$ at $T = T_c$, we obtain[48]

$$1/T_c = 1/T_c^o - \left[\frac{R}{\Delta H_o} \ln(1 + K\underline{a})\right]_{T=T_c} \qquad (3\text{-}15)$$

This equation suggests that the decrease of the product $K\underline{a}$ shifts the transition temperature T_c to higher temperature since ΔH_o is expected to be negative.

The degree of solvent binding, ϕ, is another interesting molecular average. This quantity is defined as the fraction of residues which bind dimerized active solvents. It can be expressed as[49]

$$\phi = N^{-1} \partial(\ln Z_N^o)/\partial(\ln \underline{a}) \qquad (3\text{-}16)$$

Substitution of Z_N^o given by equation (3-7) into this equation yields

$$\phi = (1 - f_N)[K\underline{a}/(1 + K\underline{a})] \qquad (3\text{-}17)$$

The factor $K\underline{a}/(1 + K\underline{a})$ represents the degree of solvent binding in the random coil portions of the polypeptide chain.

We may note that equations analogous to equations (3-9)

and (3-17) have been derived by Peller[48] and by Bixon and Lifson[49] on the basis of the independent interaction models. For active solvents such as water, alcohols, etc., the independent interaction models may be adequate, because these molecules are likely to interact with NH and CO groups independently. The formulation of the solvent effects for this case is given in Appendix.

3-2-3. Methods for Data Analysis

Since both $\underline{a}$ and ΔH_m can, in principle, be determined from vapor pressure measurements, our problem concerns the ways in which K and u_o may be evaluated from experimental data for u or ΔH given as functions of T and $\underline{a}$. Two methods are proposed for these purposes.

a) Method I

This method utilizes data for u as a function of T and $\underline{a}$. If equation (3-5) holds, then it follows that values of u^{-1} at a fixed temperature plotted against $\underline{a}$ should give a straight line whose ordinate intercept and slope are equal to u_o^{-1} and K/u_o, respectively. Thus one can evaluate u_o and K at that temperature. This operation is repeated at other temperatures to determine both u_o and K as functions of T, and finally one can obtain values of ΔH_o and ΔH_a with the aid of equations (3-11) and (3-12).

b) Method II

This method resorts to data for ΔH_c, i.e., ΔH at $T = T_c$.

It is more restrictive than Method I, since ΔH_o, ΔH_a, and ΔH_m must be assumed to be independent of temperature, and moreover, the coefficients A and B in the expressions

$$u_o = A \exp(-\Delta H_o/RT), \qquad K = B \exp(-\Delta H_a/RT) \qquad (3\text{-}18)$$

must be treated as constant. In actual cases, however, these assumptions will hold quite accurately.

It can be shown that

$$\Delta H_c = \Delta H_o - \Delta H_1 + (u_o^*)^{-1}\Delta H_1 \exp[(\Delta H_o/R)(T_c^{-1} - T^{*-1})] \qquad (3\text{-}19)$$

Here u_o^* is the value of u_o at some reference temperature T^* in the central part of the temperature region in which T_c's for chosen values of $\underline{a}$ appear. It may be determined by linear extrapolation of the u^{-1} vs. $\underline{a}$ plot to $\underline{a} = 0$.

The ordinate C_1 and slope C_2 at $T = T^*$ of a plot of ΔH_c vs. $(T_c^{-1} - T^{*-1})$ are given by

$$C_1 = \Delta H_o - \Delta H_1 + \Delta H_1/u_o^* \qquad (3\text{-}20)$$

$$C_2 = \Delta H_o \Delta H_1/Ru_o^* \qquad (3\text{-}21)$$

By solving this set of equations, with known values of u_o^*, C_1, and C_2, it is possible to obtain ΔH_o and ΔH_1. If ΔH_m is given separately, then the desired ΔH_a can be derived. Once ΔH_o and ΔH_a are known, one can determine all the necessary quantities associated with the pair interaction model.

3-3. Experimental

3-3-1. PBLA Sample

Three samples of PBLA were used. Samples S and A-I had been prepared and characterized by Hayashi, et al.[45] The other sample A-IIa was a middle fraction of an unfractionated sample ($\bar{M}_v$ = 3.7 x 10^4) extracted by fractional precipitation in chloroform-methanol mixtures. The value of $\bar{M}_n$ of this sample was determined from osmotic pressure measurements on m-cresol solutions at 43°C. Table 3.1 lists the numerical values of $\bar{M}_n$ and $\bar{M}_w$ for the three samples used. It is seen that they are relatively narrow in molecular weight distribution.

Optical-rotation data for these samples in DCA-EDC mixtures were obtained as a function of temperature.

Table 3.1. Molecular weights for PBLA samples used.

Sample code	$\bar{M}_w$ x 10^{-4}	$\bar{M}_n$ x 10^{-4}	$\bar{M}_w/\bar{M}_n$
S	24.2	23.2	1.05[a]
A-I	7.1	6.2	1.15[a]
A-IIa	3.8[b]	3.4	1.12

a) Data of Hayashi, et al.[45]

b) Viscosity-average molecular weight.

3-3-2. Determination of Activity of DCA

The activity, a, of dimerized DCA in EDC was determined from measurements of the vapor pressures of EDC as functions of temperature and composition. The measurements were carried out in the following manner. A DCA-EDC mixture was placed in a glass cell (about 30 ml capacity) equipped with a mercury manometer. It was freezed, degassed in vacuum, and melted again. This operation was repeated until no bubble evolved upon melting. Then the whole assembly was immersed in a water bath regulated to within ± 0.01°, and the vapor pressure was measured manometrically to the accuracy of 0.01 mm Hg. After the vapor pressure measurements had been completed the composition of the mixture was checked by refractometry, and found to agree with that initially determined by gravimetry. The vapor pressures of pure EDC were in good agreement with literature values[91] over the range of temperature examined.

Figure 3.1 shows vapor pressures of EDC at a number of temperatures as a function of $1 - x_D$. Here x_D stands for the mole fraction of dimerized DCA. The data points at each temperature follow a straight line quite accurately. The vapor pressure of pure DCA is as small as 0.8 mm Hg at 40°C, the highest temperature studied. Hence this substance was regarded as non-volatile. Figure 3.1 thus can be taken to indicate that, at least within the range of temperatures studied, the system of EDC and dimerized DCA behaves ideally over the entire range of composition. On the basis of this

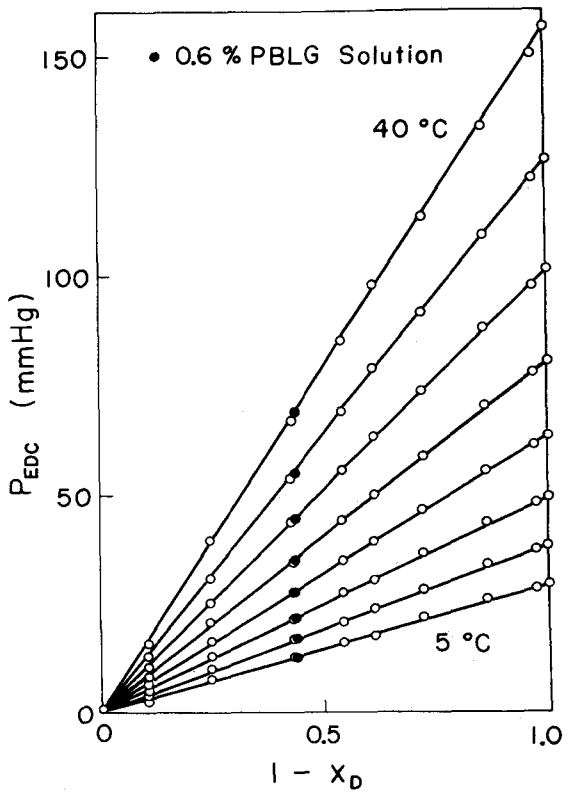

Figure 3.1. Composition dependence of vapor pressure of EDC, P_{EDC}, for mixtures of DCA and EDC at 40, 35, 30, 25, 20, 15, 10, and 5°C from top to bottom. x_D denotes the mole fraction of DCA calculated by assuming DCA to exist as dimer.

finding, we set a equal to x_D, from which it immediately follows that $\Delta H_m = 0$ for this system.

3-4. Results and Discussion

3-4-1. Helix-Coil Transition of PBLA

Figure 3.2 shows the dependence of $[\alpha]_{546}$ on temperature

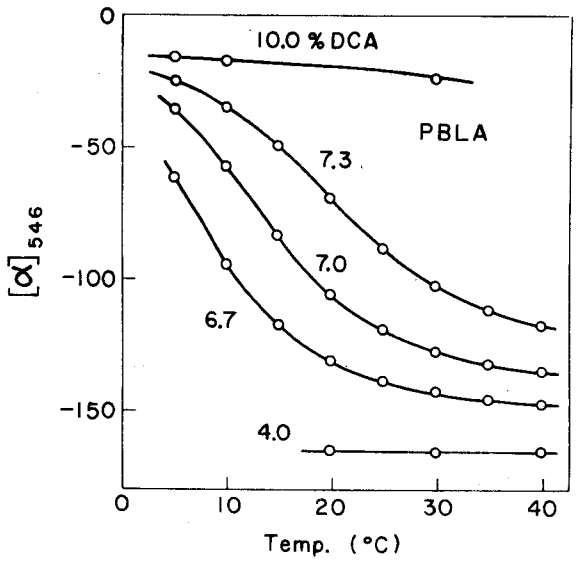

Figure 3.2. Temperature dependence of $[\alpha]_{546}$ for a PBLA sample S ($\bar{N}_n$ = 1130) in DCA-EDC mixtures. Composition of each DCA-EDC mixture is indicated by vol% of DCA at 25°C.

for sample S in various DCA-EDC mixtures. PBLA forms a left-handed α-helix,[45,92-94] and lower values of $[\alpha]_{546}$ correspond to the helical conformation. Thus it is seen that in DCA-EDC mixtures this polymer undergoes inverse transitions as does PBLG. The behavior of each curve is quite similar to that reported by Hayashi, et al.,[45] for this sample in DCA-$CHCl_3$ mixtures.

In Figure 3.3, the molecular weight dependence of transition curve is illustrated with the data for three PBLA samples in a DCA-EDC mixture (6.7 vol% DCA). The data show behavior

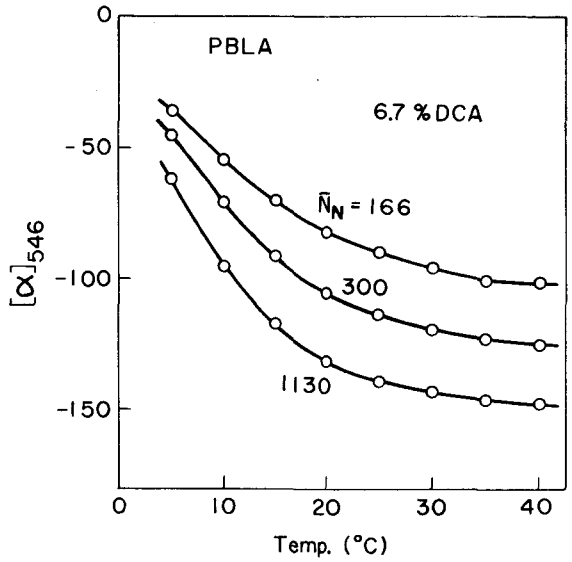

Figure 3.3. Temperature dependence of $[\alpha]_{546}$ for PBLA in a DCA-EDC mixture (6.7 vol% DCA) as a function of molecular weight.

essentially similar to those for PBLG depicted in Figure 2.6.

It has been shown that for the system PBLA-DCA-EDC the $[\alpha]_{546}$ can be related to f_N by[95]

$$f_N = -([\alpha]_{546} + 13)/157 \qquad (3\text{-}22)$$

All the measured values of $[\alpha]_{546}$ were converted to f_N with the aid of this equation.

Figures 3.4, 3.5, and 3.6 show the plots of f_N vs. $\bar{N}_n^{-1}$ for PBLA in three mixtures of DCA and EDC. The plotted points for a given solvent condition follow a straight line, as required by equation (2-39). The numerical results for $\sqrt{\sigma}$

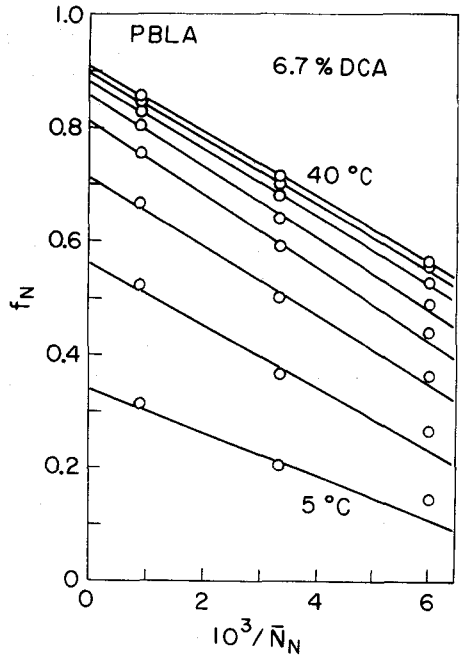

Figure 3.4. Plots of f_N vs. $\bar{N}_n^{-1}$ for PBLA in a DCA-EDC mixture (6.7 vol% DCA) at 40, 35, 30, 25, 20, 15, 10, and 5°C from top to bottom.

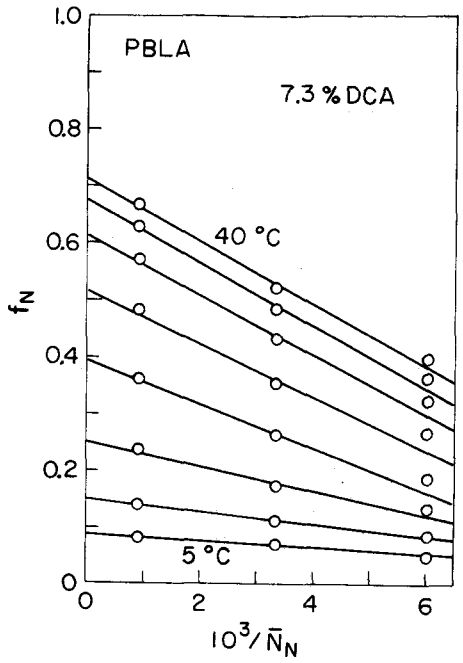

Figure 3.5. Plots of f_N vs. $\bar{N}_n^{-1}$ for PBLA in a DCA-EDC mixture (7.3 vol% DCA) at the same temperatures as those in Figure 3.4.

and u obtained from the slope and intercept of each straight line with the aid of equations (2-40) and (2-41) are summarized in Table 3.2. It is seen that all the $\sqrt{\sigma}$ values stay approximately constant irrespective of temperature and solvent composition.

Figure 3.7 shows the plots of ln u vs. 1/T for PBLA as a function of DCA-EDC composition. Each curve behaves quite similarly to those depicted for PBLG in Figure 2.10,

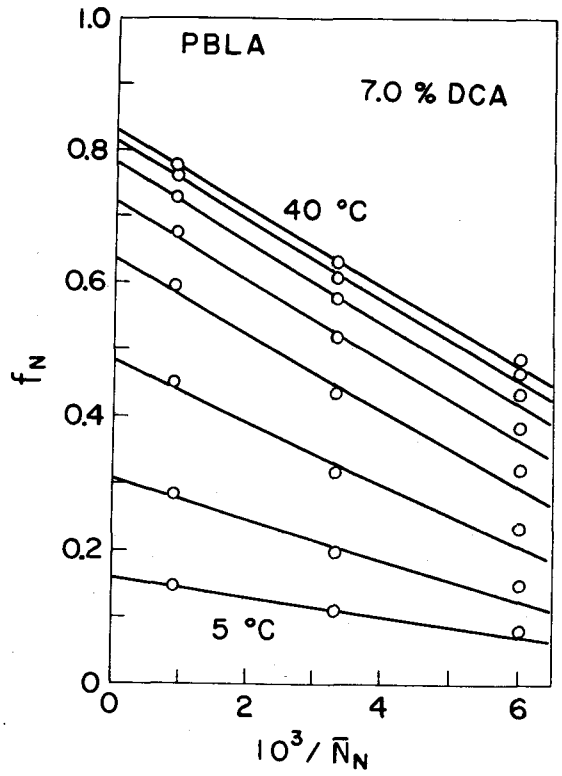

Figure 3.6. Plots of f_N vs. $\bar{N}_n^{-1}$ for PBLA in a DCA-EDC mixture (7.0 vol% DCA) at the same temperatures as those in Figure 3.4.

indicating that the transition enthalpy ΔH decreases with increasing temperature. The resulting values of ΔH_c (ΔH at $T = T_c$) are presented in the sixth column of Table 3.2. For the sake of comparison, Figure 3.8 shows plots of ln u vs. 1/T for various systems which undergo normal transitions.[45,46,96] It is seen that, in contrast to the cases of inverse transition, the data points for each

Table 3.2. Numerical values of the transition parameters σ, ln u, and ΔH for PBLA in DCA-EDC mixtures

Solvent composition (vol% of DCA at 25°C)	Temp. (°C)	f	$\sqrt{\sigma} \times 10^2$	$(\ln u) \times 10^2$	ΔH_c (cal/mol)	T_c (°C)
6.7	5	0.338	0.84	-0.57		
	10	0.562	1.01	0.25		
	15	0.713	1.06	1.00		
	20	0.811	0.98	1.56		
	25	0.858	0.94	1.93		
	30	0.881	0.95	2.25		
	35	0.897	0.94	2.45		
	40	0.910	0.89	2.56	270 ± 20	8.3
7.0	5	0.159	0.7_8	-1.4_5		
	10	0.306	0.92	-0.77		
	15	0.483	1.04	-0.07		
	20	0.637	1.07	0.61		
	25	0.721	1.09	1.08		
	30	0.780	1.07	1.45		
	35	0.814	1.05	1.69		
	40	0.830	1.05	1.85	230 ± 20	15.0
7.3	5	0.083	1.0	-3.2		
	10	0.150	0.92	-1.81		
	15	0.250	0.99	-1.15		
	20	0.394	0.99	-0.43		
	25	0.517	1.09	0.07		
	30	0.613	1.13	0.52		
	35	0.676	1.13	0.85		
	40	0.713	1.15	1.08	175 ± 15	24.1

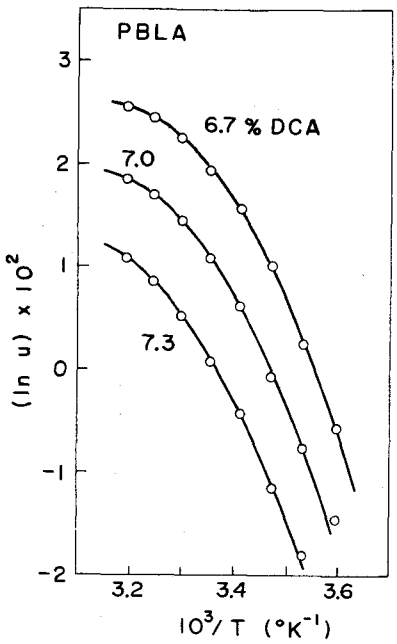

Figure 3.7. Plots of ln u vs. 1/T for PBLA in the three DCA-EDC mixtures.

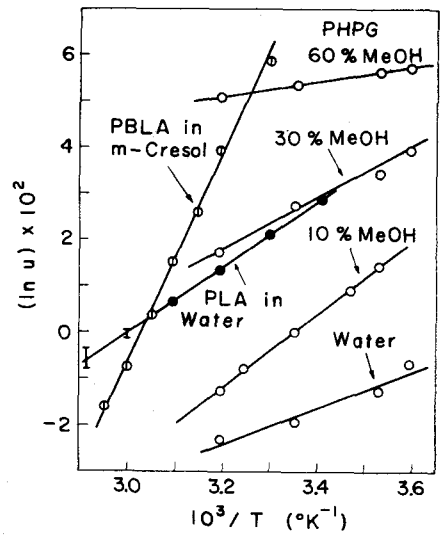

Figure 3.8. Plots of ln u vs. 1/T for various polypeptide-solvent systems in which normal transitions occur. (◐) PBLA in m-cresol,[45] (○) poly-N^5-(3-hydroxypropyl)-L-glutamine (PHPG) in water-methanol mixtures (composition is indicated by wt% of methanol),[46] and (●) poly-L-alanine (PLA) in water.[96]

polymer-solvent system follow a straight line over the range of temperatures examined. In light of equations (3-5) [or (A-4)] and (3-9), this finding may be taken to imply that the equilibrium constant of solvation for each of these systems is enough small for a normal transition with a temperature-

independent ΔH to occur.

These experimental facts show that ΔH is, in general, a function of temperature and solvent composition, and it is significantly affected by these two factors in the case of inverse transition. Therefore the curve fitting method with temperature-independent ΔH, ΔS, and σ must be used with great care for inverse transition curves.

3-4-2. Analysis of Solvent Effects

First, we analyze the data for PBLA by use of Method I. Figure 3.9 shows the plot of u^{-1} vs. $\underline{a}$ for PBLA in DCA-EDC mixtures. Although only three points are available for each temperature, they follow a straight line, as required by equation (3-5). We can obtain the values of u_o and K at each

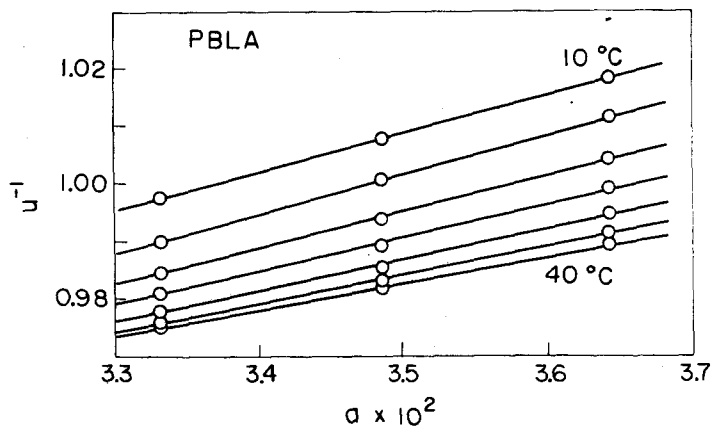

Figure 3.9. Plots of u^{-1} vs. $\underline{a}$ for PBLA in DCA-EDC mixture at 10, 15, 20, 25, 30, and 40°C from top to bottom.

temperature from the intercept and slope of each line in terms of equation (3-5), though slight scatter of the plotted points makes these values less accurate because of the very limited ranges of the ordinate and abscissa.

Figure 3.10 shows the temperature dependence of u_o and that of K thus obtained. The vertical segments indicate the uncertainty in the determinations of u_o and K. In either plot, the data points come close to a straight line. The values of ΔH_o and ΔH_a for this system were evaluated in terms of equations (3-11) and (3-12), and listed in Table 3.3.

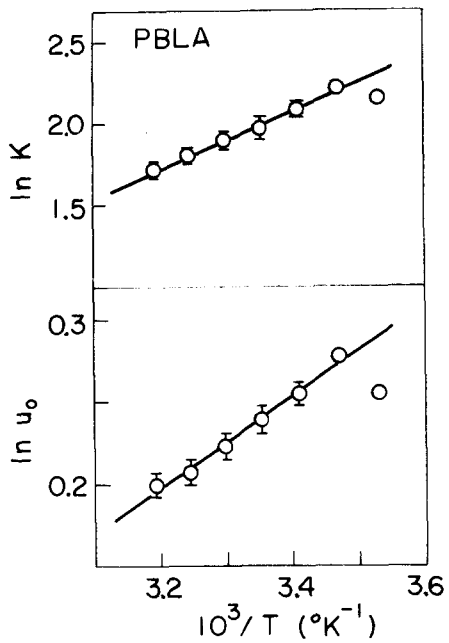

Figure 3.10. Plots of ln K vs. 1/T and of ln u_o vs. 1/T for PBLA in DCA-EDC mixtures.

Table 3.3. Thermodynamic parameters associated with helix-coil transitions of PBLA and PBLG in DCA-EDC mixtures

Poly-peptide	ΔH_o (kcal/mol)	ΔH_a (kcal/mol)	T_c^o (^oC)	u_o (at 25^oC)	K	$K\underline{a}/(1+K\underline{a})$ (at 25^oC)
PBLA	-0.56±0.06	-3.3±0.4	140 ± 20	1.27	7.2	0.20[a]
PBLG	-0.80±0.30	-3.5±0.9	210 ± 80	1.69	1.2	0.42[b]

a) 7.0 vol% DCA
b) 75 vol% DCA

Next we analyze the data for PBLG in DCA-EDC mixtures presented in Chapter 2. We use Method II for these data, since they are not accurate enough to permit the precise determinations of u_o and K as functions of temperature. Plots of ΔH_c vs. $(T^{-1} - T^{*-1})$ and of u^{-1} vs. $\underline{a}$ are presented in Figure 3.11, with 25^oC chosen as the reference temperature T^*. It is seen that the value of ΔH_c varies linearly with $(T^{-1} - T^{*-1})$ in the range indicated and also that the plotted points for u^{-1} at 25^oC follow a straight line accurately. The two lines give C_1 = 660 (cal/mol), C_2 = 81 x 10^4 (cal·deg/mol), and u_o^* = 1.69 (K = 1.2). By substituting these values into equations (3-20) and (3-21) and solving this set of equations, we obtained values of ΔH_o and ΔH_a.

The values of ΔH_o, ΔH_a, and T_c^o thus obtained for PBLA and PBLG are summarized in Table 3.3. Here we have incorporated

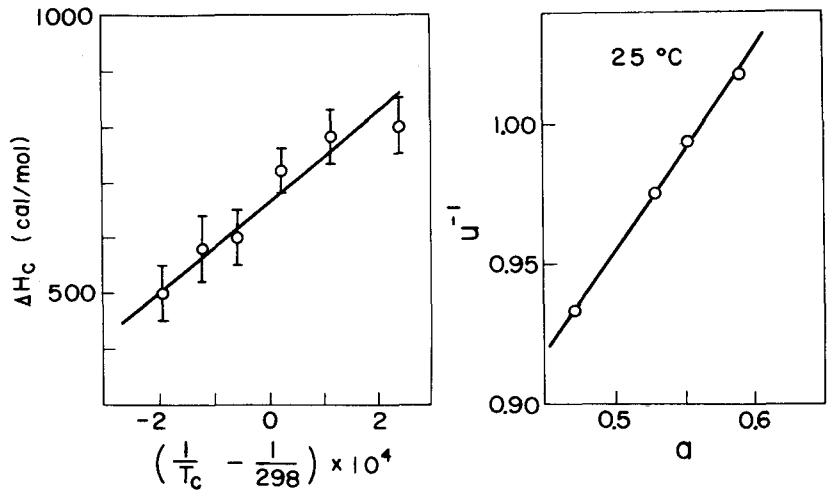

Figure 3.11. Plots of ΔH_c vs. $(\frac{1}{T} - \frac{1}{T^*})$ and of u^{-1} vs. $\underline{a}$ for PBLG in DCA-EDC mixtures. The reference temperature T^* is taken to be 298°K.

the values of u_o and K at 25°C and those of $K\underline{a}(1 + K\underline{a})$ at the indicated solvent compositions. The values of ΔH_a are about the same for PBLA and PBLG, and seem to be reasonable if we consider that ΔH_a is the enthalpy change associated with the formation of one extra hydrogen bond accompanying the binding of a pair of DCA molecules to a pair of free NH and CO goups. If a dimerized DCA were to bind independently with free CO and NH goups, we should have obtained much smaller values for ΔH_a. Such a possibility was ruled out, because the analysis of the present data with the assumption that $K_{CO} = K_{NH}$ gave nearly the same values of ΔH_o and ΔH_a as those given in Table 3.3.

On the other hand, the values for ΔH_o are, though negative as may be expected, much lower than usual hydrogen bond energies between CO and NH goups. The corresponding entropy changes per rotating bond are calculated to be -0.7 cal/deg for PBLA and -0.8 cal/deg for PBLG. It may be remarked that the entropy for fusion for an ordinary crystalline polymer is about 2 cal/deg per bond.[82] The unexpected values of ΔH_o may be ascribed either to restricted conformations in the randomly coiled state or to the possibility that the helical state in EDC is still less favorable enthalpically.

The values of T_c^o given in Table 3.3, taken literally, imply that each polypeptide in pure EDC may undergo a normal transition in a region not far above room temperature (see Figure 3.12). They are much lower than the value of about 10^3 ^oK estimated theoretically for PBLG by Baur and Nosanow,[97] who ignored the effect of solvent.

The factor $Ka/(1 + Ka)$ represents the fraction of coiled residues which bind DCA dimers. The values for this factor listed in the last column of Table 3.3 imply that there exist a considerable number of unsolvated coiled residues in either system. Bixon and Lifson[49] have reached a similar conclusion from an analysis of Yang's data[98] for PBLG in DCA-EDC mixtures at 20°C. In this connection, we wish to make a brief comment on the method of Karasz and O'Reilly,[99] who proposed the following equation to estimate ΔH:

$$d(\ln \underline{a})/d(1/T_c) = -\Delta H/R \qquad (3\text{-}23)$$

This equation is equivalent to the usual expression for the melting-point depression.

Differentiation of equation (3-15) with respect to $1/T_c$ yields

$$\frac{d(\ln \underline{a})}{d(1/T_c)} = -\frac{1}{R}\left\{\frac{1 + K\underline{a}}{K\underline{a}}\Delta H - \Delta H_m\right\}_{T=T_c} \qquad (3\text{-}24)$$

If ΔH_m can be set equal to zero, this equation becomes equivalent to Peller's expression,[48] but differs from equation (3-23) by a factor $(1 + K\underline{a})/K\underline{a}$. The slope, at a given T_c, of a ln $\underline{a}$ vs. $1/T_c$ curve must give the quantity, $(1 + K\underline{a})\Delta H/K\underline{a}$, at that temperature. Therefore, the value of ΔH estimated by equation (3-23) should be corrected for the factor $(1 + K\underline{a})/K\underline{a}$. This factor amounts to about two for PBLG in DCA-EDC mixtures (65 – 80 % DCA), which explains the contradiction[99] that the transition enthalpies obtained for PBLG in DCA-EDC mixtures by equation (3-23) were about twice as large as those obtained from heat-capacity measurements.

3-4-3. Solvent Effects on σ Values

Reported values of $\sqrt{\sigma}$ for various polypeptide-solvent systems[34,45,46,96,100,101] are collected in Table 3.4. It may be concluded that σ depends not only on polypeptide but also on solvent, in agreement with previous investigators.[34, 45,100] Nevertheless, our values of $\sqrt{\sigma}$ for either

Table 3.4. Comparison of $\sqrt{\sigma}$ values for Different systems

Poly-peptide	Solvent	Type of transition	$\sqrt{\sigma}\times10^2$	$\sqrt{\sigma}_0\times10^2$	Reference
PBLG	DCA-EDC	Inverse	0.95	2.8	This work
	DCA-CHL	Inverse	0.9_2		
PBLA	DCA-EDC	Inverse	1.0_4	1.7	
	DCA-$CHCl_3$	Inverse	0.77	1.5	45, 95
	m-cresol	Normal	1.28		45
PHPG	water-MeOH	Normal	1.79		46
PHBG[a]	water	Normal	2.59		101
PLA	water	Normal	1.2		96
PCBL[b]	DCA-$CHCl_3$	Inverse	0.35		34
PCBDB[c]	DCA-$CHCl_3$	Inverse	0.96		100
PCBO[d]	DCA-$CHCl_3$	Inverse	0.44		100

a) poly-N^5-(4-hydroxybutyl)-L-glutamine
b) poly-ε-carbobenzyloxy-L-lysine
c) poly-γ-N-carbobenzyloxy-L-α,γ-diaminobutyrate
d) poly-δ-N-carbobenzyloxy-L-ornithine

PBLG or PBLA in DCA-EDC mixtures were essentially independent of temperature and solvent composition. This suggests that $\sqrt{\sigma}$ is not affected by the solvent binding and hence all the $\sqrt{\sigma}$ values listed in Table 3.4 represent $\sqrt{\sigma}_0$. However, this idea is not readily acceptable, because if the factor $(1 + K\underline{a})^2$ scarecely varies with temperature and solvent composition in the substantial range of transition, constant values may

be obtained for $\sqrt{\sigma}_o$. In fact, the numerically calculated values of $\sqrt{\sigma}_o$ with the known values of $\sqrt{\sigma}$, K, and $\underline{a}$ for both PBLG and PBLA were constant to within the accuracy of experimental determination of $\sqrt{\sigma}$. For this reason the average values of $\sqrt{\sigma}_o$ are given in the fourth column of Table 3.4. There is a considerable difference between the $\sqrt{\sigma}_o$ values of PBLG and PBLA. Differences are also seen to exist in ΔH_o and T_c^o (see Table 3.3).

From the data of Gaskin and Yang,[100] we can find the following interesting facts; the value of $\sqrt{\sigma}$ for poly-γ-N-carbobenzyloxy-L-α,γ-diaminobutyrate (PCBDB)-DCA-$CHCl_3$ system, which undergoes a normal transition, is much larger than that for poly-δ-N-carbobenzyloxy-L-ornithine (PCBO)-DCA-$CHCl_3$ system which undergoes an inverse one. These two polypeptides differ by only one methylene group, and so the large difference in $\sqrt{\sigma}$ may be attributed chiefly to the differnce in $\underline{Ka}$ since a normal transition must be associated with a smaller $\underline{Ka}$ value than an inverse one. A similar consideration may be applied to the small value of $\sqrt{\sigma}$ obtained by Karasz, O'Reilly, and Bair[34] for poly-ε-carbobenzyloxy-L-lysine (PCBL in the same solvent mixture. One can observe that $\sqrt{\sigma}$ values associated with inverse transition are considerably smaller than those with normal transition. This can be understood if one recognizes the previous argument that a normal transition is characterized by a relatively small $\underline{Ka}$ value, while an inverse one is not. Thus it may be concluded that σ is

profoundly affected by binding of active solvent.

Since no information is available about the relationship between K_{CO} and $K_{CO'}$ and also between K_{NH} and $K_{NH'}$ (see Appendix), we cannot discuss the extent to which the σ value is affected by the binding of the independent interaction type.

3-4-4. General Features of Helix-Coil Transition

Thermally-induced helix-coil transitions of polypeptide molecules in dilute solution are classified into two types, normal and inverse, depending on the direction in which the conformational transition occurs as the temperature is raised. Thermodynamically, the normal transition is characterized by negative ΔH and ΔS, while the inverse one is characterized by positive ΔH and ΔS. Equation (3-9) shows that the sign of ΔH and hence the type of transition are determined by competition of the first and second terms on the right-hand side. Since both ΔH_0 and ΔH_1 are generally supposed to be negative, it follows that in order for ΔH to be positive, the solvent mixture must contain an active solvent with a moderately large value of K in an amount large enough for the second term to exceed the first. This prediction conforms to the observations that inverse transitions occurred only in solvent mixtures containing a strong organic acid such as DCA,[6,7] but it does not necessarily preclude the possibility that an inverse transition occurs also in a

single active solvent.

Another important prediction of equation (3-9) is that when ΔH is positive, ΔH at a fixed solvent composition should decrease with increasing temperature, since K is a decreasing function of temperature. In other words, a plot of ln u against 1/T at a fixed a should show a downward curvature. Our experimental data for both PBLG and PBLA confirm this prediction.

There may exist a certain temperature, at which the second term of equation (3-9) decreases to a value exactly cancelled by the first term, and beyond that temperature, ΔH becomes negative. Such a change in sign of ΔH should give rise to a maximum in the helical content vs. temperature curve. In fact, broad maxima were observed for PBLG in DCA-EDC at particular sets of T and a for which ΔH vanished (see Figure 2.4). To confirm this point also for PBLA, additional polarimeter measurements were carried out for sample S in a DCA-EDC mixture (7.3 vol% DCA). The results are presented in Figure 3.12, where the data for different solvent compositions are also included. A broad maximum can be found in the data for 7.3 % DCA, and the corresponding theoretical value for f_N decreases markedly upon further heating, suggesting that a second normal transition will take place. Moreover, the theoretical curve for either pure EDC or a DCA-EDC mixture (4 % DCA) predicts that in these solvents

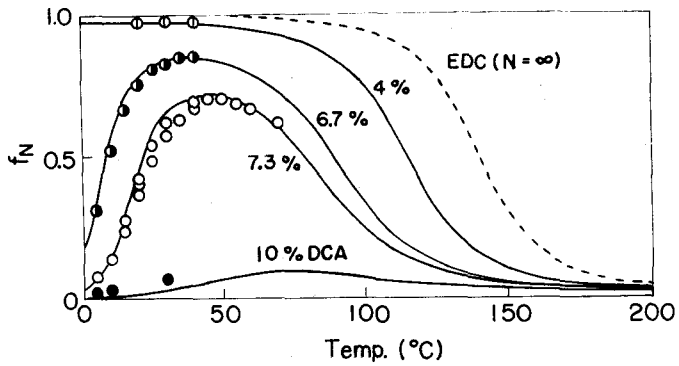

Figure 3.12. Temperature dependence of helical content f_N for a PBLA sample S in DCA-EDC mixtures of the indicated DCA contents. The solid lines and dashed line indicate the calculated curves for N = 1130, $\sqrt{\sigma}_o = 1.7 \times 10^{-2}$, and a set of the thermodynamic parameters given in Table 3.3.

PBLA may also undergo a normal transition, although it does not appear at room temperature. Theoretically, a helix-coil transition is observed in the vicinity of ln u = 0, and its type is determined by a delicate balance of two quantities u_o and 1 + K$\underline{a}$. Thus an inverse transition will be observed if u_o is smaller than 1 + K$\underline{a}$ at low temperatures and exceeds the latter at some higher temperature in the range accessible to experiment, and vice versa. Furthermore, it is easily understood that a small change in the solvent composition greatly alters the transition curve. In conclusion, the solvation mechanism proposed in this chapter explains in a consistent way not only why ΔH and σ depend on temperature and solvent composition but also the features of helix-coil transition curves in general.

Appendix

For the independent interaction model, the statistical weight for the 000 sequence, ζ, is given by[49]

$$\zeta = (1 + K_{NH}\underline{a})(1 + K_{CO}\underline{a}) \qquad (A\text{-}1)$$

since both of NH and CO groups are free to bind the active solvent molecules independently. Here K_{NH} and K_{CO} are the equilibrium constants for the formation of hydrogen bond of the active solvent with free NH and CO groups, respectively. In a similar way, we can derive the statistical weights for the rest of possible sequences necessary to construct the partition function (see Chapter 2). The factor $(1 + K_{NH}\underline{a})$ may be assigned to the statistical weight for the central residue in the 100 sequence, since only one NH group is free to bind the active solvent molecule. Similarly, the factors $(1 + K_{CO}\underline{a})$ and unity are assigned to those for the sequences of 001 and 101, respectively. Each of three residues at any end of a helical section has a free NH (or CO) group which is likely to bind the active solvent, with the equilibrium constant $K_{NH'}$ (or $K_{CO'}$). Incorporation of the three NH groups into the end residue of the helical section provides $\sqrt{\sigma}_o(1 + K_{NH'}\underline{a})^3$ as the statistical weight for the sequence of 110. Similarly, $\sqrt{\sigma}_o(1 + K_{CO'}\underline{a})^3$ must be given for 011. Consequently, for the seven sequences in question, we have

Conformations	Statistical weights
111	u_o
101	1
011	$\sqrt{\sigma}_o(1 + K_{CO'}\underline{a})^3$
001	$1 + K_{CO}\underline{a}$
110	$\sqrt{\sigma}_o(1 + K_{NH'}\underline{a})^3$
100	$1 + K_{NH}\underline{a}$
000	ζ

After normalization with respect to the central residue in the 000 sequence, the process of Nagai[27] (see Chapter 2) yields

$$Z_N = \lambda_i{}^N(\lambda_i - u)[\lambda_i{}^2 - 3(1 + u)\lambda_i + 2u]^{-1} \qquad (A\text{-}2)$$

with

$$\lambda_i{}^2(\lambda_i - u)(\lambda_i - 1) = \sigma u \qquad (A\text{-}3)$$

where

$$u = u_o/(1 + K_{NH}\underline{a})(1 + K_{CO}\underline{a}) \qquad (A\text{-}4)$$

and

$$\sqrt{\sigma} = \sqrt{\sigma}_o[(1+K_{NH'}\underline{a})(1+K_{CO'}\underline{a})/(1+K_{NH}\underline{a})(1+K_{CO}\underline{a})]^{3/2} \qquad (A\text{-}5)$$

Equations (A-2) and (A-3) are exactly the same as the corresponding equations, (2-16) and (2-9), given in Chapter 2.

Therefore, substitution of equation (2-35) into equation (3-8) gives the same expression as equation (2-38) or (2-39) for f_N. Thus, analysis of experimental data for f_N as a function of N should give u and σ which are defined by equations (A-4) and (A-5), respectively. If the solvent binding is not affected by whether free NH and CO groups belong to a randomly coiled section or helical one, i.e., if $K_{NH'} = K_{NH}$ and $K_{CO'} = K_{CO}$, equation (A-5) becomes

$$\sigma = \sigma_o \qquad \text{(A-6)}$$

This result agrees with the theoretical prediction of Gō, et al.[90]

Chapter 4

Approximate Expressions of Chain Dimensions and Light-Scattering Function of Polypeptide in the Helix-Coil Transition Region

4-1. Introduction

Rigorous expressions for the mean-square radius of gyration, $\langle S^2 \rangle$, and mean-square end-to-end distance, $\langle R^2 \rangle$, of a helix-forming polypeptide in the helix-coil transition region were first given by Nagai[27] and subsequently by Miller and Flory[50] and by Gō, Saito, and Ochiai.[53] Their equations, however, are so complicated that not only are they formidable for numerical computation but also it is troublesome to compare them with experimental observations.

This chapter attempts deriving simple approximate expressions for $\langle S^2 \rangle$ and $\langle R^2 \rangle$ from the theory of Nagai[27] under the conditions that have been imposed on σ and N in Chapter 2. Practical significance of the derived expression for $\langle S^2 \rangle$ is discussed in relation to an analysis of light-scattering data. Another topic in this chapter is the calculation of the particle scattering function $P(\theta)$ in the transition region by Nagai's model.

4-2. Mean-Square End-to-End Distance and Mean-Square Radius of Gyration

According to Nagai,[27] we take the following simplified model for a real polypeptide chain. A helical section consisting of n_1 monomeric residues is replaced by a straight rod of $n_1 a_1$ in length and a randomly coiled section consisting of n_o residues by a random flight chain of n_o steps each of which has a length a_o; these two sections are connected alternately at their ends by a universal joint. It is assumed that no excluded-volume effect is present between any pair of monomeric residues. Let $\underset{\sim}{r}_i$ $(i = 1,2,\cdots,N)$ be the displacement vector of the i-th residue. The mean-square end-to-end distance $\langle R^2 \rangle$ is then expressed by

$$\langle R^2 \rangle = \sum_{i}^{N} \langle r_i^2 \rangle + 2 \sum_{i<j} \langle \underset{\sim}{r}_i \cdot \underset{\sim}{r}_j \rangle \qquad (4\text{-}1)$$

where $\underset{\sim}{r}_i \cdot \underset{\sim}{r}_j$ is the scalar product of $\underset{\sim}{r}_i$ and $\underset{\sim}{r}_j$. Following Nagai, we rewrite this equation

$$\langle R^2 \rangle = J_1 + 2(J_2 + J_3) \qquad (4\text{-}2)$$

where

$$J_1 = \sum_{i=1}^{N} \langle r_i^2 \rangle \qquad (4\text{-}3)$$

$$J_2 = \sum_{i=2}^{N-2} \langle \underset{\sim}{r}_i \cdot \underset{\sim}{r}_{i+1} \rangle \qquad (4\text{-}4)$$

and

$$J_3 = \sum_{2 \le i < j-1 \le N-2} \langle \underset{\sim}{r}_i \cdot \underset{\sim}{r}_j \rangle \qquad (4\text{-}5)$$

Since $\langle r_i^2 \rangle$ may be written

$$\langle r_i^2 \rangle = \langle \mu_i a_1^2 + (1 - \mu_i) a_o^2 \rangle$$

with the probability, μ_i, that the i-th residue is in the helical conformation, equation (4-3) becomes

$$J_1 = a_o^2 \sum_{i=1}^{N} [1 - (1 - \frac{a_1^2}{a_o^2}) \langle \mu_i \rangle] \qquad (4\text{-}6)$$

Similarly, equations (4-4) and (4-5) can be expressed as

$$J_2 = a_1^2 \sum_{i=2}^{N-2} \langle \mu_i \mu_{i+1} \rangle \qquad (4\text{-}7)$$

$$J_3 = a_1^2 \sum_{2 \leq i < j-1 \leq N-2} \langle \mu_i \mu_{i+1} \cdots \mu_j \rangle \qquad (4\text{-}8)$$

Since we see from equation (2-17) that $\sum_{i=1}^{N} \langle \mu_i \rangle$ equals Nf_N, equation (4-6) becomes

$$J_1 = Na_o^2 [1 - (1 - \frac{a_1^2}{a_o^2}) f_N] \qquad (4\text{-}9)$$

It can be shown that

$$\langle \mu_i \mu_{i+1} \rangle = Z_N^{-1} SAE[\underset{\sim}{P}_c \underset{\sim}{P}^{i-2} \sigma(\partial \underset{\sim}{P}/\partial\sqrt{\sigma})^2 \underset{\sim}{P}^{N-i-2} \underset{\sim}{P}_a] \qquad (4\text{-}10)$$

Using the relation

$$\underset{\sim}{w}(\lambda_m) \sigma(\partial \underset{\sim}{P}/\partial\sqrt{\sigma})^2 \underset{\sim}{v}(\lambda_n) = C(\lambda_m) \lambda_m (\lambda_m + \lambda_n - u) \qquad (4\text{-}11)$$

and equation (2-19), we obtain

$$\langle \mu_i \mu_{i+1} \rangle = Z_N^{-1} (\sigma u)^{-1} \sum_{m,n} C(\lambda_m) C(\lambda_n) (\lambda_m - u)(\lambda_m + \lambda_n - u) \lambda_m^{\,i} \lambda_n^{\,N-i} \qquad (4\text{-}12)$$

Subject to the previously imposed conditions that $N \gg 1$ and $\sqrt{\sigma} \ll 1$, equation (4-12) becomes

$$\langle \mu_i \mu_{i+1} \rangle = f\left\{1 - (\lambda_2/\lambda_1)^{N-i} - (\lambda_2/\lambda_1)^i + (\lambda_2/\lambda_1)^N\right\} \times \left\{1 + [f/(1-f)](\lambda_2/\lambda_1)^N\right\}^{-1} \qquad (4\text{-}13)$$

Comparison of this equation with equation (2-37) shows that $\sum_i \langle \mu_i \mu_{i+1} \rangle$ equals Nf_N. Hence equation (4-7) reduces to

$$J_2 = N a_1^2 f_N \qquad (4\text{-}14)$$

Finally, the quantity $\langle \mu_i \mu_{i+1} \cdots \mu_j \rangle$ is expressed as

$$\langle \mu_i \mu_{i+1} \cdots \mu_j \rangle = Z_N^{-1} SAE[\underset{\sim}{P}_c \underset{\sim}{P}^{i-1} u^{j-i-1} (\partial \underset{\sim}{P}/\partial u)^{j-i-1} \underset{\sim}{P}^{N-j} \underset{\sim}{P}_a]$$
$$= Z_N^{-1} u^{j-i-2} SAE[\underset{\sim}{P}_c \underset{\sim}{P}^{i-1} u (\partial \underset{\sim}{P}/\partial u) \underset{\sim}{P}^{N-j} \underset{\sim}{P}_a] \qquad (4\text{-}15)$$

Use of equation (2-19) and the relation $\underset{\sim}{w}(\lambda_n) u (\partial \underset{\sim}{P}/\partial u) \underset{\sim}{y}(\lambda_m) = \lambda_m C(\lambda_m)$ yields

$$\langle \mu_i \mu_{i+1} \cdots \mu_j \rangle = Z_N^{-1} (\sigma u)^{-1} u^{j-i-2} \sum_{m,n} C(\lambda_m) C(\lambda_n) \lambda_m^{i+1} \lambda_n^{N-j+2} \times (\lambda_m - u)(\lambda_n - u) \qquad (4\text{-}16)$$

The imposed conditions on N and σ allow $\langle \mu_i \mu_{i+1} \cdots \mu_j \rangle$ to be written

$$\langle \mu_i \mu_{i+1} \cdots \mu_j \rangle = f(u/\lambda_1)^{j-i} \left\{1 - (\lambda_2/\lambda_1)^{N-j} - (\lambda_2/\lambda_1)^i + (\lambda_2/\lambda_1)^{N-j+i}\right\} \times \left\{1 + [f/(1-f)](\lambda_2/\lambda_1)^N\right\}^{-1} \qquad (4\text{-}17)$$

To the same degree of approximation, $(u/\lambda_1)^{j-i}$ may be written

$$(u/\lambda_1)^{j-i} = \exp\left[-(j-i)N\sqrt{\sigma}\sqrt{\frac{1-f}{f}}\right] \qquad (4\text{-}18)$$

Combination of equations (2-33), (4-17), and (4-18) with (4-8), followed by replacement of the summations by integrals gives

$$J_3 = Na_1^2 \frac{1}{\sqrt{\sigma}} \frac{f^{3/2}}{(1-f)^{1/2}} \left\{1 - \frac{3-2f}{N\sqrt{\sigma}}\sqrt{\frac{f}{1-f}} + \frac{1}{N\sqrt{\sigma}} \frac{1}{f\sqrt{f(1-f)}}\right.$$

$$\times \exp\left[-N\sqrt{\sigma}\sqrt{\frac{1-f}{f}}\right] - \left[\frac{1-f}{f} + \frac{1}{N\sqrt{\sigma}}\left(\frac{1-f}{f}\right)^{3/2}(2f+1)\right]\exp\left[-\frac{N\sqrt{\sigma}}{\sqrt{f(1-f)}}\right]$$

$$\left.\times\left\{1 + \frac{f}{1-f}\exp\left[-\frac{N\sqrt{\sigma}}{\sqrt{f(1-f)}}\right]\right\}^{-1}\right. \qquad (4\text{-}19)$$

It is to be noted that J_2 and the term multiplied by a_1^2 in J_1 are of the order of $\sqrt{\sigma}$ in comparison with J_3, and they may be neglected in our approximation. Therefore, equation (4-2) reduces to

$$\langle R^2 \rangle = Na_0^2(1 - f_N) + 2J_3$$

Although J_3 is still complicated, it may be further simplified for $N\sqrt{\sigma} > 2$ by dropping the terms associated with $\exp[-N\sqrt{\sigma}/\sqrt{f(1-f)}]$. On the other hand, $(u/\lambda_1)^N$ ($\cong \exp[-N\sqrt{\sigma}\sqrt{\frac{1-f}{f}}]$) approaches unity as f tends to unity however large $N\sqrt{\sigma}$ may be. Hence the terms associated with it must be retained even if $N\sqrt{\sigma}$ is larger than 2. Thus, subject to the conditions

that $N \gg 1$, $\sqrt{\sigma} \ll 1$, and $N\sqrt{\sigma} > 2$ along with the use of equation (2-39) for f_N, we finally obtain

$$\frac{\langle R^2 \rangle}{Na_o^2(1-f)} = 1 + \frac{2f}{\beta}\sqrt{\frac{f}{1-f}} + \frac{2}{\sqrt{\sigma}}\left(\frac{a_1}{a_o}\right)^2 \left(\frac{f}{1-f}\right)^{3/2} q(\beta,f) \qquad (4\text{-}20)$$

where

$$q(\beta,f) = 1 - \frac{3-2f}{\beta}\sqrt{\frac{f}{1-f}} + \frac{1}{\beta f\sqrt{f(1-f)}} \exp\left(-\beta\sqrt{\frac{1}{1-f}}\right) \qquad (4\text{-}21)$$

and

$$\beta = N\sqrt{\sigma} \qquad (4\text{-}22)$$

Since q tends to unity at the limit of infinite N, equation (4-20) reduces to

$$\langle R^2 \rangle / Na_o^2(1-f) = 1 + \frac{2}{\sqrt{\sigma}}\left(\frac{a_1}{a_o}\right)^2 \left(\frac{f}{1-f}\right)^{3/2} \qquad (4\text{-}23)$$

which stands in perfect agreement with the equation derived by Ptitsyn[52] from a different approach.

Next we calculate the mean-square radius of gyration, $\langle S^2 \rangle$, correct to the same degree of approximation. Generally $\langle S^2 \rangle$ is expressed by

$$\langle S^2 \rangle = N^{-2} \sum_{i<j} \langle \underset{\sim}{r}_{ij}^2 \rangle \qquad (4\text{-}24)$$

where $\underset{\sim}{r}_{ij}$ is the distance between the i-th and j-th residues. Since vector $\underset{\sim}{r}_{ij}$ is equal to $\underset{\sim}{r}_{i+1} + \underset{\sim}{r}_{i+2} + \cdots + \underset{\sim}{r}_{j}$, equation (4-24) can be written

$$\langle S^2\rangle = N^{-2}\left\{\sum_{1\le i<s\le j\le N}\langle r_s^{\,2}\rangle + 2\sum_{1\le i<s<t\le j\le N}\langle \underset{\sim}{r}_s\cdot\underset{\sim}{r}_t\rangle\right\}$$

$$= N^{-2}\left\{\sum_{1\le i<s\le j\le N}[a_1^{\,2}\langle\mu_s\rangle + a_o^{\,2}(1-\langle\mu_s\rangle)]\right.$$

$$+ 2a_1^{\,2}\Big[\sum_{1\le i<s\le j-1\le N-1}\langle\mu_s\mu_{s+1}\rangle$$

$$\left.+\sum_{1\le i<s<t-1<j-1\le N-1}\langle\mu_s\mu_{s+1}\cdots\mu_t\rangle\Big]\right\} \qquad (4\text{-}25)$$

We have already derived all the averages appearing in this equation. Replacement of the summations by integrals gives

$$\langle S^2\rangle/(1/6)Na_o^{\,2}(1-f) = 1 + \frac{12f^2}{\beta^2}\left[1 - \frac{2\sqrt{f(1-f)}}{\beta}\right]$$

$$+ \frac{2}{\sqrt{\sigma}}\left(\frac{a_1}{a_o}\right)^2\left(\frac{f}{1-f}\right)^{3/2} Q(\beta,f) \qquad (4\text{-}26)$$

where

$$Q(\beta,f) = 1 - \frac{3}{\beta}\sqrt{\frac{f}{1-f}} + \frac{6}{\beta^2}\left(\frac{f}{1-f}\right)[1 - 2(1-f)^2]$$

$$- \frac{6}{\beta^3}\left(\frac{f}{1-f}\right)^{3/2}\left\{[1-2(1-f)^2(3-2f)] - \frac{(2f-1)^2}{f^4}\exp\left[-\beta\sqrt{\frac{1-f}{f}}\right]\right\}$$

(4-27)

The first two terms on the right-hand side of equation (4-26) are contributions from randomly coiled sections, whereas the last term is that from helical sections. At fixed f and β the relative importance of these contributions is determined by a combined parameter $(1/\sqrt{\sigma})(a_1/a_o)^2$.

For infinitely large N, equation (4-26) reduces to

$$\langle S^2\rangle/(1/6)Na_o^2(1-f) = 1 + \frac{2}{\sqrt{\sigma}}\left(\frac{a_1}{a_o}\right)^2\left(\frac{f}{1-f}\right)^{3/2} \qquad (4\text{-}28)$$

Comparison of this equation with equation (4-23) gives the relation

$$\langle R^2\rangle = 6\langle S^2\rangle \qquad (4\text{-}29)$$

Nagai[27] has shown that the rigorous expressions for infinite N also satisfy this relation.

Now, combining equation (4-20) or (4-26) with equation (2-39), we can calculate $\langle R^2\rangle$ or $\langle S^2\rangle$ numerically as functions of f_N for fixed N, a_o, a_1, and σ. Figure 4.1 illustrates the curves of $\langle S^2\rangle/(1/6)Na_o^2$ vs. f_N calculated for $N = \infty$, 1200, and 600 with $\sigma = 2 \times 10^{-4}$, $a_o = 22.4$ A, and $a_1 = 1.5$ A, and the values calculated from the exact expressions of Nagai.[27] It is seen that equation (4-26) yields a fairly precise description of $\langle S^2\rangle$ over the entire range of helical content for the values of parameters chosen. The curves of $\langle R^2\rangle/Na_o^2$ vs. f_N calculated for the same parameters showed a similar degree of agreement.

The merit of equation (4-26) is not only in its simple form, which permits a straightforward computation of $\langle S^2\rangle$ and indicates explicitly its functional dependence on physical parameters N, σ, and f, but also in the fact that it can be used to determine the parameters a_o and a_1 if experimental

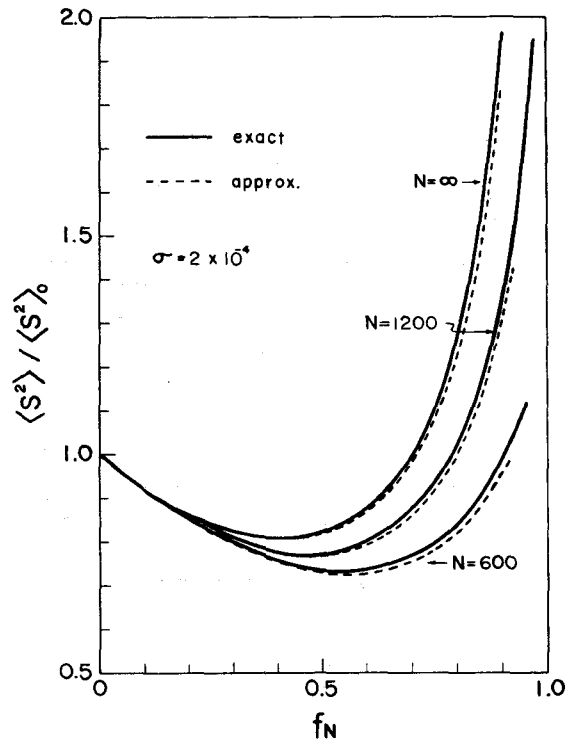

Figure 4.1. Comparison of approximate and exact[27] values of the mean-square radius of gyration $\langle S^2 \rangle$ for the parameters: $\sigma = 2 \times 10^{-4}$, $a_o = 22.4$ A, and $a_1 = 1.5$ A. $\langle S^2 \rangle_o$ denote the value of $\langle S^2 \rangle$ for random coil, i.e., $(1/6)Na_o^2$.

data are available for $\langle S^2 \rangle$ as a function of f and σ. As was shown in Chapters 2 and 3, the values of f and σ may be determined from data for f_N as a function of N. Thus the following quantities may be evaluated from experimental measu ments:

$$H_1 = \langle S^2 \rangle / N(1/6)(1 - f) \qquad (4\text{-}30)$$

$$H_2 = 1 + \frac{12f^2}{\beta^2}\left[1 - \frac{2\sqrt{f(1-f)}}{\beta}\right] \qquad (4\text{-}31)$$

and

$$H_3 = \frac{2}{\sqrt{\sigma}}\left(\frac{f}{1-f}\right)^{3/2} Q(\beta, f) \qquad (4\text{-}32)$$

Equation (4-26) predicts that a plot of H_1/H_2 against H_3/H_2 is linear and its ordinate intercept and slope are equal to a_0^2 and a_1^2, respectively, provided that both a_0 and a_1 are constant in the transition region.

4-3. Particle Scattering Function P(θ)

The particle scattering function P(θ) for an interrupted helix in solution must be evaluated by taking into account the copolymer nature of the polypeptide molecule, which stems from the experimental fact[46] that the specific refractive index increment of helical sections, $(\partial n/\partial c)_1$, is different from that of randomly coiled sections, $(\partial n/\partial c)_0$. According to Nagai,[27] the P(θ) is given by

$$P(\theta) = \left[\sum_i (\partial n/\partial c)_{\rho_i}\right]^{-2} \sum_i \sum_j (\partial n/\partial c)_{\rho_i} (\partial n/\partial c)_{\rho_j} \times$$

$$\times \langle \sin kr_{ij}/kr_{ij} \rangle_{\rho_i \rho_j} \qquad (4\text{-}33)$$

with

$$k = (4\pi/\lambda')\sin(\theta/2) \qquad (4\text{-}34)$$

where λ' is the wavelength of light in the scattering medium, θ is the scattering angle, and the subscript ρ_i means that the quantities in the parentheses refer to the i-th residue

in the state ρ_i, either helical, $\rho_i = 1$, or random coil, $\rho_i = 0$. Equation (4-33) may be expanded in powers of k^2 to give

$$P(\theta) = 1 - (k^2/3)[\sum_i (\partial n/\partial c)_{\rho_i}]^{-2} \sum_{i<j} (\partial n/\partial c)_{\rho_i} (\partial n/\partial c)_{\rho_j} \langle r_{ij}^2 \rangle_{\rho_i \rho_j}$$
$$+ (k^4/60)[\sum_i (\partial n/\partial c)_{\rho_i}]^{-2} \sum_{i<j} (\partial n/\partial c)_{\rho_i} (\partial n/\partial c)_{\rho_j} \langle r_{ij}^4 \rangle_{\rho_i \rho_j}$$
$$+ \cdots \qquad (4\text{-}35)$$

We define an apparent mean-square radius of gyration, $\langle S^2 \rangle_{app}$, by

$$\langle S^2 \rangle_{app} = [\sum_i (\partial n/\partial c)_{\rho_i}]^{-2} \sum_{i<j} (\partial n/\partial c)_{\rho_i} (\partial n/\partial c)_{\rho_j} \langle r_{ij}^2 \rangle_{\rho_i \rho_j} \qquad (4\text{-}36)$$

which is the quantity that can be obtained from light-scattering measurements. We ask what relationship exists between $\langle S^2 \rangle_{app}$ and $\langle S^2 \rangle$.

Let us define δ by

$$\delta = (\partial n/\partial c)_1/(\partial n/\partial c)_o - 1 \qquad (4\text{-}37)$$

Since

$$[\sum_i (\partial n/\partial c)_{\rho_i}]^2 = N^2 (\partial n/\partial c)_o^2 (1 + \delta f_N)^2$$

and

$$(\partial n/\partial c)_{\rho_i} (\partial n/\partial c)_{\rho_j} \langle r_{ij}^2 \rangle_{\rho_i \rho_j} = (\partial n/\partial c)_o^2 [\langle r_{ij}^2 \rangle_{00}$$
$$+ 2(1+\delta)\langle r_{ij}^2 \rangle_{10} + (1+\delta)^2 \langle r_{ij}^2 \rangle_{11}]$$

equation (4-36) becomes

$$\langle S^2\rangle_{app} = (1+\delta f_N)^{-2}N^{-2}\sum_{i<j}[\langle r_{ij}^2\rangle_{00} + 2(1+\delta)\langle r_{ij}^2\rangle_{10} + (1+\delta)^2\langle r_{ij}^2\rangle_{11}] \quad (4\text{-}38)$$

Here the subscript unity corresponds to the helical state and the subscript zero to the randomly coiled state. Hence, $\langle r_{ij}^2\rangle_{10}$, for example, is the mean-square distance between the i-th residue belonging to a helical section and the j-th residue belonging to a randomly coiled section. The mean-square radius of gyration $\langle S^2\rangle$ may be rewritten

$$\langle S^2\rangle = N^{-2}\sum_{i<j}[\langle r_{ij}^2\rangle_{00} + 2\langle r_{ij}^2\rangle_{10} + \langle r_{ij}^2\rangle_{11}] \quad (4\text{-}39)$$

so that

$$\langle S^2\rangle_{app} = \langle S^2\rangle(1 + \delta f_N)^{-2}\left\{1 + \frac{\delta}{N^2\langle S^2\rangle}\sum_{i<j}[(2+\delta)\langle r_{ij}^2\rangle_{11} + 2\langle r_{ij}^2\rangle_{10}]\right\} \quad (4\text{-}40)$$

Now, we have

$$\sum_{i<j}\langle r_{ij}^2\rangle_{11} = J_1(1,1) + 2[J_2(1,1) + J_3(1,1)] \quad (4\text{-}41)$$

where

$$J_1(1,1) = \sum_{2\le i<s\le j\le N-1}\langle r_s^2\rangle_{11} \quad (4\text{-}42)$$

$$J_2(1,1) = \sum_{2\le i<s\le j-1\le N-2}\langle \underset{\sim}{r}_s\cdot\underset{\sim}{r}_{s+1}\rangle_{11} \quad (4\text{-}43)$$

$$J_3(1,1) = \sum_{2\le i<s<t-1\le j-1\le N-2} \langle \underset{\sim}{r}_s \cdot \underset{\sim}{r}_t \rangle_{11} \qquad (4\text{-}44)$$

$J_1(1,1)$ can be written

$$J_1(1,1) = a_o^2 \sum_{2\le i<s\le j\le N-1} [\langle \mu_i \mu_j \rangle - (1 - \frac{a_1^2}{a_o^2}) \langle \mu_i \mu_s \mu_j \rangle] \qquad (4\text{-}45)$$

The expressions for $\langle \mu_i \mu_j \rangle$ and $\langle \mu_i \mu_s \mu_j \rangle$ can be derived in the same way as $\langle \mu_i \rangle$, $\langle \mu_i \mu_{i+1} \rangle$, etc., have been derived. Thus

$$\langle \mu_i \mu_j \rangle = Z_N^{-1} (\sigma u)^{-1} \sum_{m,n,p} C(\lambda_m) C(\lambda_n) C(\lambda_p) \lambda_m^{i-1} \lambda_n^{N-i-2} \lambda_p^{N-j}$$

$$\times (\lambda_m - u)(\lambda_p - u)[\lambda_m \lambda_n + \lambda_m(\lambda_m - u) + \lambda_n(\lambda_n - u)]$$

$$\times [\lambda_n \lambda_p + \lambda_n(\lambda_n - u) + \lambda_p(\lambda_p - u)] \qquad (4\text{-}46)$$

and

$$\langle \mu_i \mu_s \mu_j \rangle = Z_N^{-1} (\sigma u)^{-1} \sum_{m,n,p,q} C(\lambda_m) C(\lambda_n) C(\lambda_p) C(\lambda_q) \lambda_m^{i-1} \lambda_n^{s-i-2}$$

$$\times \lambda_p^{j-s-2} \lambda_q^{N-j} (\lambda_m - u)(\lambda_q - u)[\lambda_m \lambda_n + \lambda_m(\lambda_m - u) + \lambda_n(\lambda_n - u)]$$

$$\times [\lambda_n \lambda_p + \lambda_n(\lambda_n - u) + \lambda_p(\lambda_p - u)]$$

$$\times [\lambda_p \lambda_q + \lambda_p(\lambda_p - u) + \lambda_q(\lambda_q - u)] \qquad (4\text{-}47)$$

In a similar way, it can be shown that

$$J_2(1,1) = a_1^2 \sum_{2\le i<s\le j-1\le N-2} \langle \mu_i \mu_s \mu_{s+1} \mu_j \rangle \qquad (4\text{-}48)$$

$$J_3(1,1) = a_1^2 \sum_{2\le i<s<t-1\le j-1\le N-2} \langle \mu_i \mu_s \mu_{s+1} \cdots \mu_t \mu_j \rangle \qquad (4\text{-}49)$$

with

$$\begin{aligned} \langle \mu_i \mu_s \mu_{s+1} \mu_j \rangle = {} & Z_N^{-1} (\sigma u)^{-1} \sum_{m,n,p,q} C(\lambda_m) C(\lambda_n) C(\lambda_p) C(\lambda_q) \lambda_m^{i-1} \\ & \times \lambda_n^{s-i-1} \lambda_p^{j-s-2} \lambda_q^{N-j} (\lambda_m - u)(\lambda_q - u)(\lambda_n + \lambda_p - u) \\ & \times [\lambda_m \lambda_n + \lambda_m (\lambda_m - u) + \lambda_n (\lambda_n - u)] \\ & \times [\lambda_p \lambda_q + \lambda_p (\lambda_p - u) + \lambda_q (\lambda_q - u)] \end{aligned} \qquad (4\text{-}50)$$

and

$$\begin{aligned} \langle \mu_i \mu_s \mu_{s+1} \cdots \mu_t \mu_j \rangle = {} & Z_N^{-1} (\sigma u)^{-1} u^{t-s-2} \sum_{m,n,p,q} C(\lambda_m) C(\lambda_n) C(\lambda_p) \\ & \times C(\lambda_q) \lambda_m^{i-1} \lambda_n^{s-i} \lambda_p^{j-t} \lambda_q^{N-j} (\lambda_m - u)(\lambda_q - u) \\ & \times [\lambda_m \lambda_n + \lambda_m (\lambda_m - u) + \lambda_n (\lambda_n - u)] \\ & \times [\lambda_p \lambda_q + \lambda_p (\lambda_p - u) + \lambda_q (\lambda_q - u)] \end{aligned} \qquad (4\text{-}51)$$

Writing

$$\sum_{i<j} \langle r_{ij}^2 \rangle_{10} = J_1(1,0) + 2[J_2(1,0) + J_3(1,0)] \qquad (4\text{-}52)$$

with $J_1(1,0)$, $J_2(1,0)$, and $J_3(1,0)$ defined as

$$J_1(1,0) = \sum_{2\le i<s\le j\le N} \langle r_s^2 \rangle_{10} \qquad (4\text{-}53)$$

$$J_2(1,0) = \sum_{2\le i<s\le j-2\le N-2} \langle \underset{\sim}{r}_s \cdot \underset{\sim}{r}_{s+1} \rangle_{10} \tag{4-54}$$

$$J_3(1,0) = \sum_{2\le i<s<t-1\le j-2\le N-2} \langle \underset{\sim}{r}_s \cdot \underset{\sim}{r}_t \rangle_{10} \tag{4-55}$$

we obtain

$$J_1(1,0) = a_o^2 \sum_{2\le i<s\le j\le N} \Big\{ \langle \mu_i \rangle - (1 - \frac{a_1^2}{a_o^2}) \langle \mu_i \mu_s \rangle - [\langle \mu_i \mu_j \rangle - (1 - \frac{a_1^2}{a_o^2}) \langle \mu_i \mu_s \mu_j \rangle] \Big\} \tag{4-56}$$

$$J_2(1,0) = a_1^2 \sum_{2\le i<s\le j-2\le N-2} [\langle \mu_i \mu_s \mu_{s+1} \rangle - \langle \mu_i \mu_s \mu_{s+1} \mu_j \rangle] \tag{4-57}$$

$$J_3(1,0) = a_1^2 \sum_{2\le i<s<t-1\le j-2\le N-2} [\langle \mu_i \mu_s \mu_{s+1} \cdots \mu_t \rangle - \langle \mu_i \mu_s \mu_{s+1} \cdots \mu_t \mu_j \rangle] \tag{4-58}$$

where

$$\langle \mu_i \mu_s \mu_{s+1} \rangle = Z_N^{-1} (\sigma u)^{-1} \sum_{m,n,p} C(\lambda_m) C(\lambda_n) C(\lambda_p) \lambda_m^{i-1} \lambda_n^{s-i-1} \times \lambda_p^{N-s} (\lambda_m - u)(\lambda_p - u)(\lambda_n + \lambda_p - u)[\lambda_m \lambda_n + \lambda_m(\lambda_m - u) + \lambda_n(\lambda_n - u)] \tag{4-59}$$

$$\langle \mu_i \mu_s \mu_{s+1} \cdots \mu_t \rangle = Z_N^{-1} (\sigma u)^{-1} u^{t-s-2} \sum_{m,n,p} C(\lambda_m) C(\lambda_n) C(\lambda_p) \lambda_m^{i-1} \times \lambda_n^{s-i} \lambda_p^{N-t+2} (\lambda_m - u)(\lambda_p - u)[\lambda_m \lambda_n + \lambda_m(\lambda_m - u) + \lambda_n(\lambda_n - u)] \tag{4-60}$$

We calculated $J_1(1,1),\cdots, J_3(1,0)$ subject to $N \gg 1$, $\sqrt{\sigma} \ll 1$, and $N\sqrt{\sigma} > 2$ with the summations being replaced by integrals. We also found that all the J_2 terms were of the order of $\sqrt{\sigma}$ relative to the corresponding J_3 terms. The results obtained, however, were yet so complicated because of the terms multiplied by $\exp[-\beta\sqrt{(1-f)/f}]$. Therefore we imposed the restriction that this exponential function may be neglected in comparison with unity. The resulting expression for $\langle S^2\rangle_{app}$ then reads

$$\langle S^2\rangle_{app}/\langle S^2\rangle = (1 + \delta f_N)^{-2}\Big\{(1 + \delta f)^2 + [(\delta f)^2 K_1 + 2\delta f K_2]\frac{(1-f)Na_o^2}{6\langle S^2\rangle}\Big\} \tag{4-61}$$

where

$$K_1 = I_1(\beta,f) + \frac{2}{\sqrt{\sigma}}\frac{a_1^2}{a_o^2}\left(\frac{f}{1-f}\right)P_1(\beta,f) \tag{4-62}$$

$$K_2 = I_2(\beta,f) + \frac{2}{\sqrt{\sigma}}\frac{a_1^2}{a_o^2}\left(\frac{f}{1-f}\right)P_2(\beta,f) \tag{4-63}$$

with

$$I_1(\beta,f) = -\frac{12}{\beta}\sqrt{f(1-f)}\left[1 - \frac{5-6f}{\beta}\sqrt{\frac{f}{1-f}} + \frac{2f(5-6f)}{\beta^2}\right] \tag{4-64}$$

$$P_1(\beta,f) = \frac{6}{\beta}\Big\{1-2f + \frac{1}{\beta}\sqrt{\frac{f}{1-f}}\left[1-8f+10f^2 - \frac{2f}{1-f}(1-3f+f^2)\right] - \frac{1}{\beta^2}\left[(1-f)(2-6f+5f^2) + f(9-4f^2) + \frac{2f(2f-1)}{1-f}\right]\Big\} \tag{4-65}$$

$$I_2(\beta,f) = -\frac{6}{\beta}\sqrt{f(1-f)}\left[1 - \frac{3-4f}{\beta}\sqrt{\frac{f}{1-f}} + \frac{4f(1-f)}{\beta^2}\right] \qquad (4\text{-}66)$$

$$P_2(\beta,f) = \frac{3}{\beta}\left\{1-2f - \frac{2}{\beta}(3-8f+4f^2)\sqrt{\frac{f}{1-f}}\right.$$

$$\left. + \frac{2}{\beta^2}\left[2f(2-5f+2f^2) + \frac{f(1-2f)}{1-f}\right]\right\} \qquad (4\text{-}67)$$

The imposed condition is satisfied quite well if $\beta\sqrt{(1-f)/f} > 5$. Thus if $\beta = 10$, the values of f for which equation (4-61) is useful must be smaller than 0.8.

When δ is zero, equation (4-61) gives $\langle S^2\rangle_{app} = \langle S^2\rangle$, as should be expected. In the limit of infinitely large N, K_1 and K_2 tend to zero, f_N approaches f, and $\langle S^2\rangle/N$ remains finite (see equation (4-28)). Thus, unless $f = 1$, we find

$$\lim_{N\to\infty} \langle S^2\rangle_{app} = \langle S^2\rangle \qquad (4\text{-}68)$$

irrespective of the difference in refractive index increment between helical and randomly coiled sections. Okita, Teramoto, and Fujita[46] estimated δ for poly-N^5-(3-hydroxypropyl)-L-glutamine in methanol and in water from the dependence of $(\partial n/\partial c)$ on molecular weight at fixed solvent conditions, and found values of δ ranging 0.2 – 0.4. We calculated $\langle S^2\rangle_{app}$ for the range $0.1 < f < 0.9$ by assigning the following numerical values: $\delta = 0.2$, $a_o = 12$ A, $a_1 = 1.5$ A, $\sigma = 10^{-4}$, and $N = 10^3$ (thus $\beta = 10$). The resulting values of $\langle S^2\rangle_{app}$ agreed with the corresponding $\langle S^2\rangle$ to within 1 % at all f examined. Additional calculations with $\delta = 0.4$ gave $\langle S^2\rangle_{app}$

which did not exceed $\langle S^2 \rangle$ more than 2 %. From these results it appears quite safe to conclude that except under very special circumstances, the slope of a $P(\theta)^{-1}$ vs. $k^2/3$ plot for a polypeptide sample is essentially equal to its mean-square radius of gyration even when the molecule is in the state of interrupted helix.

On the assumptiom that the higher terms in equation (4-35) are not affected by the copolymer nature, the $P(\theta)$ function may be put in the form:

$$P(\theta) = 1 - \frac{k^2}{3}\langle S^2 \rangle + \frac{k^4}{60N^2} \sum_{i<j} \langle r_{ij}^4 \rangle - \frac{k^6}{2520N^2} \sum_{i<j} \langle r_{ij}^6 \rangle + \cdots \qquad (4\text{-}69)$$

We now consider the average fourth moment of $\underset{\sim}{r}_{ij}$ to calculate the third term on the right-hand side of this equation. It can be shown that

$$r_{ij}^4 = \Big(\sum_{i<m\leq j} r_m^2\Big)\Big(\sum_{i<n\leq j} r_n^2\Big) + 4\Big(\sum_{i<m\leq j} r_m^2\Big)\Big(\sum_{i<s<t\leq j} \underset{\sim}{r}_s \cdot \underset{\sim}{r}_t\Big) + 4\Big(\sum_{i<m<n\leq j} \underset{\sim}{r}_m \cdot \underset{\sim}{r}_n\Big)\Big(\sum_{i<s<t\leq j} \underset{\sim}{r}_s \cdot \underset{\sim}{r}_t\Big) \qquad (4\text{-}70)$$

Averaging over all conformations of the molecule, we obtain

$$\langle r_{ij}^4 \rangle =$$

$$\sum_{i<m\leq j} \langle r_m^4 \rangle + \frac{32}{3} \sum_{i<m<n\leq j} \langle \overline{r_m^2 r_n^2} \rangle + \frac{68}{3} \sum_{i<m<s<t\leq j} \langle \overline{r_m^2 r_s r_t} \rangle$$

$$+ \frac{10}{3} \sum_{i<m<n\leq j} \langle r_m^2 r_n^2 \rangle + \frac{40}{3} \sum_{i<m<s<t\leq j} \langle r_m^2 \, \overline{r_s r_t} \rangle$$

$$+ \frac{40}{3} \sum_{i<m<s<t<n\leq j} \langle \overline{r_m r_s} \; \overline{r_t r_n} \rangle + \frac{32}{3} \sum_{i<m<s<t<n\leq j} \langle \overline{r_m r_s r_t r_n} \rangle \qquad (4\text{-}71)$$

where bars attached to the products of r_i's indicate that the residues are in the same helical section. We proceed, confining ourselves to the case where $N \gg 1$. Then the first three terms in equation (4-71) may be dropped, giving

$$\langle r_{ij}^4 \rangle = \frac{10}{3} (J_1^* + 4J_2^* + 4J_3^* + \frac{16}{5} J_4^*) \qquad (4\text{-}72)$$

where

$$J_1^* = \sum_{i<m<n\leq j} \langle r_m^2 r_n^2 \rangle \qquad (4\text{-}73)$$

$$J_2^* = \sum_{i<m<s<t\leq j} \langle r_m^2 \, \overline{r_s r_t} \rangle \qquad (4\text{-}74)$$

$$J_3^* = \sum_{i<m<s<t<n\leq j} \langle \overline{r_m r_s} \; \overline{r_t r_n} \rangle \qquad (4\text{-}75)$$

$$J_4^* = \sum_{i<m<s<t<n\leq j} \langle \overline{r_m r_s r_t r_n} \rangle \qquad (4\text{-}76)$$

It can be shown that

$$J_1^* = \sum_{i<m<n\leq j} \Big\{ \langle \mu_m \mu_n \rangle a_1^4 + (\langle \mu_m \rangle + \langle \mu_n \rangle - 2\langle \mu_m \mu_n \rangle) a_1^2 a_o^2 + (1 - \langle \mu_m \rangle - \langle \mu_n \rangle + \langle \mu_m \mu_n \rangle) a_o^4 \Big\} \tag{4-77}$$

J_2^* may be divided into two groups depending on whether $s = t + 1$ or $s < t + 1$. Thus

$$J_2^* = \sum_{i<m<s<j-1} \langle r_m^2 \overline{r_s r_{s+1}} \rangle + \sum_{i<m<s<t-1<j-1} \langle r_m^2 \overline{r_s r_t} \rangle \tag{4-78}$$

Our approximate treatment has shown that the first sum in this equation, being of the order of $\sqrt{\sigma}$ in comparison with the second one, may be neglected. Thus we have for J_2^*

$$J_2^* = \sum_{i<m<s<t<j} \Big\{ \langle \mu_m \mu_s \mu_{s+1} \cdots \mu_t \rangle a_1^4 + [\langle \mu_s \mu_{s+1} \cdots \mu_t \rangle - \langle \mu_m \mu_s \mu_{s+1} \cdots \mu_t \rangle] a_1^2 a_o^2 \Big\} \tag{4-79}$$

Similarly, we obtain for J_3^* and J_4^*

$$J_3^* = a_1^4 \sum_{i<m<s<t<n<j} \langle \mu_m \mu_{m+1} \cdots \mu_s \mu_t \mu_{t+1} \cdots \mu_n \rangle \tag{4-80}$$

and

$$J_4^* = a_1^4 \sum_{i<m<s<t<n<j} \langle \mu_m \mu_{m+1} \cdots \mu_n \rangle \tag{4-81}$$

All the averages of products μ_i's appearing in these equations have already been evaluated except for $\langle \mu_m \mu_{m+1} \cdots \mu_s \mu_t \mu_{t+1} \cdots \mu_n \rangle$, which is given by

$$\langle \mu_m \mu_{m+1} \cdots \mu_s \mu_t \mu_{t+1} \cdots \mu_n \rangle =$$

$$Z_N^{-1} (\sigma u)^{-1} u^{n-m-t+s-4} \sum_{p,q,w} C(\lambda_p) C(\lambda_q) C(\lambda_w)$$

$$\times \lambda_p^{m+1} \lambda_q^{t-s+2} \lambda_w^{N-n+2} (\lambda_p - u)(\lambda_w - u) \qquad (4\text{-}82)$$

Although the sums can be evaluated in principle by integral with the condition that $N \gg 1$, $\sqrt{\sigma} \ll 1$, and $N\sqrt{\sigma} > 2$, the resulting equation involves too many terms to be manageable. Therefore, we here impose the same additional condition, $\beta\sqrt{(1-f)/f} > 5$, as in the calculation of $\langle S^2 \rangle_{app}$. The result then obtained is summed over i and j to give

$$\sum_{i<j} \langle r_{ij}^4 \rangle / 5N^2 = (Na_o^2/6)^2 (1-f)^2 \left\{ K_1^* + \frac{4}{\sqrt{\sigma}} \left(\frac{a_2}{a_o}\right)^2 \left(\frac{f}{1-f}\right)^{3/2} K_2^* \right.$$

$$\left. + \frac{4}{\sigma} \left(\frac{a_1}{a_o}\right)^4 \left(\frac{f}{1-f}\right)^3 K_3^* \right\} \qquad (4\text{-}83)$$

where

$$K_1^* = 1 + (4/\beta) f^{3/2} (1-f)^{-1/2} + 12(f/\beta)^2$$

$$- (24/\beta^3) f^{5/2} (3-5f)(1-f)^{-1/2} + (120/\beta^4) f^3 (1-2f) \qquad (4\text{-}84)$$

$$K_2^* = 1 - (4/\beta)(2-f)[f(1-f)]^{1/2} + (12f/\beta^2)(2-f^2)(1-f)^{-1}$$

$$- (24/\beta^3)(f/1-f)^{3/2} [2-f^2 + (1-f)^2 (5f-2)]$$

$$+ (24/\beta^4)(f/1-f)^2 [2-f^2 + 3f(1-f)^2$$

$$-(1-f)^3 (7-10f)] \qquad (4\text{-}85)$$

$$K_3^* = 1 + \frac{4}{\beta}\frac{1}{f(1-f)}\left[(1-f)^2 - 2f + \frac{4}{5}\right] + \frac{12}{\beta^2}\left[f^2 + 2f - 6 + \frac{3(1-f)}{5}\right] + \frac{24}{\beta^3}\frac{f^{1/2}}{(1-f)^{3/2}}\left[(1-f)^3(5f-1) + (1-f)^2\left(2f + \frac{17}{5}\right) + 4\left(\frac{6-5f}{5}\right)\right] - \frac{24}{\beta^4}\left\{10f^2(1-f)(2-f) + f(5f-8)\frac{[(1-f)^3-1]}{(1-f)^2} + \frac{26f^2}{5}\right\} \qquad (4\text{-}86)$$

For infinitely large N, K_1^*, K_2^*, and K_3^* become unity, and equation (4-83) is simplified to

$$\sum_{i<j} \langle r_{ij}^4 \rangle / 5N^2 = (Na_o^2/6)^2(1-f)^2\left\{1 + \frac{2}{\sqrt{\sigma}}\frac{a_1}{a_o}^2\left(\frac{f}{1-f}\right)^{3/2}\right\}^2 \qquad (4\text{-}87)$$

It is seen from equation (4-28) that the right-hand side of equation (4-87) is identical to $\langle S^2 \rangle^2$. Thus unless f = 1, $\sum_{i<j} \langle r_{ij}^4 \rangle$ for infinite N obeys the relation expected for Gaussian chains.

Simple analytical expressions for the averages of higher even moments $\langle r_{ij}^{2p} \rangle$ (p > 2) do not seem to be derivable when N is finite. However, an asymptotic expression for $\langle r_{ij}^6 \rangle$ valid at the limit of infinite N can be obtained without difficulty. It reads

$$\langle r_{ij}^6 \rangle = \frac{70}{3}\left\{\sum_{i<m<s<n\le j} \langle r_m^2 r_s^2 r_n^2 \rangle + 6\sum_{i<m<s<t<n\le j} \langle r_m^2 \overline{r_s r_t}\, r_n^2 \rangle + 12\sum_{i<m<s<t<h<n\le j} \langle r_m^2 \overline{r_s r_t}\, \overline{r_h r_n} \rangle\right.$$

$$+ 8 \sum_{i<m<s<t<h<k<n\leq j} \langle \overline{r_m r_s}\ \overline{r_t r_h}\ \overline{r_k r_n} \rangle \Big\} \qquad (4\text{-}88)$$

If a procedure similar to that used for the derivation of equation (4-87) is applied, this eventually gives

$$\sum_{i<j} \langle r_{ij}^6 \rangle = 42N^2 \langle S^2 \rangle^3 \qquad (4\text{-}89)$$

unless f = 1. This relation is known for Gaussian coils. Thus substitution of equations (4-87) and (4-89) into equation (4-69) gives

$$\lim_{N\to\infty} P(\theta) = 1 - \frac{k^2\langle S^2\rangle}{3} + \frac{k^4\langle S^2\rangle^2}{12} - \frac{k^6\langle S^2\rangle^3}{60} + \cdots \qquad (4\text{-}90)$$

which agrees that for Gaussian coils at least up to the term of k^6. In passing, equation (4-90) can be shown to hold even if each term in it is calculated by taking the copolymer nature into account.

Now we define a quantity G by

$$G = \sum_{i<j} \langle r_{ij}^4 \rangle / 5N^2 \langle S^2 \rangle^2 \qquad (4\text{-}91)$$

Since it tends to unity for a Gaussian coil and to 24/25 for a rigid rod, this quantity will be very insensitive to the geometry of the molecule. In Figure 4.2 are presented the curves of G against f for various N and $\sigma = 10^{-4}$, $a_0 = 15$ A, and $a_1 = 1.5$ A. We have restricted the numerical calculations to f smaller than the value which fulfills the condition,

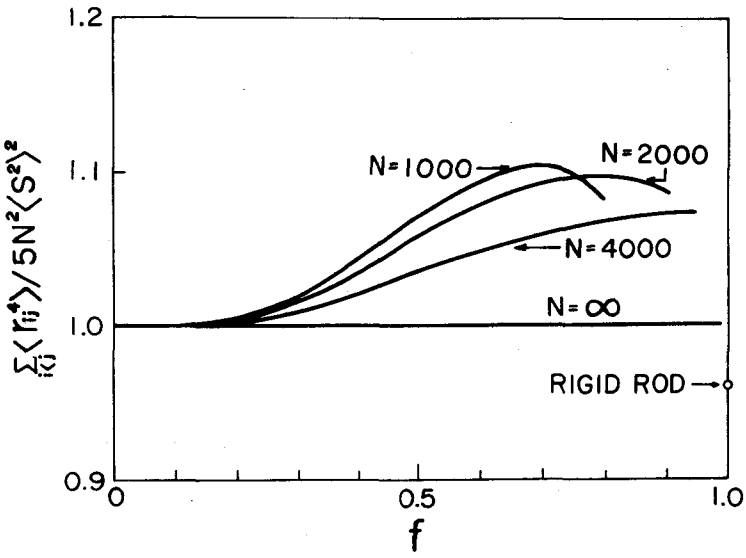

Figure 4.2. Plots of G ($= \sum_{i<j} \langle r_{ij}^4 \rangle / 5N^2 \langle S^2 \rangle^2$) against f as a function of N. The parameters chosen are: $\sigma = 10^{-4}$, a_o = 15 A, and a_1 = 1.5 A. The value of G at f = 1 (rigid rod) indicated by a circle is 24/25.

$\beta\sqrt{(1-f)/f} > 5$, on which $\sum_{i<j} \langle r_{ij}^4 \rangle$ was derived. Interestingly, G attains a broad maximum before decreasing to the value for a rod and the Gaussian behavior characteristic of infinite chain is not approached even at an N as large as 4000. This latter feature is associated with the fact, evident from equations (4-26) and (4-83), that it is the parameter β, not N itself, that primarily governs deviations of finite chains from the Gaussian limit.

In terms of equation (4-91), equation (4-69) may be recast in the form:

$$P(\theta)^{-1/2} = 1 + \frac{k^2\langle S^2\rangle}{6} + \frac{k^4}{24}(1 - G)\langle S^2\rangle^2 \qquad (4\text{-}92)$$

with the omission of terms higher than k^6. Plots of $P(\theta)^{-1/2}$ vs. $k^2\langle S^2\rangle$ for a Gaussian coil should follow the initial tangent over a relatively wide range of $k^2\langle S^2\rangle$, because the third term on the right-hand side of equation (4-92) vanishes for this type of chain.[102] The coefficient of this third term is as small as 1/600 for a rigid rod. Indeed, numerical calculations indicate that equation (4-92) gives a good approximation to the exact $P(\theta)^{-1/2}$ for both coils and rods if $k^2\langle S^2\rangle < 3$.[103] We therefore discuss $P(\theta)$ for polypeptide molecules in terms of this equation.

The solid lines in Figure 4.3 present values of $P(\theta)^{-1/2}$ at fixed f as a function of $\sin^2(\theta/2)$ for typical values of the parameters: $N = 2000$, $\sigma = 10^{-4}$, $a_0 = 15$ A, $a_1 = 1.5$ A, and $\lambda' = 3113$ A; the lines at $f = 0$ and 1 have been calculated from the exact light-scattering functions relevant for each.[103] The dotted lines in the figure represent the initial tangents to the solid lines. It is seen that $P(\theta)^{-1/2}$ vs. $\sin^2(\theta/2)$ follows the initial tangent over an extended range, provided that f is not too close to unity. Thus, this type of plot will allow $\langle S^2\rangle$ of a polypeptide molecule to be determined from light-scattering data even when the molecule is in the state of interrupted helix.

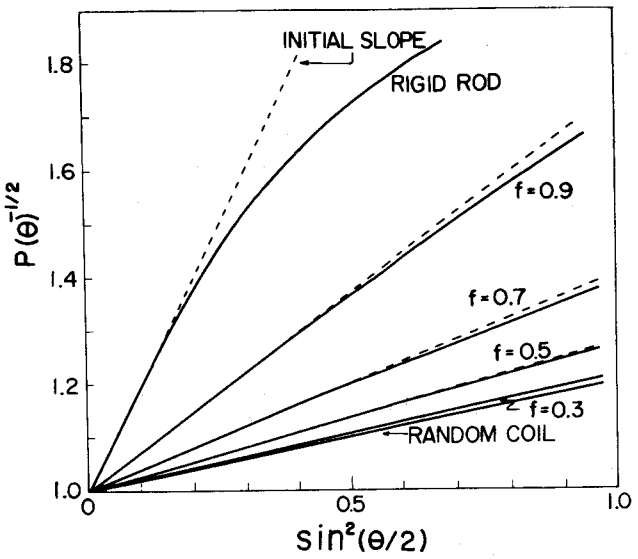

Figure 4.3. $P(\theta)^{-1/2}$ at fixed f as functions of $\sin^2(\theta/2)$ for the parameters: N = 2000, $\sigma = 10^{-4}$, a_0 = 15 A, a_1 = 1.5 A, and λ' = 3113 A. The solid lines for intermediate f represent the values calculated according to equation (4-92), and the dotted lines indicate the initial tangents to the solid lines. The solid lines for rigid rod and random coil denote the values calculated from the exact light-scattering functions.[103]

4-4. Calculations of $\langle R^4 \rangle$ and Higher Even Moments

The average fourth moment of the end-to-end distance, $\langle R^4 \rangle$, of a polypeptide molecule was calculated by Gō, Saito, and Ochiai[53] on the basis of the Lifson-Roig theory.[28] However, their equation and numerical results were in error, as pointed out recently by Saito himself[104] and by Birshtein.[105] The latter author has given the correct form of $\langle R^4 \rangle$, which

can be recast in the form of equation (4-71) with i = 0 and j = N. Our approximate treatment allows a straightforward calculation of $\langle R^4 \rangle$. Substitution of i = 0 and j = N into equations (4-72) – (4-81) and replacement of the summations by integrals, subject to the conditions that $N \gg 1$, $\sqrt{\sigma} \ll 1$, and $N\sqrt{\sigma} > 2$, lead to

$$\langle R^4 \rangle = \frac{5}{3}(Na_o^2)^2(1-f)^2\left\{Y_1 + \frac{4}{\sqrt{\sigma}}\left(\frac{a_1}{a_o}\right)^2\left(\frac{f}{1-f}\right)^{3/2}Y_2 + \frac{4}{\sigma}\left(\frac{a_1}{a_o}\right)^4\left(\frac{f}{1-f}\right)^3 Y_3\right\} \tag{4-93}$$

where

$$Y_1 = 1 + \frac{6}{\beta}\frac{f^{3/2}}{\sqrt{1-f}} + \frac{6}{\beta^2}f^2(2f-1)(1-f) \tag{4-94}$$

$$Y_2 = 1 - \frac{6}{\beta}\sqrt{f(1-f)} + \frac{12}{\beta^2}f(1-f) \tag{4-95}$$

and

$$Y_3 = 1 + \frac{6}{\beta}\frac{1}{\sqrt{f(1-f)}}\left[(1-f)^2 - \frac{2}{5}\right] + \frac{2}{\beta^2}\left[(1-f)(6f-5) + 4\left(f-\frac{2}{5}\right) + \frac{15f-12}{5(1-f)}\right] + W(\beta,f)\exp\left[-\beta\sqrt{\frac{1-f}{f}}\right] \tag{4-96}$$

with $W(\beta,f)$ defined by

$$W(\beta,f) = \frac{4}{5f^3} + \frac{2}{\beta\sqrt{f(1-f)}}\left[f - 2 + \frac{(1+f)(1-f)^3}{f^3} + \frac{8(2f-1)}{5f^3}\right] + \frac{2}{\beta^2}\left[\frac{(f-4)}{(1-f)} + \frac{4(2+f)}{5f(1-f)} + \frac{3(1-f)}{f^2} + \frac{8(1-2f)(1-f)}{5f^3} - \frac{(15f-7)(1-f)^3}{5f^4}\right] \tag{4-97}$$

At the limit of infinite N, Y_1, Y_2, and Y_3 tend to unity. So equation (4-93) reduces to

$$\langle R^4 \rangle = (5/3)(Na_o^2)^2(1-f)^2\left[1 + \frac{2}{\sqrt{\sigma}}\left(\frac{a_1}{a_o}\right)^2\left(\frac{f}{1-f}\right)^{3/2}\right]^2 \qquad (4\text{-}98)$$

It follows from this equation and equation (4-23) that unless f = 1,

$$\langle R^4 \rangle = \frac{5}{3}\langle R^2 \rangle^2 \qquad (4\text{-}99)$$

Although we have omitted the first sum in equation (4-78) to derive equation (4-93), equation (4-99) is strictly valid for infinite N unless f = 1. Similarly, from equation (4-88) for $\langle r_{ij}^6 \rangle$ valid at the limit of infinite N, we obtain

$$\langle R^6 \rangle = \frac{35}{9}\langle R^2 \rangle^3 \qquad (4\text{-}100)$$

provided that f < 1. These equations also satisfy

$$\langle R^{2p} \rangle = \frac{(2p+1)!}{6^p\, p!}\langle R^2 \rangle^p$$

which is valid for Gaussian coils. This and other arguments so far presented would suffice to conclude that a polypeptide chain with infinite N behaves as a Gaussian coil unless f = 1. In fact, this conclusion derives, without recourse to a particular molecular model, from the general consideration of

Nagai[106] on the conformation of stereoregular polymer molecules.

The ratio of $\langle R^4 \rangle$ to $(5/3)\langle R^2 \rangle^2$ varies from unity for a Gaussian coil to 3/5 for a rigid rod. Figure 4.4 illustrates how this ratio for given N varies with f for the case where $\sigma = 10^{-4}$, $a_0 = 15$ A, and $a_1 = 1.5$ A. The ratio is almost equal to unity for $f < 1/2$ and decreases gradually toward 3/5 as f approaches unity. The deviation from Gaussian behavior becomes less pronounced as N increases. Very recently, Gō and Saito[107] made a revised calculation of $\langle R^4 \rangle$ on the basis of the theory of Lifson and Roig[28] and arrived at substantially the same results as shown here.

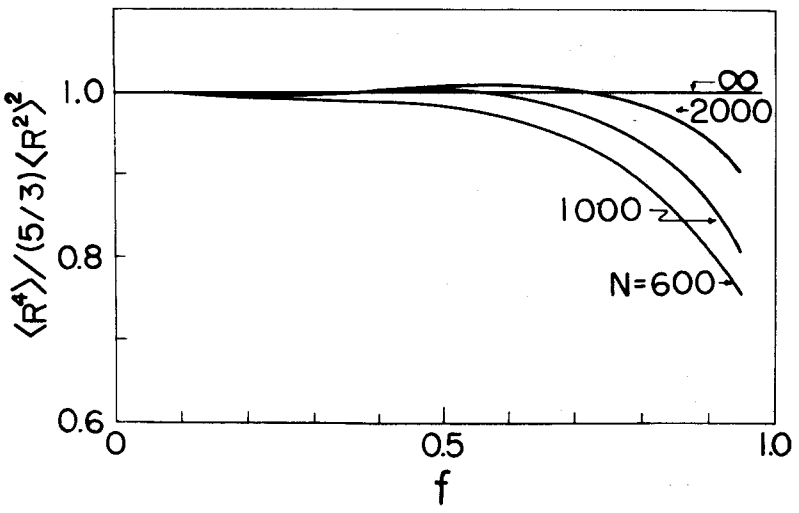

Figure 4.4. Fourth moment of the end-to-end distance $\langle R^4 \rangle$ relative to $(5/3)\langle R^2 \rangle^2$ for various N. The parameters chosen are the same as those in Figure 4.2. The value of the moment at f = 1 (rigid rod) is 0.6.

Chapter 5

Light-Scattering Study of Poly(γ-Benzyl L-glutamate) in the Helix-Coil Transition Region

5-1. Introduction

It has been shown in Chapter 4 that Nagai's exact expression[27] for the mean-square radius of gyration, $\langle S^2 \rangle$, of a helix-forming polypeptide in solution can be simplified to a form which is amenable to a comparison with experiment. Such a comparison was performed in a recent paper of Okita, Teramoto, and Fujita,[58] who treated poly-N^5-(3-hydroxypropyl) L-glutamine (PHPG) in mixtures of water and methanol. This chapter concerns a similar study made with PBLG in a mixture of DCA and cyclohexanol (CHL). Dimensions of this polypeptide in a helicogenic solvent DMF are also investigated, with special interest in the molecular weight dependence of the pitch of helix per monomeric residue.

5-2. Experimental

5-2-1. Polypeptide Samples

In addition to PBLG samples E-1 and E-3 used in Chapter 2, the following three samples were chosen for the present investigation. One of them was a gift from Dr. Yamashita, who had polymerized it with a mixture of $P(C_4H_9)_3$ and $N_i(OCOCH_3)_2 \cdot 4H_2O$ as an initiator.[108] It was fractionated in

the manner described in Chapter 2, and a middle fraction F-2 was chosen. Two other samples, E-2 and A-X, were appropriate middle fractions of previously prepared samples.

Solutions of PBLG in a DCA-CHL mixture (91.7 wt% DCA) were made up as in Chapter 2. In spite of the experimental difficulty mentioned there, we chose this particular solvent mixture, because, as had been found by Strazielle, Dufour, and Marchal,[59] the refractive indices of the two components were almost identical so that effects of preferential adsorption might be minimized.

5-2-2. Specific Refractive Index Increments

Measurements of specific refractive index increment $(\partial n/\partial c)$ were carried out on a differential refractmeter of the modified Schulz-Cantow type at 25°C. The calibration of the instrument was made with aqueous solutions of highly purified KCl, and the data of Kruis[109] were taken as the reference value. The results were 0.121_0 (ml/g) at the wavelength of 436 nm and 0.117_1 at 546 nm for DMF, and 0.092_5 at 546 nm for the DCA-CHL mixture. The values for DMF are in agreement with those of previous workers.[4,59–65,72] Since we found no detectable dependence of $(\partial n/\partial c)$ on molecular weight, the δ value defined by equation (4-37) was taken to be zero, and hence the copolymer nature of interrupted helices was neglected in the subsequent treatments.

5-2-3. Light-Scattering Photometry

Use was made of a Shimazu light-scattering photometer with cylindrical cells. The circular uniformity of each cell was checked with a dilute solution of fluorescein (about 10^{-6} mol/liter). The apparatus was calibrated with pure benzene of 25°C using unpolarized light of the wavelengths of 436 and 546 nm. The Rayleigh ratios of benzene of 25°C at right angle to the incident beam were taken to be 46.5 x 10^{-6} and 16.1 x 10^{-6} for 436 nm and 546 nm, respectively.[110] Solutions and solvents were made free of dust and microgels by centrifugation for an hour at 20,000 g, and then they were directly pipetted into the cell.

Measurements were made with unpolarized light of the wavelenths of 436 nm and 546 nm in the angular range from 35° to 135°. DMF solutions were examined at a single temperature of 25°C, at 436 nm for five samples and also at 546 nm for sample E-1. DCA-CHL solutions were examined for samples E-1 and F-2 at 546 nm in the temperature range from 10° to 30°C. The temperatures of each test solution were regulated to within ± 0.02° of the selected temperatures. The data were corrected for the back reflection of the incident beam by the method of Kratohvil.[111]

5-3. Results and Data Analysis

5-3-1. Analysis of Light-Scattering Data in DMF Solutions

If the effects of copolymer nature and preferential

adsorption can be ignored, the reduced intensity, R_θ, of scattered light from a dilute polymer solution is given by

$$\frac{Kc}{R_\theta} = \frac{1}{\bar{M}_w P(\theta)} + 2A_2 c \frac{P_2(\theta)}{[P(\theta)]^2} + O(c^2) \qquad (5\text{-}1)$$

Here K is the familiar light-scattering constant, $\bar{M}_w$ the weight-average molecular weight of the dissolved polymer, c its concentration, θ the scattering angle, A_2 the second virial coefficient of the solution, and $P(\theta)$ and $P_2(\theta)$ the intra- and intermolecular scattering functions, respectively.

Recent investigations[102,112,113] of randomly coiled polymers have shown that a plot of $(Kc/R_\theta)^{1/2}$, rather than Kc/R_θ, vs. c facilitates a determination of $P(\theta)$. We expected that this might be the case for polypeptides regardless of their conformations.

Figure 5.1 shows this type of plot for sample E-1 in DMF at 25°C. It can be seen that the data points at fixed θ follow a straight line and allow the ordinate intercept to be estimated with accuracy. The values of $(Kc/R_\theta)_{c=0}$ thus obtained are related to $\langle S^2 \rangle$ by

$$(Kc/R_\theta)_{c=0} = [\bar{M}_w P(\theta)]^{-1}$$

$$= (1/\bar{M}_w)[1 + (k^2/3)\langle S^2 \rangle + \cdots] \qquad (5\text{-}2)$$

where k^2 is a constant proportional to $\sin^2(\theta/2)$ defined by equation (4-34). Thus $\langle S^2 \rangle$ can be determined from the initial

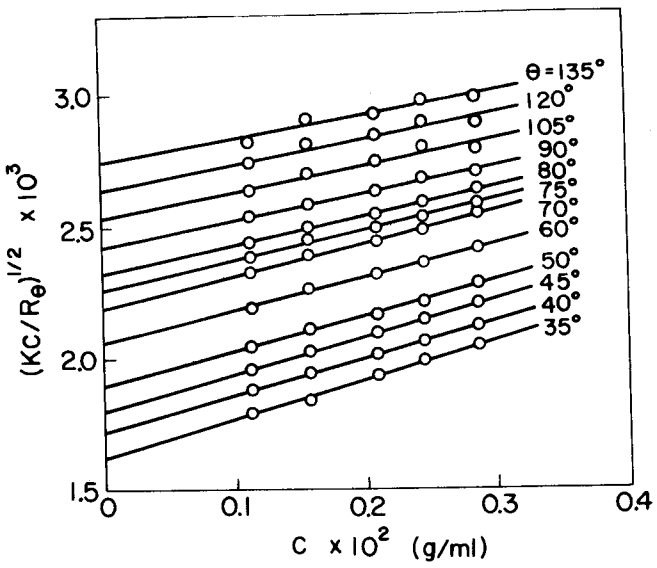

Figure 5.1. Concentration dependence of $(Kc/R_\theta)^{1/2}$ at the wavelenth of 436 nm for PBLG sample E-1 in DMF of 25°C at the indicated scattering angles.

slope of a plot of $(Kc/R_\theta)_{c=o}$ vs. $\sin^2(\theta/2)$. Note that it was shown in Chapter 4 (Figure 4.3) that if the sample is homogeneous, a plot of $P(\theta)^{-1/2}$, rather than $P(\theta)^{-1}$, vs. $\sin^2(\theta/2)$ follows the initial tangent over a broader range irrespective of its conformation. However, it should be noted that the $P(\theta)^{-1}$ plot for a polydisperse rigid rod is likely to follow the initial tangent over a wide range of $\sin^2(\theta/2)$ than the corresponding square-root plot does.

Figure 5.2 shows the data for five samples in DMF at 25°C. The dashed lines indicate the initial tangents from which $\langle S^2 \rangle$ for these samples have been estimated. There exists a fairly wide range of linear portion in either type

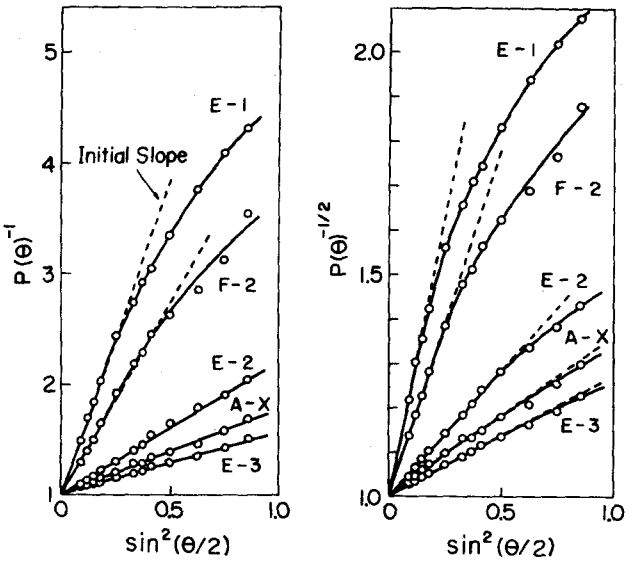

Figure 5.2. Plots of $P(\theta)^{-1}$ and $P(\theta)^{-1/2}$ vs. $\sin^2(\theta/2)$ at 436 nm for PBLG samples studied in DMF at 25°C. The dashed lines indicate the initial tangent from which $\langle S^2 \rangle$ for each sample has been evaluated.

of plot for samples E-2, A-X, and E-3. So the $\langle S^2 \rangle$ of these samples can be evaluated accurately. On the other hand, for samples E-1 and F-2, we must rely only on a few data points at low scattering angles in order to determine the initial slope. This gives rise to a considerable uncertainty in the estimate of $\langle S^2 \rangle$. A correct value of $\langle S^2 \rangle$ may presumably lie between the values obtained by the two types of plot. Therefore, their averages have been taken as the desired ones.

Since both $P(\theta)$ and $P_2(\theta)$ tend to unity at $\theta = 0$, equation (5-1) becomes

$$Kc/R_o = 1/\bar{M}_w + 2A_2c + \cdots \qquad (5\text{-}3)$$

which may be rewritten

$$(Kc/R_o)^{1/2} = (1/\bar{M}_w)^{1/2} + A_2\bar{M}_w^{1/2}c + \cdots \qquad (5\text{-}4)$$

The latter equation is expected to give a better representation of experimental data for the reason mentioned before.

Figure 5.3 shows plots of $(Kc/R_o)^{1/2}$ vs. c for the five PBLG samples in DMF at 25°C. Each plot follows a straight line, whose ordinate intercept and slope permit the precise determination of $\bar{M}_w$ and A_2. Numerical data thus obtained are summarized in Table 5.1. Here the estimated uncertainty of

Table 5.1. Light-scattering data for PBLG in DMF at 25°C

Sample code	$\bar{M}_w \times 10^{-4}$	$A_2 \times 10^4$ (ml mol/g^2)	$\langle s^2 \rangle^{1/2}$ (A)	h (A)
E-1	$56._7$	2.2_4	1020 ± 70	1.36 ± 0.09
F-2	$47._7$	2.5_4	765 ± 15	1.22 ± 0.02
E-2	$23._7$	2.4_6	450 ± 10	1.44 ± 0.03
A-X	$18._8$	2.5_3	36_8	1.4_8
E-3	$15._8$	2.7_8	31_5	1.5_1

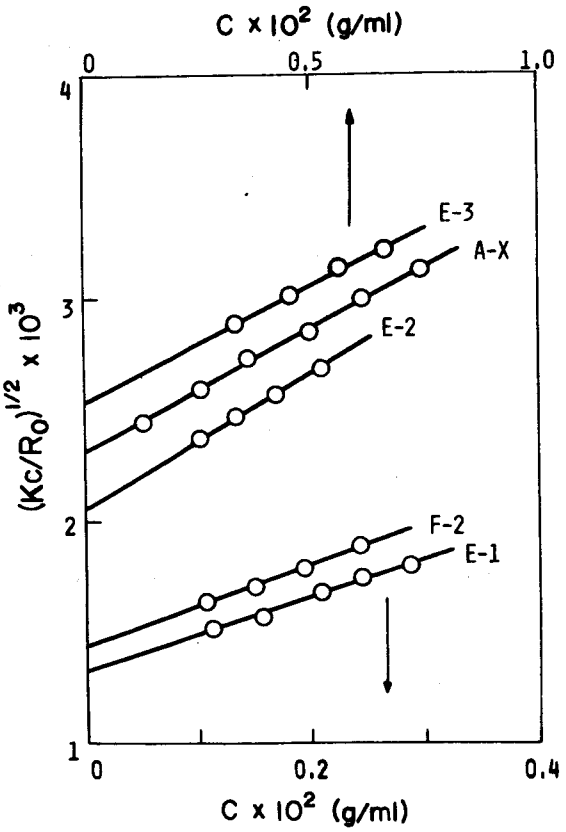

Figure 5.3. Plots of $(Kc/R_o)^{1/2}$ vs. c for the five samples in DMF at 25°C; the upper c scale for E-3, A-X, and E-2 and the lower c scale for F-2 and E-1.

$\langle S^2 \rangle^{1/2}$ is also recorded. The last column lists the values of h, the helical pitch per monomeric residue calculated by assuming a straight rod for the molecular shape. The h values decreases gradually with increasing molecular weight from 1.5 A characteristic of the α-helix. A detailed discussion of these results will be given later.

5-3-2. Data in s DCA-CHL Mixture

Figure 5.4 illustrates plots of $(Kc/R_o)^{1/2}$ vs. c for sample E-1 in the DCA-CHL mixture (91.7 wt% DCA) at 25°C. Here the data for the same sample in DMF at 436 and 546 nm are also shown for comparison. The plots for the different experimental conditions converge to a common ordinate intercept, yielding the same value for $\overline{M}_w$. This same behavior was observed for sample F-2. These results indicate that the preferential adsorption of DCA molecules, if any, had

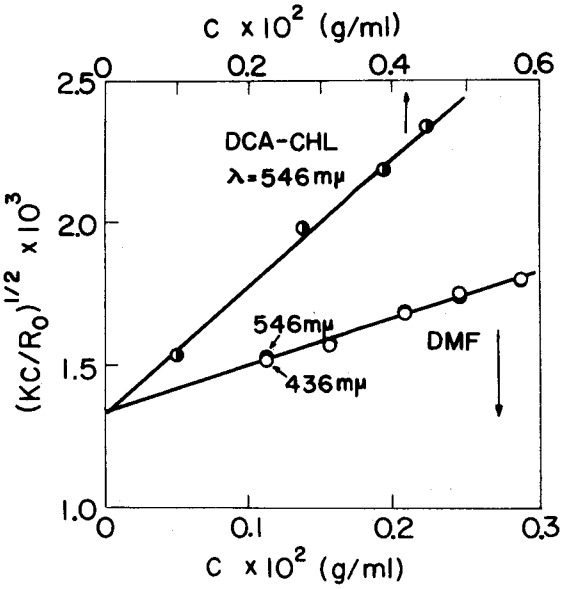

Figure 5.4. Representative plots of $(Kc/R_o)^{1/2}$ vs. c for sample E-1 in a DCA-CHL mixture (91.7 wt% DCA) and in DMF at 25°C. (◑) DCA-CHL at 546 nm, (○) DMF at 436 nm, and (●) DMF at 546 nm.

negligible effect on the molecular quantities derived from light-scattering measurements. This is consistent with an approximate equality of the refractive indices of the solvent components and with the observation by Strazielle, et al.[59] The data points for DMF at the two wavelengths come very close to each other, which implies a consistency of both sets of data.

Figure 5.5 shows plots of $P(\theta)^{-1/2}$ vs. $\sin^2(\theta/2)$ for sample E-1 in the DCA-CHL mixture at 546 nm as a function of temperature, in which the data for the same sample in DMF are also presented. The initial slope of the curve for the DCA-CHL

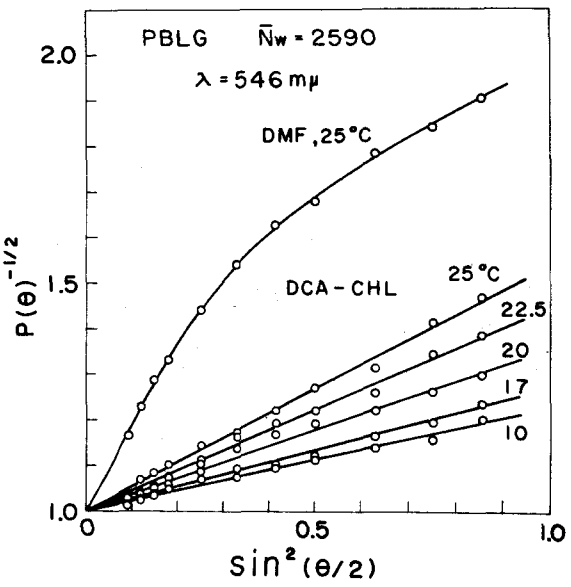

Figure 5.5. Representative plots of $P(\theta)^{-1/2}$ vs. $\sin^2(\theta/2)$ at 546 nm for E-1 in the DCA-CHL mixture and in DMF at the indicated temperatures.

mixture increases as the temperature is raised, which is an indication of the occurrence of a transition from coil to helix.

Figure 5.6 illustrates how $\langle S^2 \rangle^{1/2}$ of samples E-1 and F-2 in the DCA-CHL mixture vary with temperature. Comparison with Figure 2.6 shows that both $[\alpha]_{546}$ and $\langle S^2 \rangle^{1/2}$ display similar temperature dependence with an abrupt increase near 20°C. It must be noted, however, that PBLG is far from being perfectly helical in the DCA-CHL mixture even at the highest

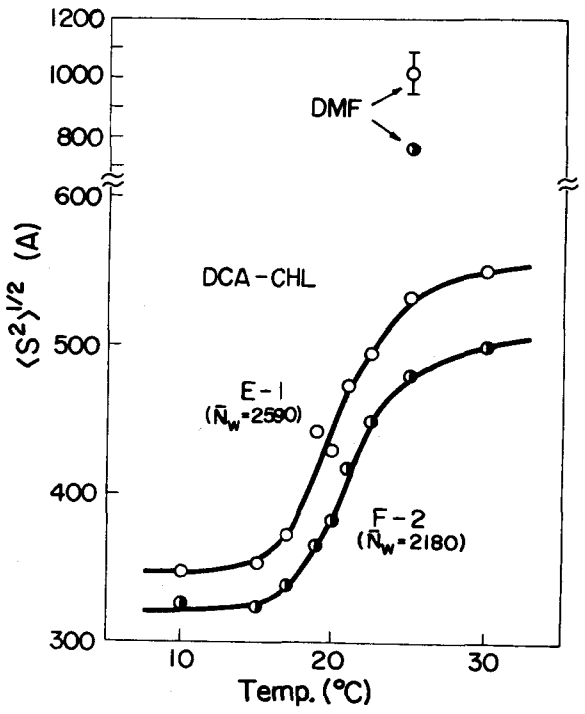

Figure 5.6. Temperature dependence of the root-mean-square radius of gyration $\langle S^2 \rangle^{1/2}$ for the indicated samples in the DCA-CHL mixture.

temperature studied. The $\langle S^2 \rangle^{1/2}$ vs. temperature curve for E-1 has close resembrance to that reported by Strazielle, et al.,[59] for a PBLG sample ($\bar{M}_w$ = 58 x 10^4) in a DCA-cyclohexane mixture, although these authors observed a shallow minimum in the neighborhood of the transition temperature. Figure 5.7 represents the change of $\langle S^2 \rangle^{1/2}$ with helical content f_N. The shape of each curve is substantially similar to that reported by Okita, et al.,[58] for PHPG in water-methanol mixtures. The relevant light-scattering data in the

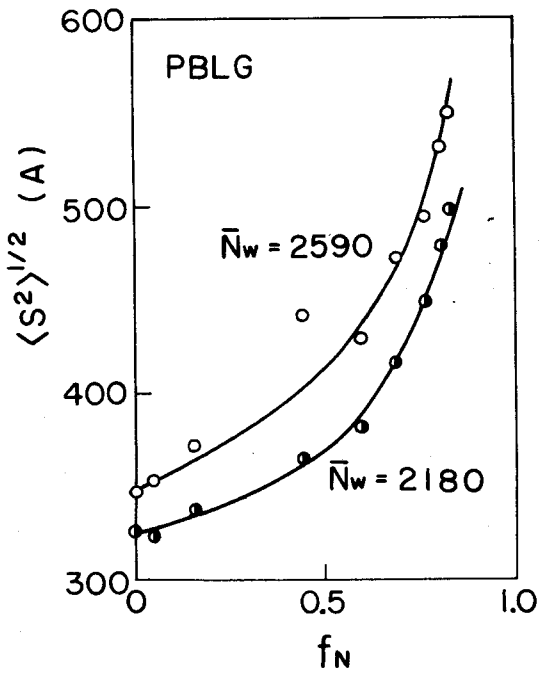

Figure 5.7. Changes in $\langle S^2 \rangle^{1/2}$ with helical content f_N for PBLG samples E-1 (○) and F-2 (◑) in the DCA-CHL mixture.

DCA-CHL mixture are summarized in Table 5.2.

Table 5.2. Numerical results of $\langle S^2 \rangle^{1/2}$ and A_2 for PBLG E-1 and F-2 in a DCA-CHL mixture (91.7 wt% DCA)

Temp. (°C)	E-1 ($\overline{M}_w$ = 56.7 x 10^4) $\langle S^2 \rangle^{1/2}$ (A)	E-1 A_2 x 10^4 (ml mol/g^2)	F-2 ($\overline{M}_w$ = 47.7 x 10^4) $\langle S^2 \rangle^{1/2}$ (A)	F-2 A_2 x 10^4 (ml mol/g^2)
10	34_7	3.3_2	32_6	3.3_0
15	35_3	3.6_2	32_4	3.2_2
17	37_2	3.2_5	33_8	3.2_7
19	44_2	2.8_4	36_6	3.4_5
20	43_0	3.1_4	38_2	2.7_7
21	47_3	3.2_5	41_7	2.8_8
22.5	49_5	2.8_9	44_9	2.8_8
25	53_2	2.9_7	48_0	2.8_5
30	55_0	2.7_6	49_9	2.5_7

5-4. Discussion

5-4-1. Analysis of $\langle S^2 \rangle$ Data for Interrupted Helices

It has been shown in Chapter 4 that Nagai's exact expression[27] for $\langle S^2 \rangle$ can be replaced approximately by

$$H_1/H_2 = a_o^2 + a_1^2 H_3/H_2 \qquad (5\text{-}5)$$

where H_1, H_2, and H_3 are defined by

$$H_1 = 6\langle S^2 \rangle / N(1 - f)$$

$$H_2 = 1 + \frac{12f^2}{\beta^2}\left[1 - \frac{2\sqrt{f(1-f)}}{\beta}\right]$$

and

$$H_3 = \frac{2}{\sqrt{\sigma}}\left(\frac{f}{1-f}\right)^{3/2} Q(\beta, f)$$

respectively (see Chapter 4). If both a_o and a_1 are constant in the substantial range of the transition, a plot of H_1/H_2 vs. H_3/H_2 should give a straight line whose slope and ordinate intercept are equal to a_1^2 and a_o^2, respectively. We can now compute H_1/H_2 and H_3/H_2 for PBLG in the DCA-CHL mixture by making use of the $\langle S^2 \rangle$ data and the values of $\sqrt{\sigma}$ and f given in Table 2.4. Figure 5.8 shows the resulting plot of H_1/H_2 vs. H_3/H_2 for samples E-1 and F-2 in this solvent mixture. The plotted points are approximately fitted by a straight line, yielding $a_1 = 1.5_3 \pm 0.10$ A and $a_o = 16.9 \pm$

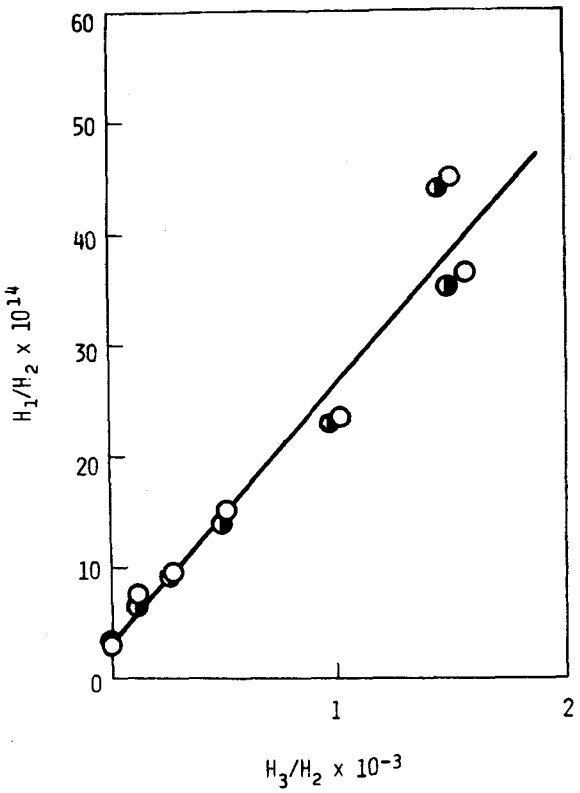

Figure 5.8. Analysis of the $\langle S^2 \rangle$ data for PBLG in the DCA-CHL mixture (91.7 wt% DCA) in terms of equation (5-5). The symbols of the plotted points are the same as those in Figure 5.7.

0.2 A. Actually, the latter value was estimated directly from the values of $\langle S^2 \rangle$ for the two samples at 10°C where their helical contents were zero. The value of a_o is in agreement with 16.7 A calculated from the $\langle S^2 \rangle$ data of Strazielle, et al.,[59] for a PBLG sample ($\overline{M}_w = 58 \times 10^4$) in a DCA-cyclohexane mixture at 15°C.

Okita, et al.,[58] reported a similar analysis of $\langle S^2 \rangle$

data for PHPG in mixtures of water and methanol. Table 5.3 summarizes the values of a_1 and a_0 for PBLG and PHPG. The values of a_1 compare well to 1.5 A expected for the α-helix. On the other hand, the values of 16.9 and 15 A for a_0 are much larger than 11.3 A deduced for unperturbed polypeptide chains by Brant and Flory[114] (see also 6-3-2 of Chapter 6). The excluded-volume effects may be a dominant factor for the disparity among these a_0 values. Brant and Flory obtained a value of 1.51 for the linear expansion factor of PBLG in DCA. This value multiplied by 11.3 A leads to a_0 = 17.1 A, which is in good agreement with the present value, 16.9 A.

The data shown in Figure 5.8, for all the conformity to

Table 5.3. Size parameters a_0 and a_1 characterizing the chain dimensions of polypeptides in solution

Polypeptide	Solvent	a_0 (A)	a_1 (A)	Reference
PBLG	DCA-CHL	16.9±0.2	1.53±0.10	This work
PHPG	water-methanol	15.0±0.5	1.65±0.05	Okita, et al.[58]
unperturbed chain		11.3	---	Brant-Flory[114]
		11.2±0.5	---	This work (see Chapter 6)
α-helix		---	1.5	

the theoretical prediction, do not necessarily imply that a_0 is strictly constant, since the intercept of the straight line is so small that the behavior of the plot may be insensitive to the change in a_0. The slope of this type of plot is substantially determined by the values of H_3 for f larger than about 0.5, and all that needed is is that a_1 is nearly constant in such a region.

In conclusion, the above results lend experimental support to Nagai's theory[27] and subsequent developments[50-53] on the mean dimensions of polypeptide molecules in the helix-coil transition region. Another important conclusion is that the helical sections of interrupted helices consist of the α-helix.

5-4-2. Average Dimensions in Helicogenic Solvents

Figure 5.9 shows a plot of h vs. $\bar{M}_w$ for PBLG in DMF at 25°C. For comparison, the data of previous workers[65,72,115,116] for this polymer in DMF and in EDC are also plotted.* The data points of these authors combined with the present data establish a definite trend of h as a function of $\bar{M}_w$. As has already been mentioned in Chapter 1, this trend implies that the α-helix formed by PBLG in helicogenic solvent either (1) is intact but has a certain flexibility as a whole or (2)

---

* The data of Fujita, et al.,[72] are reanalyzed with the square root plot and the value of 46.5×10^{-6}, instead of 48.5×10^{-6}, taken for the Rayleigh ratio for pure benzene of 25°C at 436 nm.

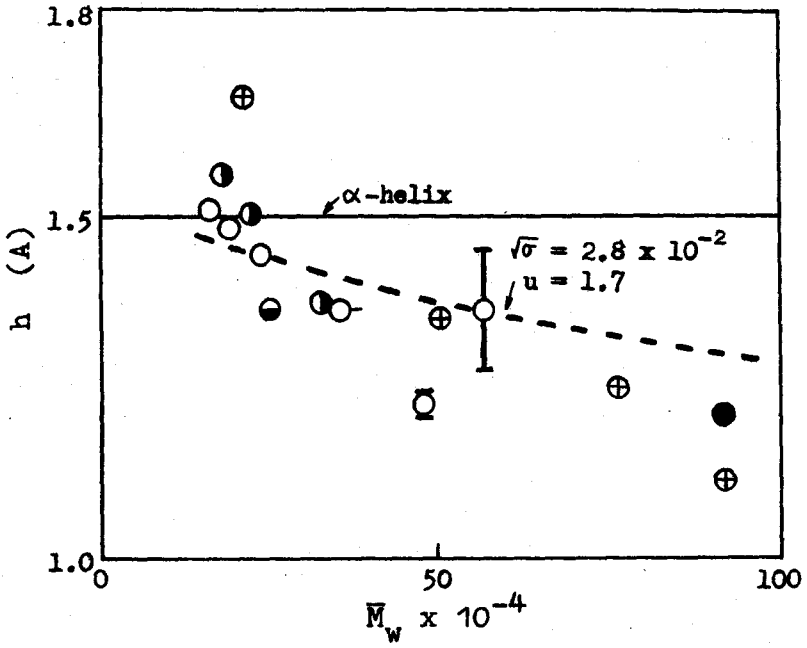

Figure 5.9. Molecular weight dependence of the pitch per monomeric residue, h, for PBLG in DMF and in EDC derived from light-scattering measurements. Data in DMF: (○) present work, (◎) Fujita, et al.,[72] (see text), and (⊕) Moha, et al.[65] Data in EDC: (●) Moha, et al.,[65] (◑) Wallach and Benoit,[115] and (◒) Jennings and Jerrard.[116] The thin line is the value expected for the α-helix and the dashed line indicates the theoretically calculated curve from Nagai's exact expression[27] for $\langle S^2 \rangle$ by using the transition parameters indicated (see text).

contains one or more breaks in its middle portion. In the case (1), the molecule is compatible with the wormlike chain of Kratky and Porod,[74] whereas in the case (2), the molecule is the limiting form of an interrupted helix in which the content

of randomly coiled portions is very small.

Several workers[65-69] favored the wormlike chain for interpretation of light-scattering and hydrodynamic data in helicogenic solvents, and some of them concluded that the molecular conformation would be different from the α-helix. The most serious argument against this conclusion is the existence of ample evidence for the α-helical conformation in solution.[117,118]

On the other hand, Miller and Flory[50] have presented for the interrupted helix model several sets of values for σ and u which allow the calculated chain dimensions to be in reasonable agreement with experimental data. However, there arises a question of whether the values of σ and u chosen for their numerical computations were really descriptive of PBLG in helicogenic solvents. The direct answer is difficult because the evaluation of these parameters in helicogenic solvents are not feasible. Here we simply remark that $\sqrt{\sigma} = 2.8 \times 10^{-2}$ and u = 1.7 for PBLG in pure EDC at 25°C deduced in Chapter 3 from the analysis of the solvent effects are consistent with the values assigned by Miller and Flory.

The dashed line in Figure 5.9 has been calculated for this set of $\sqrt{\sigma}$ and u by Nagai's exact equation.[27] It fits fairly well the data for both DMF and EDC solutions. This is taken to indicate the soundness of our values for σ and u. It is to be noted that the f value calculated for these values of parameters amounts to 0.9990.

The average number of helical sections in the molecule calculated by the exact expression of Nagai[27] with the same set of parameters were 1.2 for N = 500, 1.4 for N = 1000, and 2.2 for N = 3000. These numbers mean that a PBLG with N = 2560 (M = 56 x 10^4) in EDC consists, on the average, of two helical sections. A once-broken rod with a single break on its central portion gives 1.19 A for h. On the other hand, if the break appears at any portion on the chain with equal probability, h becomes 1.34 A. Interestingly, the latter value is in agreement with the value at $\bar{M}_w$ = 56 x 10^4 interpolated from the dashed line in Figure 5.9.

Chapter 6

Viscosity Behavior of Poly(γ-Benzyl L-glutamate) in Dilute Solution

6-1. Introduction

Limiting viscosity number (or intrinsic viscosity) $[\eta]$ is one of the fundamental quantities for the investigation of macromolecules in dilute solution. Several sets of experimental data[45,46,52,55-57,119-121] for $[\eta]$ of polypeptides in the region of helix-coil transition have been reported. In some cases,[45,46,52,55-57] they were compared with theories of mean dimensions. In quantitative terms, however, the chain dimensions, e.g., $\langle S^2 \rangle$, cannot be deduced from $[\eta]$ unless a relevant relation between them is established.

In this chapter, we examine viscosity behavior of PBLG in the helix-coil transition region, with the primary interest in the variations of $[\eta]$ with molecular weight and helical content. A brief discussion of the relationship between $[\eta]$ and $\langle S^2 \rangle$ is given on the basis of the data in a mixture of dichloroacetic acid (DCA) and cyclohexanol (CHL).

6-2. Experimental

The PBLG samples used were the same as those for the polarimetric and light-scattering measurements described in the previous chapters. All of them were examined in DCA and

dimethylformamide (DMF) at 25°C. Three samples, E-1, F-2, and E-2, were studied in DCA-ethylene dichloride (EDC) mixtures of various compositions which covered the entire range of helix-coil transition, and two samples, E-1 and F-2, in a DCA-CHL mixture (91.7 wt% DCA) at various temperatures between 10° and 30°C.

The viscometers used were of the Ubbelohde suspended-level type and of the ordinary Ostwald type, designed to have negligible kinetic-energy corrections under all conditions chosen for the present measurements. Temperature fluctuations were kept within ± 0.01°C. Correction for the shear-rate effect was unnecessary, except for samples E-1 and F-2 in DMF and in DCA-EDC mixtures (3, 10, and 50 vol% DCA) at 25°C, and for E-1 in a DCA-EDC mixture (65 vol% DCA) at temperatures above 15°C. For these systems, use was made of a rotating cylinder viscometer of the Zimm-Crothers type,[122] in which the temperature was regulated to within ± 0.02°C.

6-3. Results and Discussion

6-3-1. Relationships between $[\eta]$ and $\bar{M}_w$ for PBLG in DMF and in DCA

Results from the viscosity measurements on DMF and DCA solutions are summarized in Table 6.1. In Figure 6.1 are shown double-logarithmic plots of $[\eta]$ vs. weight-average molecular weight $\bar{M}_w$ for PBLG in DMF and DCA at 25°C.

Table 6.1. Viscosity data for PBLG in DMF and in DCA at 25°C

Sample code	$\bar{M}_w \times 10^{-4}$	$[\eta]$ (dl/g)	
		DMF	DCA
E-1	$56._7$	$12._8$	2.4_8
F-2	$47._7$	9.2_0	2.1_7
E-2	$23._7$	3.6_2	1.22
A-X	$18._8$	2.4_2	0.98_0
E-3	$15._8$	1.94	0.89_8
E-4	8.0_8	0.70_8	0.54_7
A-IV	6.3_5	0.52_6	0.45_0
A-6	3.7_0	0.238[a)]	0.301[a)]

a) Data of Nakagawa, et al.[79]

For comparison the data of Doty, Bradbury, and Holtzer[4] are included. Our data points in either solvent fall on a straight line over the range of $\bar{M}_w$ studied, yielding

$$[\eta]_{DMF} = 5.8_2 \times 10^{-8} \bar{M}_w^{1.45} \qquad (6\text{-}1)$$

$$[\eta]_{DCA} = 1.0_2 \times 10^{-4} \bar{M}_w^{0.76} \qquad (6\text{-}2)$$

The slope 1.45 for DMF, which is fair agreement with

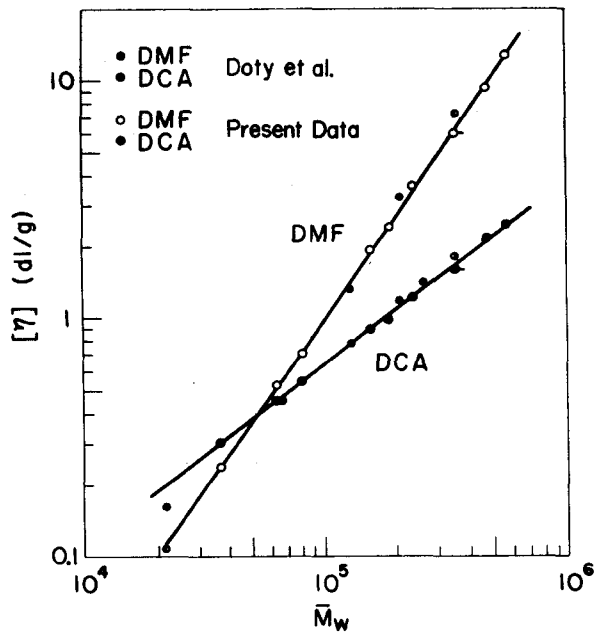

Figure 6.1. Relationships between intrinsic viscosity $[\eta]$ and weight-average molecular weight $\bar{M}_w$ for PBLG in DMF and in DCA at 25°C. (○) DMF and (●) DCA. The data points with the horizontal pip are those of Fujita, et al.,[123] (see text). Small circles (⦶) and (◑) are the data of Doty, et al.,[4] for DMF and DCA, respectively.

1.58 obtained by Spach, et al.,[71] but appreciably smaller than 1.7 expected for rigid rod molecules,[124] indicates that PBLG molecules in DMF are not rigid straight rods. This conclusion is consistent with the one from the light-scattering data in Chapter 5, but disagrees with Doty, et al.,[4] who found for this polypeptide in helicogenic solvents a larger slope compatible with the rigid rod model. Later, Fujita, et al.,[123] have confirmed the observation of Doty,

et al., in the range of relatively high molecular weights. However, since all the published data[4,71,123] give a single smooth curve when $[\eta]_{DMF}$ are plotted against $[\eta]_{DCA}$, the disparity among the reported slopes may be attributed to errors in molecular weight determination. In order to check this possibility, we reanalyzed the original light-scattering data of Fujita, et al.,[123] by the procedure adopted in Chapter 5 (see 5-4-2). The corrected data, indicated by circles with a horizontal pip in Figure 6.1, are now consistent with our data.

The value of 0.76 for the exponent for DCA solutions is typical of a randomly coiled polymer in a good solvent. Combination of Yamakawa's asymptotic solution of the excluded-volume effect[125] with the Flory-Fox relation[126] gives a value of 0.8 as the upper limit for this exponent. The value of 0.87 for PBLG in DCA reported by Doty, et al.,[4] exceeds this limit.

6-3-2. Unperturbed Dimension of PBLG

Recent studies[102,112,127] of the excluded-volume effects on randomly coiled polymers in dilute solution favor the fifth-power law for the linear expansion factor of statistical radius. However, as pointed out by Kawahara, Norisuye, and Fujita,[128] and subsequently by Tanaka, Imai, and Yamakawa,[129] the viscosity data still may be analyzed by the procedure of Kurata and Stockmayer[130] or of Stockmayer and Fixman[131] based

on the third-power law. This procedure makes use of the relation:

$$[\eta]/\bar{M}_w^{1/2} = K_\theta + CBA^{-3}\,\bar{M}_w^{1/2} \qquad (6\text{-}3)$$

where C is a numerical constant, B and A denote the long-range interaction and short-range interaction parameters, respectively, and K_θ is defined by

$$K_\theta = [\eta]_\theta/\bar{M}_w^{1/2} \qquad (6\text{-}4)$$

with $[\eta]_\theta$ being the value of $[\eta]$ at the θ-condition.

The Kurata-Stockmayer-Fixman plot for our data on PBLG in DCA is shown in Figure 6.2. The plotted points follow a straight line and yield a value of 1.00×10^{-3} for K_θ. The monomer length a_θ in the unperturbed state is related to K_θ by

$$a_\theta = (K_\theta/\Phi_\theta)^{1/3}\,M_o^{1/2} \qquad (6\text{-}5)$$

where M_o is the molecular weight of the monomeric residue and Φ_θ is the Flory constant at the theta state. Assuming Φ_θ to be $(2.3 \pm 0.3) \times 10^{21}$ and substituting $K_\theta = 1.00 \times 10^{-3}$ into equation (6-5), we obtain 11.2 ± 0.5 A for a_θ, which is in excellent agreement with 11.3 A deduced by Brant and Flory.[114] Our K_θ differs appreciably from the value 0.58×10^{-3} reported by Kurata and Stockmayer,[130] who deduced it from the viscosity data of Doty, et al.[4]

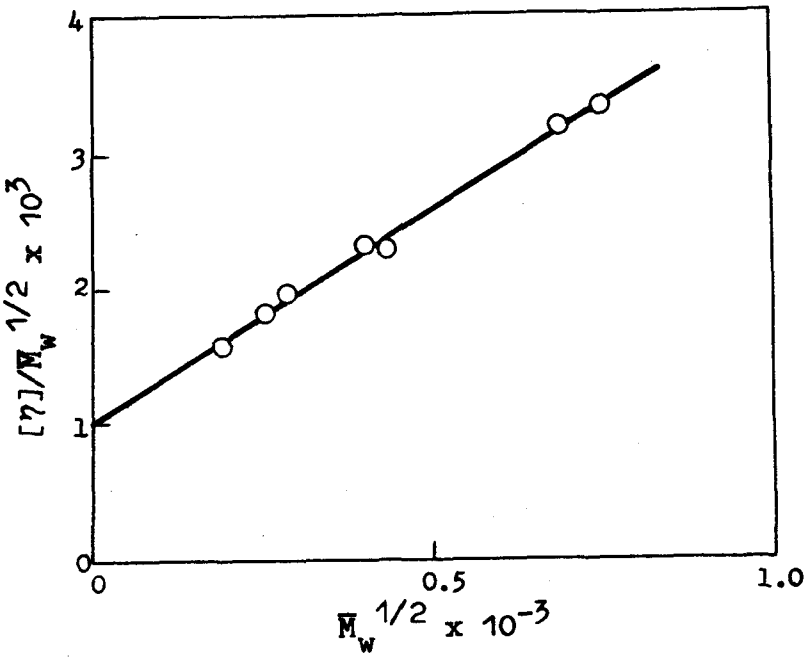

Figure 6.2. The Stockmayer-Fixman plot for PBLG in DCA at 25°C.

6-3-3. Viscosity Behavior in the Transition Region

Viscosity data for PBLG in DCA-EDC mixtures and in a DCA-CHL mixture (91.7 wt% DCA) are summarized in Table 6.2. The $[\eta]$ values of samples E-1 and F-2 in the DCA-CHL mixture at 10°C are appreciably smaller than the corresponding values in DCA at 25°C and those in a DCA-EDC mixture (70 vol% DCA) at 5°C. The disagreement may be accounted for by an excluded-volume effect, because PBLG molecules are randomly coiled in these solvents.

Figure 6.3 shows the temperature dependence of $[\eta]$ for

Table 6.2. Viscosity data for PBLG in DCA-EDC mixtures and in a DCA-CHL mixture

Solvent	Temp. (°C)	[η] (dl/g) Sample E-1	F-2	E-2
DCA-EDC				
70 (vol% of DCA)	5	2.5_1	2.1_6	1.24
	10	2.6_5	2.2_1	1.26
	12.5	2.9_9	2.3_4	1.29
	15	3.5_0	2.6_6	1.51
	17.5	4.4_2	3.3_2	1.76
	20	5.0_4	4.0_9	2.00
	25	5.5_4	4.6_0	2.2_5
65	5	3.5_2	2.4_1	1.31
	10	5.2_9	4.0_0	1.93
	15	6.3_4	4.7_1	2.3_6
	20	6.8_6	5.0_6	2.5_0
	25	7.0_4	5.1_6	2.5_4
50	25	8.2_8	6.0_2	2.7_8
10	25	10.3	7.3_2	3.2_3
3	25	10.9	8.0_6	3.3_8
DCA-CHL (91.7 wt% DCA)	10	2.2_2	1.86	
	15	2.2_5	1.90	
	17	2.4_6	1.99	
	19	3.7_9	2.7_3	
	20	4.7_3	3.6_3	
	21	5.5_1	4.1_7	
	22.5	5.8_0	4.6_9	
	25	6.1_9	4.8_5	
	30	6.2_8	5.0_0	

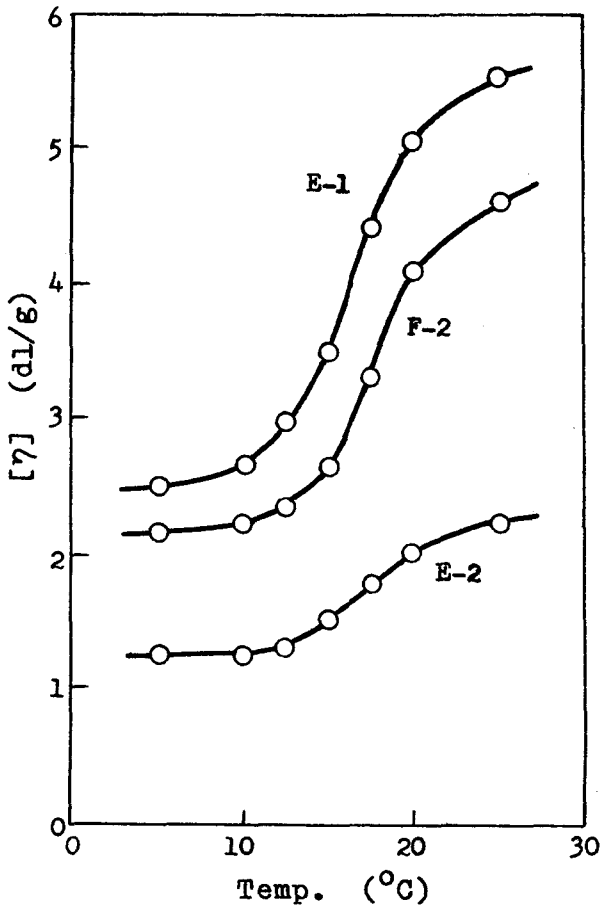

Figure 6.3. Temperature dependence of $[\eta]$ for PBLG E-1, F-2, and E-2 in a DCA-EDC mixture (70 vol% DCA).

samples E-1, F-2, and E-2 in a DCA-EDC mixture (70 vol% DCA). Similar plots for samples E-1 and F-2 in the DCA-CHL mixture are shown in Figure 6.4. These curves have close resembrance to those of optical rotation depicted in Figure 2.6 and of $\langle S^2 \rangle^{1/2}$ in Figure 5.6.

We now examine the variation of $[\eta]$ with helical content

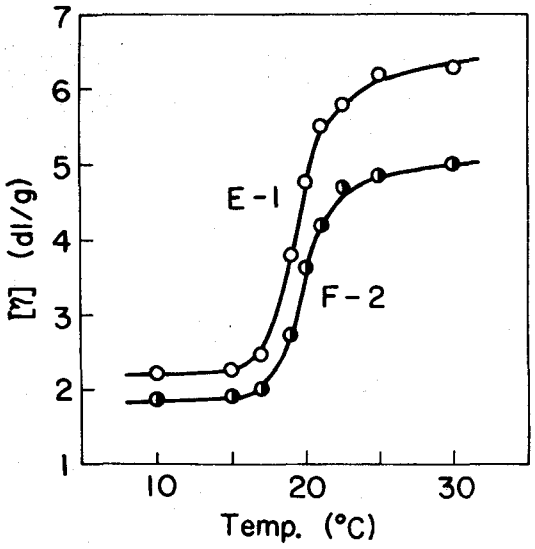

Figure 6.4. Temperature dependence of $[\eta]$ for PBLG E-1 and F-2 in a DCA-CHL mixture (91.7 wt% DCA).

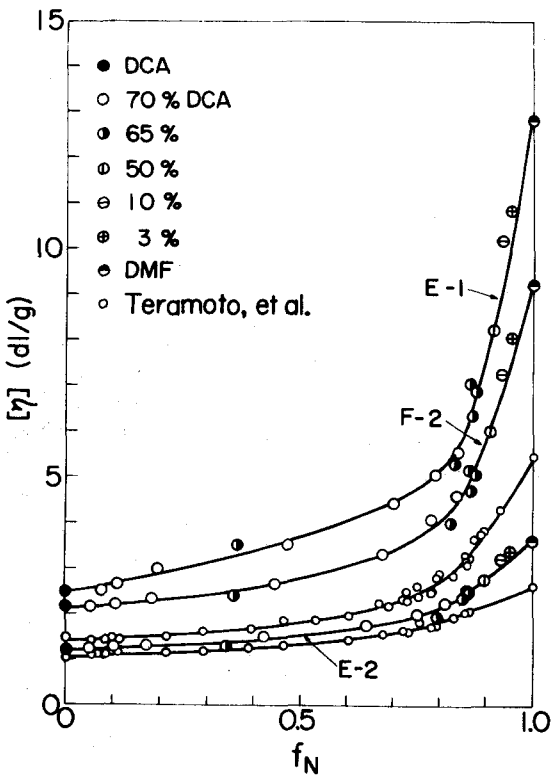

Figure 6.5. Variation of $[\eta]$ with helical content f_N for PBLG E-1, F-2, and E-2 in mixtures of DCA and EDC. (⊕) 3 % (vol % of DCA), (⊖) 10 %, (◑) 50 %, (◑) 65 %, (○) 70 %, (●) DCA, and (◓) DMF. Small circles are the data of Teramoto, et al.,[55] in DCA-EDC mixtures and in DMF.

f_N. Figure 6.5 illustrates it in DCA-EDC mixtures of various compositions, where the data of Teramoto, Nakagawa, and Fujita[55] are included for comparison. Our data for each sample in different solvent conditions form a single composite curve, and $[\eta]$ for higher molecular weight samples increases remarkably in the vicinity of $f_N = 1$. The data of Teramoto, et al., exhibt similar behavior. Figure 6.6 shows results in the DCA-CHL mixture. The merger of $[\eta]$ vs. f_N data on a

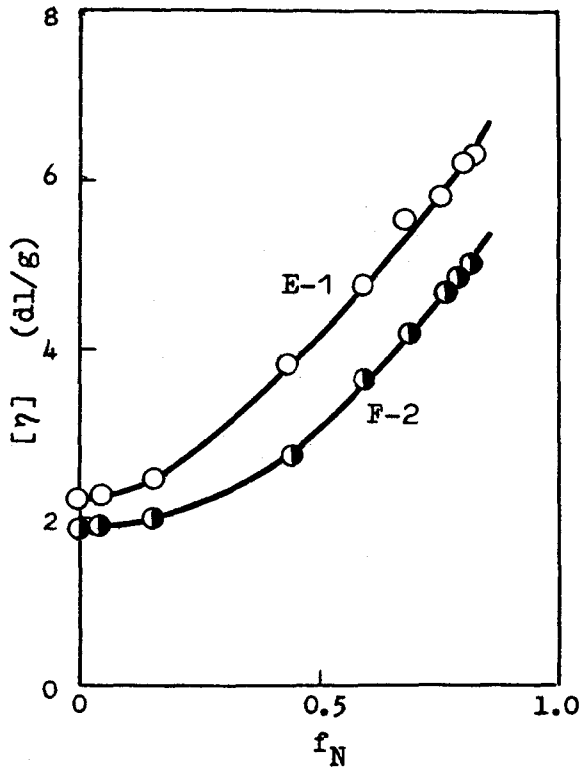

Figure 6.6. Dependence of $[\eta]$ on f_N for samples E-1 and F-2 in the DCA-CHL mixture

single curve is consistent with the finding in Chapter 2 that the σ values for PBLG in DCA-EDC mixtures depend scarcely on temperature and solvent composition.

6-3-4. Relationship between $[\eta]$ and $\langle S^2 \rangle$

The usual practice in the treatment of randomly coiled polymers is to write a relation[126]

$$[\eta] = \Phi(6\langle S^2 \rangle)^{3/2}/\overline{M}_w \qquad (6\text{-}6)$$

We apply this formalism to interrupted helices, and examine how the Flory constant Φ varies with the extent of deviation of interrupted helices from random coils.

Figure 6.7 shows values of Φ plotted against helical content f for samples E-1 and F-2 in the DCA-CHL mixture. For comparison, the data for these samples in DMF are also plotted at f = 1. The values of Φ are almost constant (ca. 1.9×10^{21}) for f below 0.6, and then decreases to those for DMF as f approaches unity. The value 1.9×10^{21} compares favorably to 2.1×10^{21} known as an average for randomly coiled polymers in a very good solvent.[82] As has been demonstrated in Chapter 4, an interrupted helix behaves like a Gaussian coil with respect to the mean-square dimensions and higher even moments, provided that the molecular weight is sufficiently large and the helical content is not equal to unity. Hence, for such a polypeptide molecule, the uniform expansion model of Kurata and Yamakawa[132] is expected

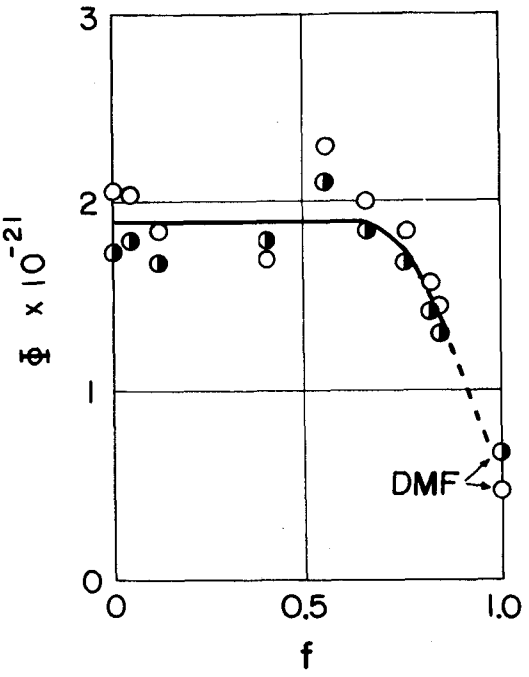

Figure 6.7. Variation of the Flory constant Φ with helical content f for samples E-1 (○) and F-2 (◑) in the DCA-CHL mixture.

to yield the Flory-Fox relation and hence an approximately constant Φ. The deviation from the limiting behavior may become appreciable as the molecular weight is lowered and the helical content approaches unity. Comparison of Figure 6.7 with Figure 4.4 validates this inference.

Substitution of equation (6-6) into equation (4-26) gives

$$\frac{([\eta]/\bar{M}_w^{1/2})^{2/3}}{H_2(1-f)} = \frac{\Phi^{2/3}}{M_o}\left(a_o^2 + a_1^2 \frac{H_3}{H_2}\right) \qquad (6\text{-}7)$$

For infinitely large molecular weight, this equation reduces

to

$$\frac{([\eta]/\bar{M}_w^{1/2})^{2/3}}{(1-f)} = \frac{\Phi^{2/3}}{M_o}\left[a_o^2 + \frac{2a_1^2}{\sqrt{\sigma}}\left(\frac{f}{1-f}\right)^{3/2}\right] \qquad (6\text{-}8)$$

Ptitsyn and coworkers[52,57,133-136] used this equation for a determination of σ, although they applied it to finite molecular weight by replacing f by f_N. For the application of equation (6-8) to finite molecular weights, it is necessary to assume that f is equal to f_N and $Q(\beta,f) = 1$. Since $Q(\beta,f)$ decreases from unity as f increases from zero, the resulting plot of $([\eta]/\bar{M}_w^{1/2})^{2/3}/(1-f_N)$ vs. $(\Phi^{2/3}a_1^2/M_o)(f_N/1-f_N)^{3/2}$ should have a smaller slope than that expected from equation (6-7), yielding a larger σ if Φ is assumed to be constant (see Figure 2 of ref. 137). Barskaya, Bolotina, and Ptitsyn[134] obtained a $\sqrt{\sigma}$ value of 1.4×10^{-2} for PBLG in DCA-EDC from such an analysis, which is larger than our value of 0.95×10^{-2}.

In conclusion, $[\eta]$ and $\langle S^2 \rangle$ for interrupted helices of PBLG in the DCA-CHL mixture obey the Flory-Fox relation for helical contents below 0.6. In general, the $[\eta] - \langle S^2 \rangle$ relation may be influenced by the molecular weight, the parameter σ, and other factors. Since the present data span only limited ranges of these factors, further study is needed to ascertain the applicability of the above conclusion to other polypeptide-solvent systems. This type of work is interesting and perhaps of great importance in connection with

hydrodynamic properties of semi-flexible macromolecules in dilute solution.

Summary and Conclusions

This thesis has dealt with two main subjects: conformational transition from coil to helix of polypeptide molecules in dilute solution and dimensional changes accompanying the transition. Emphasis was put on the analyses of experimental data in terms of the statistical mechanical theory. Throughout this work, poly(γ-benzyl L-glutamate) (PBLG) was chiefly used as polypeptide sample, and mixtures of dichloroacetic acid (DCA) and ethylene dichloride (EDC) and a mixture of DCA and cyclohexanol (CHL) were chosen as solvents.

1. Determination of the helix-coil transition parameters

Since the conformation of a polypeptide molecule is governed by three basic parameters, N, σ, and u, the first part of the present investigation was focussed on the determination of these parameters for PBLG in the mixed solvent systems mentioned above. Here N is the number of monomeric residues in the molecule, σ the helix-initiation or cooperativity parameter, and u the equilibrium constant for the formation of helix from coil. To this end, the approximate expression of Okita, et al., for the helical content f_N,

$$f_N = f - 2f^{3/2}(1 - f)^{1/2}/\bar{N}_n\sqrt{\sigma} \qquad (1)$$

was applied to optical rotation data taken as a function of number-average degree of polymerization $\bar{N}_n$. Here f stands for the value of f_N for infinitely large N. This process gave, with a moderate precision, values of u, σ, and f as functions of temperature and solvent composition. The values of $\sqrt{\sigma}$ obtained were substantially independent of temperature and DCA-EDC composition, yielding the average values of 0.95×10^{-2} for DCA-EDC mixtures and 0.92×10^{-2} for the DCA-CHL mixture.

The enthalpy change ΔH accompanying the helix-coil transition was evaluated from the dependence of ln u on temperature. It was found that the value of ΔH varied significantly with temperature and solvent composition. This finding suggested that ΔH might involve certain concomitant heats in addition to the intramolecular hydrogen bond energy, and that calorimetric measurements should yield certain averages of ΔH. In fact, our ΔH values for PBLG in DCA-EDC mixtures, when properly averaged, were in excellent agreement with the calorimetric values reported for the same system, and the discrepancy in calorimetric data themselves was ascribed to the difference in the averaging processes involved. The agreement of our ΔH values with the calorimetric data substantiated the reliability of our determination of the transition parameters.

2. Solvent effects on the helix-coil transition

The remarkable dependence of ΔH on temperature and solvent composition found for PBLG suggested that helix-coil transitions of inverse type would be pronouncedly affected by interactions of peptide residues with active solvent molecules such as DCA capable of forming hydrogen bond. A statistical theory which took such interactions into consideration was developed on the assumption that the active solvent exists in the form of dimer and that the dimerized molecules hydrogen bond with a pair of free CO and NH groups of peptide residues. The following expressions for ΔH, u, and σ were derived:

$$\Delta H = \Delta H_o - \frac{K\underline{a}}{1 + K\underline{a}} (\Delta H_a - \Delta H_m) \tag{2}$$

$$u = u_o/(1 + K\underline{a}) \tag{3}$$

$$\sqrt{\sigma} = \sqrt{\sigma}_o/(1 + K\underline{a})^2 \tag{4}$$

where K is the equilibrium constant for the binding reaction assumed, ΔH_a the enthalpy change for this binding, ΔH_m the partial molar enthalpy of the dimerized active solvent in the mixture considered, $\underline{a}$ the thermodynamic activity of this solvent, and ΔH_o, u_o, and σ_o the values of ΔH, u, and σ in the system containing no active solvent. Either equation (2) or (3) was used to analyze the experimental

data for PBLG and poly(β-benzyl L-aspartate) (PBLA) in DCA-EDC mixtures. The value of ΔH_a so obtained was about -3 kcal/mol for both PBLG and PBLA, which was favorably compared to the values for heats of association (per hydrogen bond) of amides in ordinary organic liquids. On the other hand, the values of ΔH_o for both polypeptides were, though negative as they should be, appreciably lower than those expected for the ordinary hydrogen bonds between CO and NH groups. The values of the thermodynamic parameters associated with the solvent effect made it possible to understand not only why and how the observed values of ΔH depended on temperature and solvent composition, but also the general features of inverse transitions in quantitative terms. Furthermore, equation (4) gave a possible interpretation for the experimental fact that, against the hypothesis of Zimm and Bragg, σ depended upon the kind of solvent. Equations (3) and (4) provided an indirect method to estimate the transition parameters u_o and σ_o in a pure inert solvent (e.g., EDC).

3. Dimensional changes in the transition region

Approximate expressions for mean dimensions and particle scattering function P(θ) of a polypeptide chain were derived from Nagai's theory on the assumption that $N \gg 1$, $\sqrt{\sigma} \ll 1$, and $N\sqrt{\sigma} > 2$. Here θ denotes the scattering angle. The result shows that the usual procedure of plotting $P(\theta)^{-1/2}$ against $\sin^2(\theta/2)$ allows one to determine the mean-square radius of

gyration $\langle S^2 \rangle$ even for a molecule in the form of interrupted helix. Moreover, Nagai's exact expression for $\langle S^2 \rangle$ was shown to be simplified in the form:

$$H_1/H_2 = a_0^2 + a_1^2(H_3/H_2) \tag{5}$$

with

$$H_1 = 6\langle S^2 \rangle / N(1 - f) \tag{6}$$

$$H_2 = 1 + (12f^2/\beta^2)[1 - 2f^{1/2}(1-f)^{1/2}/\beta] \tag{7}$$

and

$$H_3 = \frac{2}{\sqrt{\sigma}}\left(\frac{f}{1-f}\right)^{3/2}\left\{1 - \frac{3}{\beta}\left(\frac{f}{1-f}\right)^{1/2} + \frac{6}{\beta^2}\left(\frac{f}{1-f}\right)[1 - 2(1-f)^2]\right.$$
$$- \frac{6}{\beta^3}\left(\frac{f}{1-f}\right)^{3/2}[1 - 2(1-f)^2(3-2f)$$
$$\left. - \frac{(1-2f)^2}{f^4}\exp(-\beta\sqrt{\frac{f}{1-f}})]\right\} \tag{8}$$

where β stands for $N\sqrt{\sigma}$ and a_0 and a_1 indicate the monomer lengths for randomly coiled and helical residues, respectively.

Light-scattering measurements for PBLG were performed with a DCA-CHL mixture (91.7 wt% DCA) and with a helicogenic solvent dimethylformamide (DMF). The $\langle S^2 \rangle$ data obtained for the DCA-CHL mixture were analyzed by making use of equation (5) along with the values of σ and f determined from polarimetric data. The results confirmed the validity of equation (5), yielding 16.9 ± 0.2 A for a_0 and 1.53 ± 0.10 A for a_1. The former

value is significantly larger than 11.3 A deduced by Brant and Flory for the unperturbed chain, which indicates that PBLG molecules in randomly coiled state are profoundly affected by excluded-volume effects. On the other hand, the value of 1.53 A for a_1 is in excellent agreement with that of 1.5 A expected for the α-helix. Thus, the present results for PBLG lend support to the theoretical developments by Nagai and by subsequent workers for the mean-square dimensions of a polypeptide chain.

The pitch of helix, h, per monomeric residue derived from the $\langle S^2 \rangle$ data for PBLG in DMF decreases slightly with increasing molecular weight, in agreement with the reported data for this polymer in both DMF and EDC. These experimental data were compared favorably to the theoretical values calculated in terms of the interrupted helix model with the values of 2.8×10^{-2} for $\sqrt{\sigma}_o$ and 1.7 for u_o obtained in EDC.

As a conformation-dependent property in dilute solution, viscosity behavior of PBLG in the helix-coil transition region was also examined with DCA, DMF, DCA-EDC mixtures, and the DCA-CHL mixture as solvents. The double-logarithmic plots of intrinsic viscosity $[\eta]$ and weight-average molecular weight $\bar{M}_w$ for DMF and DCA accurately followed straight lines with very different slopes, 1.45 for DMF and 0.76 for DCA, over the whole range of $\bar{M}_w$ studied. These results confirmed that PBLG molecules assume a rodlike shape in DMF and random coil in DCA. The Stockmayer-Fixman plot for PBLG in DCA gave the

value of 11.2 ± 0.5 A for a_o in the unperturbed state, which stood in excellent agreement with the value of Brant-Flory and proved the larger value of 16.9 A obtained for a_o from $\langle S^2 \rangle$ data to be due to the excluded-volume effect.

The data of $[\eta]$ for each PBLG sample in DCA-EDC mixtures of different compositions, when plotted against f_N, formed a single composite curve regardless of temperature and solvent composition. The curves for high-molecular-weight samples were characterized by steep upswing in the vicinity of $f_N = 1$. Comparison of the viscosity data with those of $\langle S^2 \rangle$ for PBLG in the DCA-CHL mixture revealed that $[\eta]$ and $\langle S^2 \rangle$ of this system obeyed the Flory-Fox relation for helical contents lower than 0.6 and that the deviation from the Flory-Fox relation became more appreciable as the helical content approached unity.

References

1. E.R. Blout, R.H. Karlson, P. Doty, and B. Hargitay, Polypeptides. I. The Synthesis and the Molecular Weight of High Molecular Weight Polyglutamic Acids and Esters, J. Amer. Chem. Soc., 76, 4492 (1954).
2. P. Doty, A.M. Holtzer, J.H. Bradbury, and E.R. Blout, Polypeptides. II. The Configuration of Polymers of γ-Benzyl-L-glutamate in Solution, J. Amer. Chem. Soc., 76, 4493 (1954).
3. E.R. Blout and R.H. Karlson, Polypeptides. III. The Synthesis of High Molecular Weight Poly-γ-benzyl-L-glutamate, J. Amer. Chem. Soc., 78, 941 (1956).
4. P. Doty, J.H. Bradbury, and A.M. Holtzer, Polypeptides. IV. The Molecular Weight, Configuration and Association of Poly-γ-benzyl-L-glutamate in Various Solvents, J. Amer. Chem. Soc., 78, 947 (1956).
5. L. Pauling, R.B. Corey, and H.R. Branson, The Structure of Proteins: Two Hydrogen-Bonded Helical Configuration of the Polypeptide Chain, Proc. Natl. Acad. Sci., 37, 205 (1951)
6. P. Doty and J.T. Yang, Polypeptides. VII. Poly-γ-Benzyl-L-glutamate: The Helix-Coil Transition in Solution, J. Amer. Chem. Soc., 78, 498 (1956).
7. G.D. Fasman, Factors Responsible for Conformational Stability, in "Poly-α-Amino Acids," G.D. Fasman Ed.,

Marcel Dekker, Inc., New York, 1967, Chapter 11, p 499.

8. M. Calvin, J. Hermans, Jr., and H.A. Scheraga, Effect of Deuterium on the Strength of Hydrogen Bonds, J. Amer. Chem. Soc., 81, 5048 (1959).

9. S. Hanlon, S.F. Russo, and I.M. Klotz, Protonation of Amide Groups of Polypeptides by "Helix-Breaking" Solvents, J. Amer. Chem. Soc., 85, 2024 (1963).

10. S. Hanlon and I.M. Klotz, Protonation of Polypeptides in "Helix-Breaking" Solvents: Spectral and Optical-Rotatory Properties in Solvents Containing Strong Organic Acids, Biochemistry, 4, 37 (1965).

11. M.A. Stake and I.M. Klotz, Protonation of Polypeptides in Helix-Breaking Solvents. Electrical Conductance, Biochemistry, 5, 1726 (1966).

12. S. Hanlon, The Protonation of Poly-γ-benzyl-L-glutamate in Mixed Solvents Containing Dichloroacetic Acid, Biochemistry, 5, 2049 (1966).

13. W.E. Stewart, L. Mandelkern, and R.E. Glick, Proton Nuclear Magnetic Resonance Studies of Model Polypeptides. Aspects of the Helix-Random Coil Interconversion, Biochemistry, 6, 143 (1967).

14. K.J. Liu and S.J. Lignowski, PMR Chemical Shifts of TFA in Poly(γ-benzyl L-Glutamate) Solutions, Biopolymers, 9, 739 (1970).

15. J.A. Ferretti and B.W. Ninham, Nuclear Magnetic Resonance Investigation of the Helix to Random Coil Transformation

in Poly(α-amino acid). II. Poly(γ-benzyl L-glutamate), Macromolecules, 3, 30 (1970).

16. K. Sato and A. Nishioka, NMR Studies on Poly(γ-methyl-L-glutamate) Solutions, Polymer J., 2, 379 (1971).

17. P. Urnes and P. Doty, Optical Rotation and the Conformation of Polypeptides and Proteins, Adv. Protein Chem., 16, 401 (1961).

18. J.T. Yang, Optical Rotatory Dispersion, in "Poly-α-Amino Acids," G.D. Fasman Ed., Marcel Dekker, Inc., New York, 1967, Chapter 6, p 239.

19. J.A. Schellman, The Thermodynamics of Urea Solutions and Heat of Formation of the Peptide Hydrogen Bond, Compt. Rend. Trav. Lab. Carlsburg, Ser Chim., 29, 223 (1955).

20. P. Doty, Configurations of Biologically Important Macromolecules in Solution, in "Biophysical Science - A Study Program," J.L. Oncley, F.O. Schmitt, R.C. Williams, M.D. Rosenberg, and R.H. Bolt Ed., John Wiley & Sons, Inc., New York, 1959, p 107.

21. S.A. Rice, A. Wada, and E.P. Geiduschek, Some Comments on the Theory of Denaturation, Discussions Farady Soc., 25, 130 (1958).

22. B.H. Zimm and J.K. Bragg, Theory of the Phase Transition between Helix and Random Coil in Polypeptide Chains, J. Chem. Phys., 31, 526 (1959).

23. L. Peller, On a Model for the Helix-Random Coil

Transition in Polypeptides. I. The Model and Its Thermal Behavior, J. Phys. Chem., 63, 1194 (1959).

24. J.H. Gibbs and E.A. DiMarzio, Statistical Mechanics of Helix-Coil Transitions in Biological Macromolecules, J. Chem. Phys., 30, 271 (1959).

25. T.L. Hill, Generalization of the One-Dimensional Ising Model Applicable to Helix Transitions in Nucleic Acids and Proteins, J. Chem. Phys., 30, 383 (1959).

26. A. Miyake, Local Regularity of Chain Substance. II, J. Polymer Sci., 46, 169 (1960).

27. K. Nagai, Dimensional Change of Polypeptide Molecules in the Helix-Coil Transition Region. II, J. Chem. Phys., 34, 887 (1961).

28. S. Lifson and A. Roig, On the Theory of Helix-Coil Transition in Polypeptides, J. Chem. Phys., 34, 1963 (1961).

29. B.H. Zimm, P. Doty, and K. Iso, Determination of the Parameters for Helix Formation in Poly-γ-Benzyl-L-glutamate, Proc. Natl. Acad. Sci., 45, 1601 (1959).

30. J. Applequist, On the Helix-Coil Equilibrium in Polypeptides, J. Chem. Phys., 38, 934 (1963).

31. T. Ackermann and H. Rüterjans, a) Der Temperaturverlauf der spezifischen Wärme von Lösungen des Poly-γ-benzyl-L-glutamats im Bereich der Helix-Coil Umwandlung, Z. Physik. Chem. (Frankfurt), 41, 116 (1964);

b) Kalorimetrische Messungen zur Helix-Coil-Umwandlung

von Nucleinsäuren und synthetischen Polypeptiden in Lösung, Ber. Bunsenges. Physik. Chem., 68, 850 (1964).

32. T. Ackermann and E. Neumann, Experimental Thermodynamics of the Helix-Random Coil Transition. I. Influence of Polymer Concentration and Solvent Composition in the PBG-DCA-EDC System, Biopolymers, 5, 649 (1967).

33. F.E. Karasz, J.M. O'Reilly, and H.E. Bair, Thermal Helix-Coil Transition in Poly-γ-benzyl-L-glutamate, Nature, 202, 693 (1964).

34. F.E. Karasz, J.M. O'Reilly, and H.E. Bair, Helix-Coil Transition in Poly-ε-carbobenzoxy-L-lysine, Biopolymers, 3, 241 (1965).

35. F.E. Karasz and J.M. O'Reilly, Deuteration and Solvent Composition Effects in the Helix-Coil Transition of Poly-γ-benzyl-L-glutamate, Biopolymers, 4, 1015 (1966).

36. A. Kagemoto and F.E. Karasz, The Molecular Weight Dependence of the Transition Enthalpy of Poly-γ-benzyl-L-glutamate, Analytical Calorimetry, 2, 147 (1970).

37. A. Kagemoto and R. Fujishiro, The Heat of the Coil-Helix Transition of Poly-γ-benzyl-L-glutamate in the Solution, Macromol. Chem., 114, 139 (1968).

38. A. Kagemoto and R. Fujishiro, Enthalpy Change of the Coil-Helix Transition of Poly(γ-benzyl L-Glutamate) in Dichloroacetic Acid — 1.2-Dichloroethane Mixtures, Biopolymers, 6, 1753 (1968).

39. G. Giacometti and A. Turolla, Heat of Solution of

Poly-γ-Benzyl-L-Glutamate in Dichloroethane-Dichloroacetic Acid Mixtures, Z. Physik. Chem. (Frankfurt), 51, 108 (1966).

40. G. Giacometti, A. Turolla, and R. Boni, Enthalpy of Helix-Coil Transitions from Heats of Solution. I. Polyglutamate, Biopolymers, 6, 441 (1968).

41. G. Giacometti, A. Turolla, and R. Boni, Enthalpy of Helix-Coil Transitions from Heats of Solution. II. Poly-ε-carbobenzoxy-L-lysine and Copolymers with L-phenyl-alanine, Biopolymers, 9, 979 (1970).

42. G. Giacometti, A. Turolla, and A.S. Verdini, Calorimetric Measurements on the "Normal" Temperature-Induced Helix-Coil Transition of Poly(N-γ-Carbobenzoxy-α,γ-diamino butylic acid), J. Amer. Chem. Soc., 93, 3092 (1971).

43. G. Rialdi and J. Hermans, Jr., Calorimetric Heat of the Helix-Coil Transition of Poly-L-glutamic Acid, J. Amer. Chem. Soc., 88, 5719 (1966).

44. P.Y. Chou and H.A. Scheraga, Calorimetric Measurement of Enthalpy Change in the Isothermal Helix-Coil Transition of Poly-L-lysine in Aqueous Solution, Biopolymers, 10, 657 (1971).

45. Y. Hayashi, A. Teramoto, K. Kawahara, and H. Fujita, Solution Properties of Synthetic Polypeptides. V. Helix-Coil Transition in Poly(β-benzyl L-Aspartate), Biopolymers, 8, 403 (1969).

46. K. Okita, A. Teramoto, and H. Fujita, Solution Properties of Synthetic Polypeptides. VI. Helix-Coil Transition of Poly-N^5-(3-hydroxypropyl)-L-glutamine, Biopolymers, 9,717 (1970).

47. J.A. Schellman, a) The Stability of Hydrogen-Bonded Peptide Structures in Aqueous Solution, Compt. Rend. Trav. Lab. Carlsburg, Ser. Chim., 29, 230 (1955); b) The Factors Affecting the Stability of Hydrogen-Bonded Polypeptide Structures in Solution, J. Phys. Chem., 62, 1485 (1958).

48. L. Peller, On a Model for the Helix-Random Coil Transition in Polypeptides. II. The Influence of Solvent Composition and Charge Interactions on the Transition. J. Phys. Chem., 63, 1199 (1959).

49. M. Bixon and S. Lifson, Solvent Effects on the Helix-Coil Transition in Polypeptides, Biopolymers, 4, 815 (1966).

50. W.G. Miller and P.J. Flory, Dimensions of Polyptptide Chains in Helicogenic Solvents, J. Mol. Biol., 15, 298 (1966).

51. O.B. Ptitsyn and A.M. Skvortsov, Theory of Helix-Coil Transition in Biopolymers. V. Method for Determination of Cooperativeness of Helix-Coil Transition in Polypeptide Chains Using Changes in Dimensions of Macromolecules in the Transition Region. Biofizika, 10, 909 (1965).

52. O.B. Ptitsyn, The Co-operativity of Helix-Coil Transitions in Polypeptide Chains, in "Conformation of Biopolymers," G.N. Ramachandran Ed., Acad. Press, London and New York, 1967, vol. 1, p 381.

53. M. Gō, N. Saito, and M. Ochiai, Conformation of Polypeptides in Helix-Coil Transition Region, J. Phys. Soc. Japan, 22, 227 (1967).

54. T.M. Birshtein, V.A. Zubkov, and M.V. Volkenshtein, Conformational Characteristics of Polymorphous Optically Active Macromolecues: A Statistical Zigzag Model, J. Polymer Sci. A-2, 8, 177 (1970).

55. A. Teramoto, K. Nakagawa, and H. Fujita, Solution Properties of Synthetic Polypeptides. III. Viscosity Behavior of Poly-γ-Benzyl-L-Glutamate in the Helix-Coil Transition Region, J. Chem. Phys., 46, 4197 (1967).

56. O.B. Ptitsyn, The Cooperativity of Helix-Coil Transitions in Polypeptide Chains, Conform. Biopolym., Pap. Int. Symp., Madras, 1, 381 (1967).

57. O.B. Ptitsyn, T.V. Barskaya, I.A. Bolotina, and I.G. Illarionova, Synthetic Polypeptides. III. Comparison of the Cooperative Degree of Poly-L-glutamic Acid Helical State in Different Solvents, Biofizika, 12, 386 (1967).

58. K. Okita, A. Teramoto, and H. Fujita, Solution Properties of Synthetic Polypeptides. IX. Light-Scattering Study of Poly-N^5-(3-hydroxypropyl)-L-glutamine in the

Helix-Coil Transition Region, Polymer J., 1, 582 (1970).

59. C. Strazielle, C. Dufour, and E. Marchal, Transition Helice-Chaine du Poly-γ-glutamate de Benzyle dans les Melanges de Solvants – I Etude par Diffusion de la Lumiere, Eur. Polym. J., 6, 1133 (1970).

60. A. Wada, a) Dielectric Properties of Polypeptide Solutions. Measurements of the Dielectric Properties of the α-Helix by the Low-Frequency Bridge Method, Bull Chem. Soc. Japan, 33, 822 (1960); b) Dielectric Properties of Polypeptide Solutions. I. The Electric Dipole Moment of α-Helix in Dioxane, J. Chem. Phys., 29, 674 (1958); c) II. Relation between the Electric Dipole Moment and the Molecular Weight of α-Helix, J. Chem. Phys., 30, 328 (1959); d) III. Elucidation of the Critical Frequency of Dielectric Dispersion from the Molecular Shape of the α-Helix, J. Chem. Phys., 30, 329 (1959).

61. I. Tinoco, Jr., Dynamic Electrical Birefringence Studies of Poly-γ-benzyl-L-glutamate, J. Amer. Chem. Soc., 79, 4336 (1957).

62. J.T. Yang, a) Concentration Dependence of Flow Birefringence of Polymer Solutions, J. Amer. Chem. Soc., 80, 5139 (1958); b) Comparison of the Use of Intrinsic Viscosity and Flow Birefringence for the Determination of Lengths of Rigid Particles, J. Polymer Sci., 54, S14 (1961).

63. C.T. O'Konski, K. Yoshioka, and W.H. Orttung, Electric Properties of Macromolecules. IV. Determination of Electric and Optical Parameters from Saturation of Electric Birefringence in Solution, J. Phys. Chem., 63, 1558 (1959).

64. J.T. Yang, a) Non-Newtonian Viscosity of Poly-γ-benzyl-L-glutamate Solutions, J. Amer. Chem. Soc., 80, 1783 (1958); b) Factors Affecting the Non-Newtonian Viscosity of Rigid Particles, J. Amer. Chem. Soc., 81, 3902 (1959).

65. P. Moha, G. Weill, and H. Benoit, Longueur de Persistance du Poly-L-glutamate de Benzyle en Solution, J. chim. phys., 61, 1240 (1964).

66. J. Applequist and P. Doty, α-Helix Formation in Poly-ε-Carbobenzoxy-L-Lysine and Poly-L-Lysine, in "Polyamino Acids, Polypeptides, and Proteins," M.A. Stahmann Ed., Univ. Wisconsin Press, Madison, 1962, p 161.

67. V.N. Tsvetkov, Yu.V. Mitin, I.N. Shtennikova, V.R. Glushenkova, G.V. Tarasova, V.S. Skazka, and N.A. Nikitin, Sedimentation, Diffusion and Viscosity of Poly-γ-Benzyl-L-glutamate in Solution, Vysokomolekul. Soedin., 7, 1098 (1965).

68. J. Marchal and C. Lapp, II. Analyse Hydrodynamique des Dimensions des Macromoléqules Hélicoïdales de Poly-DL-Phénylalanine et de Poly-L-γ-glutamate de Benzyl, J. chim. phys., 61, 999 (1964).

69. V. Luzzati, M. Cesari, G. Spach, F. Masson, and J.M. Vincent, La Structure du Poly-L-γ-Glutamate de Benzyle en Solution. Configuration en Hélice Différent de l'Hélice α et Transitions entre Formers Helicoïdales, J. Mol. Biol. 3, 566 (1961).

70. G. Boeckel, J.C. Genzling, G. Weill, and H. Benoit, Étude par Effet Kerr du Poly-L-glutamate de Benzyle en Solution, J. chim. phys., 59, 999 (1962).

71. G. Spach, L. Freund, M. Daune, and H. Benoit, Détermination de la Dimension des Molécules de Poly-L-γ-glutamate de Benzyle et de Poly-L-ε-carbobenzoxy-L-lysine par des Méthodes Hydrodynamiques-Effets de la Flexibilité, J. Mol. Biol. 7, 468 (1963).

72. H. Fujita, A. Teramoto, K. Okita, T. Yamashita, and S. Ikeda, Solution Properties of Synthetic Polypeptides. I. Light Scattering and Osmometry of Poly-γ-benzyl-L-glutamate in Helicogenic Solvents, Biopolymers, 4, 769 (1966).

73. M. Terbojevich, E. Peggion, A. Cosani, G. D'Este, and E. Scoffone, Solution Properties of Synthetic Polypeptides. Light Scattering and Viscosity of Poly-γ-ethyl-L-glutamate in Dichloroacetic Acid and Trifluoroethanol, Eur. Polym. J., 3, 681 (1967).

74. O. Kratky and G. Porod, Röntgenuntersuchung Gelöster Fadenmoleküle, Rec. Trav. Chim., 68, 1106 (1949).

75. D. Poland and H.A. Scheraga, in "Theory of Helix-Coil

in Biopolymers," Academic Press, Inc., New York, 1970, p 70.

76. H.A. Kramers and G.H. Wannier, Statistics of the Two-Dimensional Ferromagnet. Part I, Phys. Rev., 60, 252 (1941).

77. G.F. Newell and E.W. Montroll, On the Theory of the Ising Model of Ferromagnetism, Rev. Mod. Phys., 25, 353 (1953).

78. A. Cosani, E. Peggion, E. Scoffone, and A.S. Verdini, Chromatographic Fractionation of Primary Amine Initiated Poly-γ-Benzyl-L-Glutamate, Macromol. Chem., 97, 113 (1966).

79. K. Nakagawa, N. Nishioka, A. Teramoto, and H. Fujita, Solution Properties of Synthetic Polypeptides. XIV. Synthesis and Characterization of Broken-rod Polypeptides, Polymer J., in press.

80. R.D. Lundberg and P. Doty, Polypeptides. XVII. A Study of the Kinetics of the Primary Amine-initiated Polymerization of N-Carboxy-anhydrides with Special Reference to Configurational and Streochemical Effects, J. Amer. Chem. Soc., 79, 3961 (1957).

81. W. Moffitt and J.T. Yang, The Optical Rotatory Dispersion of Simple Polypeptides. I, Proc. Natl. Acad. Sci., 42, 596 (1956).

82. P.J. Flory, in "Principles of Polymer Chemistry," Cornell Univ. Press, Ithaca, N.Y., 1953.

83. J.Y. Cassim and E.W. Taylor, The Effects of Solvent Environment on the Optical Rotatory Dispersion Parameters of Polypeptides. I. Studies on Poly-γ-Benzyl-L-Glutamate, Biophys. J., 5, 553 (1965).

84. A. Nakajima and T. Hayashi, Effects of Temperature on Molecular Conformations of Poly-γ-methyl-L-glutamate in Solvents, Bull. Inst. Chem. Res., Kyoto Uni., 46, 62 (1968).

85. A. Teramoto, T. Yamashita, and H. Fujita, Solution Properties of Synthetic Polypeptides. IV. Trimethylenediamine-Initiated Poly-γ-Benzyl-L-Glutamate, J. Chem. Phys., 46, 1919 (1967).

86. A. Teramoto and T. Norisuye, Solution Properties of Synthetic Polypeptides. XII. Enthalpy Changes Accompanying Helix-Coil Transition of Polypeptide, Biopolymers, 11, 1693 (1972).

87. G.C. Pimentel and A.L. McClellan, in "The Hydrogen Bond," Freemen & Co., Fan Francisco and London, 1959.

88. T.M. Birshtein and O.B. Ptitsyn, in "Conformations of Macromolecules," John Wiley & Sons, New York· London· Sydney, 1966, Chapter 10, p 277.

89. D. Puett and A. Ciferri, Conformational Studies on Concentrated Solutions of Poly(γ-benzyl L-Glutamate), Biopolymers, 10, 547 (1971).

90. M. Gō, N. Gō, and H.A. Scheraga, Molecular Theory of the Helix-Coil Transition in Polyamino Acids. I.

Formulation, Proc. Natl. Acad. Sci., 59, 1030 (1968); II. Numerical Evaluation of s and σ for Polyglycine and Poly-L-alanine in the Absence (for s and σ) and Presence (for σ) of Solvent, J. Chem. Phys., 52, 2060 (1970); III. Evaluation and Analysis of s and σ for Polyglycine and Poly-L-alanine in Water, J. Chem. Phys., 54, 4489 (1971).

91. "Organic Solvents," A. Weissberger, F.S. Proskauer, J.A. Riddick, and E.E. Toops, Jr. Ed., Interscience Publishers, Inc., New York, 1955, p 195.

92. E.M. Bradbury, A.R. Downie, A. Elliott, and W.E. Hanby, The Stability and Screw Sense of the α-Helix in Poly-β-Benzyl-L-aspartate, Proc. Roy. Soc. (London), A259, 110 (1960).

93. R.H. Karlson, K.S. Norland, G.D. Fasman, and E.R. Blout, The Helical Sense of Poly-β-benzyl-L-aspartate. Synthesis and Rotatory Dispersion of Copolymers of β-Benzyl-L and D-aspartate with γ-Benzyl-L-glutamate, J. Amer. Chem. Soc., 82, 2268 (1960).

94. C. Toniolo, M.L. Falxa, and M. Goodman, Conformational Aspects of Polypeptides. XXV. Solvent and Temperature Effects on the Conformations of Copolymers of Benzyl and Methyl L-Aspartate with Nitrobenzyl-L-Aspartate, Biopolymers, 6, 1579 (1968).

95. A. Teramoto, unpublished data.

96. R.T. Ingwall, H.A. Scheraga, N. Lotan, A. Berger, and

E. Katchalski, Conformational Studies of Poly-L-Alanine in Water, Biopolymers, 6, 331 (1968).

97. M.E. Baur and L.H. Nosanow, Simple Model for the Helix-Random Coil Transition in Polypeptides, J. Chem. Phys., 38, 578 (1963).

98. J.T. Yang, Optical Rotatory Dispersion of Polypeptides and Proteins, Tetrahedron, 13, 143 (1961).

99. F.E. Karasz and J.M. O'Reilly, Enthalpy Changes in the Helix-Coil Transition of Poly(γ-benzyl L-glutamate), Biopolymers, 5, 27 (1967).

100. F. Gaskin and J.T. Yang, Helix-Coil Transition of Poly-γ-N-Carbobenzoxy-L-α,γ-diaminobutyrate and Poly-δ-N-Carbobenzoxy-L-ornithine, Biopolymers, 10, 631 (1971).

101. P.H. von Dreele, N. Lotan, V.S. Ananthanarayanan, R.H. Andreattam D. Poland, and H.A. Scheraga, Helix-Coil Stability Constants for the Naturally Occuring Amino Acids in Water. II. Characterization of the Host Polymers and Application of the Host-Guest Technique to Random Poly(hydroxypropylglutamine-co-hydroxybutyl-glutamine), Macromolecules, 4, 408 (1971).

102. G.C. Berry, Thermodynamic and Conformational Properties of Polystyrene. I. Light-Scattering Studies on Dilute Solutions of Linear Polystyrenes, J. Chem. Phys., 44, 4550 (1966).

103. K.A. Stacey, in "Light-Scattering in Physical Chemistry," Butterworths, London, 1956.

104. N. Saito, private communication.

105. T.M. Birshtein, Conformation of Polypeptide in the Helix-Coil Transition Region, Biopolymers, 7, 443 (1969).

106. K. Nagai, Non-Gaussian Character of Real Polymer Chains, J. Chem. Phys., 38, 924 (1963).

107. M. Gō and N. Saito, Conformation of Polypeptides in the Helix-Coil Transition Region. II. Revised Calculation and Discussion, J. Phys. Soc. Japan, 28, 467 (1970).

108. S. Yamashita, Stereospecific Polymerization of α-Amino Acid N-Carboxy Anhydrides, Ph. D. Thesis, Osaka Univ., (1971).

109. A. Kruis, Die Äquivalentdispersion von starken Elektrolyten in Lösung im Sichtbaren, Z. Physik. Chem., 34B, 13 (1936).

110. Gj. Dežělić and J. Vavra, Angular Dependence of the Light Scattering in Pure Liquids, Croat. Chim. Acta, 38, 35 (1966).

111. J.P. Kratohvil, Calibration of Light-Scattering Instruments IV. Correction for Reflection Effects, J. Colloid Interface Sci., 21, 498 (1966).

112. T. Norisuye, K. Kawahara, A. Teramoto, and H. Fujita, Excluded-Volume Effects in Dilute Polymer Solutions. I. Equilibrium Properties, J. Chem. Phys., 49, 4330 (1968).

113. H. Utiyama, N. Sugi, M. Kurata, and M. Tamura, Precise Light-Scattering Studies on Dilute Polymer Solutions II. Low-Angle Light-Scattering Photometer Model LS-1.

114. D.A. Brant and P.J. Flory, The Configuration of Random Polypeptide Chains. I. Experimental Results, J. Amer. Chem. Soc., 87, 2788 (1965).

115. M. Wallach and H. Benoit, Light Scattering by Poly-L-Benzyl Glutamate Solutions Subjected to an Electrical Field, J. Polymer Sci., 57, 41 (1962).

116. B.R. Jennings and H.G. Jerrard, Light Scattering by Poly-γ-benzyl-L-glutamate Solutions Subjected to Electric Fields, J. Phys. Chem., 69, 2817 (1965).

117. D.A.D. Parry and A. Elliott, X-Ray Diffraction Patterns of Liquid Crystalline Solutions of Poly(γ-benzyl L-glutamate), Nature, 206, 616 (1965).

118. P. Saludjian and V. Luzzati, The α-Helix Conformation of Polypeptides in Solution: A Re-evaluation of the Small-angle X-Ray Scattering Evidence, J. Mol. Biol., 15, 681 (1966).

119, P. Doty, A. Wada, J.T. Yang, and E.R. Blout, Polypeptides. VIII. Molecular Configurations of Poly-L-glutamic Acid in Water-Dioxane Solution, J. Polymer Sci., 23, 851 (1957).

120. R. Sakamoto, The Stability of Helices of Poly-L-glutamic Acid Esters in Solution, J. Chem. Soc. Japan Pure Chem. Sect., 85, 17 (1964).

121. A.J. Byerley, B.R. Jennings, and H.G. Jerrard, Conformation Parameter and Gradient Dependency of Poly-γ-benzyl-L-glutamate by Viscometry, J. Chem. Phys., 48, 5526 (1968).

122. B.H. Zimm and D.M. Crothers, Simplified Rotating Cylinder Viscometer for DNA, Proc. Natl. Acad. Sci., 48, 905 (1962).

123. H. Fujita, A. Teramoto, T. Yamashita, K. Okita, and S. Ikeda, Solution Properties of Synthetic Polypeptides. II. Sedimentation and Viscosity of Poly-γ-benzyl-L-glutamate in Dimethylformamide, Biopolymers, 4, 781 (1966).

124. R. Simha, The Influence of Brownian Movement on the Viscosity of Solutions, J. Phys. Chem., 44, 25 (1940).

125. H. Yamakawa, Asymptotic Solution of the Excluded-Volume Problems in a Linear Polymer Chain, J. Chem. Phys., 48, 3845 (1968).

126. P.J. Flory and T.G Fox, Treatment of Intrinsic Viscosities, J. Amer. Chem. Soc., 73, 1904 (1951).

127. H. Yamakawa, in "Modern Theory of Polymer Solutions," Harper and Row, New York, 1971.

128. K. Kawahara, T. Norisuye, and H. Fujita, Excluded-Volume Effects in Dilute Polymer Solutions. II. Limiting Viscosity Number, J. Chem. Phys., 49, 4339 (1968).

129. G. Tanaka, S. Imai, and H. Yamakawa, Experimental Test of the Two-Parameter Theory of Dilute Polymer Solutions: Poly-p-methylstyrene, J. Chem. Phys., 52, 2639 (1970).

130. M. Kurata and W.H. Stockmayer, Intrinsic Viscosities and Unperturbed Dimensions of Long Chain Molecules, Fortschr. Hochpolym. Forsch., 3, 196 (1963).

131. W.H. Stockmayer and M. Fixman, On the Estimation of Unperturbed Dimensions from Intrinsic Viscosities, J. Polymer Sci. C, 1, 137 (1963).

132. M. Kurata and H. Yamakawa, Theory of Dilute Polymer Solution. II. Osmotic Pressure and Frictional Properties, J. Chem. Phys., 29, 311 (1958).

133. O.B. Ptitsyn and A.M. Skvortsov, Theory of Helix-Coil Transition in Biopolymers. V. Method for Determination of Cooperativeness of Helix-Coil Transition in Polypeptide Chains Using Changes of Dimensions of Macromolecules in the Transition Region, Biofizika, 10, 909 (1965).

134. T.V. Barskaya, I.A. Bolotina, and O.B. Ptitsyn, Comparison of the Degree of Cooperation of the Helix-Coil Transitions in the Esters of Poly(L-glutamic acid), Molekul. Biol. (SSSR), 2, 700 (1968).

135. V.E. Bychkova, O.B. Ptitsyn, and T.V. Barskaya, Thermodynamic Parameters of Helix-Coil Transition in Polypeptide Chains. I. Poly-(L-glutamic Acid), Biopolymers, 10, 2161 (1971).

136. T.V. Barskaya and O.B. Ptitsyn, Thermodynamic Parameters of Helix-Coil Transition in Polypeptide Chains. II. Poly-L-Lysine, Biopolymers, 10, 2181 (1971).

137. A. Teramoto, T. Norisuye, and H. Fujita, Solution Properties of Synthetic Polypeptides. VII. Approximate Expressions for Important Physical Quantities of Polypeptide Molecules, Polymer J., 1, 55 (1970).

List of Publications

The results of the present study have been published in the following papers:

(1) Solution Properties of Synthetic Polypeptides. VII. Approximate Expressions for Important Physical Quantities of Polypeptide Molecules, Polymer J., 1, 55 (1970). (Chapters 2 and 4).

(2) VIII. Further Study of the Light-Scattering Function, Polymer J., 1, 341 (1970). (Chapter 4).

(3) X. Transition Parameters for Poly(γ-Benzyl-L-glutamate), Polymer J., 1, 691 (1970). (Chapter 2).

(4) XI. Solvent Effect on Helix-Coil Transition in Polypeptides, Polymer J., 3, 538 (1972). (Chapter 3).

(5) XII. Enthalpy Changes Accompanying Helix-coil Transition of Polypeptide, Biopolymers, 11, 1693 (1972). (Chapter 2).

(6) XIII. Dimensions of Interrupted Helices of Poly(γ-benzyl L-glutamate), Polymer J., ~~in press.~~ 4, 323 (1973). (Chapter 5).